MOUSE AND STEM CELL MODELS OF FRONTOTEMPORAL DEMENTIA

by

Miranda Ethel Orr

A dissertation submitted in partial fulfillment
of the requirements for the degree

of

Doctor of Philosophy

in

Neuroscience

MONTANA STATE UNIVERSITY
Bozeman, Montana

January 2012

APPROVAL

of a dissertation submitted by

Miranda Ethel Orr

This dissertation has been read by each member of the dissertation committee and has been found to be satisfactory regarding content, English usage, format, citation, bibliographic style, and consistency, and is ready for submission to The Graduate School.

Dr. George A. Carlson (Co-Chair)

Dr. Frances B. Lefcort (Co-Chair)

Approved for the Department Cell Biology and Neuroscience

Dr. Thomas E. Hughes

Approved for The Graduate School

Dr. Carl A. Fox

STATEMENT OF PERMISSION TO USE

In presenting this dissertation in partial fulfillment of the requirements for a doctoral degree at Montana State University, I agree that the Library shall make it available to borrowers under rules of the Library. I further agree that copying of this dissertation is allowable only for scholarly purposes, consistent with "fair use" as prescribed in the U.S. Copyright Law. Requests for extensive copying or reproduction of this dissertation should be referred to ProQuest Information and Learning, 300 North Zeeb Road, Ann Arbor, Michigan 48106, to whom I have granted "the exclusive right to reproduce and distribute my dissertation in and from microform along with the non-exclusive right to reproduce and distribute my abstract in any format in whole or in part."

Miranda Ethel Orr

January 2012

ACKNOWLEDGEMENTS

I owe my deepest gratitude to my advisor, Dr. George Carlson, for the experiences he provided me, his commitment to my scientific training, and continuous guidance and support, both personally and professionally. For their time, dedication, and constructive comments throughout my training, I thank my dissertation committee: Dr. Frances Lefcort, Dr. Roger Bradley, Dr. Linda Hyman, Dr. Richard Bessen and Dr. Rich Bridges; and our collaborator, Dr. Karen Ashe, University of Minnesota. I thank Dr. Peter Davies, Albert Einstein College of Medicine, for donating several of the antibodies used in my research. I am grateful for the awards, Ruth L. Kirschstein National Research Service Award and COBRE grant, that funded my salary and travel.

I thank the McLaughlin Research Institute scientists, administration, and Animal Resource Center staff for their advice and assistance. For histology, I thank Amanda and Andrea for their dedicated time. I especially thank the Carlson lab research assistants, Rose, Rebecca, and Chris for making every day thoroughly enjoyable. Together with Cabin lab members, MegAnne and Jessica, they provided companionship, humor, and social outlet. My fellow graduate students and close friends, Will and Jaishree, always offered advice, console, and comic relief and I am truly grateful for their comradery.

My family and close friends have encouraged me and supported my professional goals, thank you all. Most importantly, I thank my husband, Tim, whose courage, honesty, and dedication inspire me daily. He is my role model and my best friend. Lastly, in loving memory my research was inspired by my grandma, Vivian Siewing, who passed away with Alzheimer's disease in 2002.

TABLE OF CONTENTS

LIST OF TABLES

LIST OF FIGURES

LIST OF FIGURES--CONTINUED

NOMENCLATURE

Mouse gene symbols are italicized with only the first letter uppercase (e.g. *Mapt*). Human gene symbols are regular type with all letters uppercase (e.g. MAPT). Superscript indicates whether the allele is present (+) or absent (0). Subscript designates a protein mutation (e.g. tau_{P301L} indicates a proline to leucine mutation at residue 301.

ABSTRACT

Alzheimer's disease (AD) is the most prevalent brain disease in the United States, and an escalating health concern. AD patient brains acquire hallmark protein aggregates, referred to as senile Aβ plaques and neurofibrillary tangles (NFTs), that coincide with brain cell loss and dementia. A subset of AD patients carry mutant genes. Our understanding of AD largely relies on model systems that express these gene variants. Mice engineered to express AD-mutant human genes develop Aβ plaques, but fail to develop the tau-containing NFTs or cell loss. Mutant tau variants are required to induce NFTs and neuronal loss in mice, but AD patients carry normal tau genes. The inability of mouse tau to become a pathogenic protein in the presence of AD-mutant gene variants, and the general insufficiency of the current systems to recapitulate AD, inspired the research described here. To determine if species differences between mouse and human tau inhibit the progression of AD in mice, I utilized a well-characterized mouse model of a related disease, frontotemporal dementia (FTD). FTD mice carry mutant human tau and develop NFTs and cell loss. I ablated mouse tau in FTD mice and looked for signs of more severe pathology. I compared the FTD mice, with and without mouse tau, to FTD mice with and without wild type human tau to investigate potential tau species-specific differences. My studies indicated that wild type tau, mouse or human, dampened the pathological effects of FTD tau implying a general, not mouse-specific, effect of normal tau protein. Our data suggest that unknown factors, distinct from endogenous mouse tau, contribute to the inability of mice to model AD. The recent interest in patient-specific stem cell (SC) models to study disease necessitates a thorough evaluation of their ability to recapitulate key characteristics of disease, reproducibility, and longevity. I generated and characterized brain SC cultures from FTD fetal mice and compared them to those generated from mice with normal human tau. Significant genotype associated differences were discovered in the SC system and later verified in adult mice to reinforce the potential of patient-specific SC models to study disease.

INTRODUCTION

Neurodegenerative Diseases and Mouse Models

Alzheimer's Disease

Over one hundred years ago German psychiatrist and neuropathologist, Dr. Alois Alzheimer, described a 51-year-old patient with progressive forgetfulness, inappropriate behavior, and dementia. Despite diminishing cognitive function, this patient's motor skills remained unaffected. While accustomed to treating these behavioral issues in elderly residents, this patient, Auguste Deter, presented with symptoms at an unusually young age. When Auguste died over four years later Dr. Alzheimer conducted a postmortem histological examination on her brain tissue. In his 1907 case report, Alzheimer noted an evenly atrophied brain with vascular changes [1]. He described striking neurofibrils stained with the Bielschowsky method, a newly developed histological assay. Approximately 25-33% of all cortical neurons contained Bielschowsky staining. Some cells had degenerated leaving only a tangle of fibrils. The fibrils co-existed with ubiquitous miliary deposits observable without staining. Today, post-mortem presence of these protein aggregates, now known as neurofibrillary tangles (NFTs) and Aβ senile plaques, respectively, is necessary to conclusively diagnose the "Disease of Forgetfulness," later named Alzheimer's dementia (AD) in honor of Dr. Alzheimer's discovery.

Currently in the US, AD is the most prevalent neurodegenerative disease, the sixth leading cause of death across all ages, and impacts over 5.4 million Americans [2]. Due to the slowly progressing nature of AD, patients survive an average of four to eight

years, but can live decades resulting in a prolonged low quality of life [3-6]. Advanced disease renders patients completely unable to conduct daily living tasks and necessitates full-time care. While AD is a terminal illness, patients typically die from infection or pneumonia, not cognitive failure. Early diagnosis is critical to delay disease progression. While medical advances in cognitive testing, brain imaging, and cerebral spinal fluid biomarkers continue to improve [7], postmortem brain examination is still required to conclusively confirm an AD diagnosis.

AD predominantly affects the cerebral cortex; specifically, the entorhinal cortex is the first to develop signs of pathology. The cerebral cortex is the outer, evolutionarily youngest, and most highly developed portion of the human brain responsible for processing complex cognitive functions. As disease progresses pathology encompasses a more primitive brain region, the hippocampus, which is recognized primarily for memory consolidation. Due to the brain regions affected, patients display signs of cognitive decline affecting memory, attention, language, and executive functions.

The vast majority of AD cases, >95%, have no defining genetic factor and are considered sporadic, or late-onset. Conversely, early-onset or familial AD (FAD) refers to a small subset of patients with a clear genetic component. Both familial and sporadic forms display the same cellular pathological characteristics: amyloid plaques, comprised of Aβ peptides; and NFTs, comprised of misprocessed tau protein. These protein aggregates coincide with neuron loss, brain atrophy and dementia [8]. Congruencies between familial and sporadic disease pathologies suggest that they arise through similar

mechanisms. Progress in the field relies heavily on data gathered from familial cases. Such studies have revealed key molecular players of disease.

To date, three autosomal dominant FAD genes have been identified: amyloid precursor protein (APP) [9-13], and presenilins 1 (PS1) and 2 (PS2) [14-16]. Mutations in any of these three genes result in elevated APP-derived Aβ, the primary component of senile plaques [17]. Aβ is generated by consecutive proteolytic cleavage of APP, first extracellularly by β-secretase followed by γ-secretase within its membrane-spanning region. Both PS1 and PS2 are subunits of the enzyme γ-secretase, and certain mutations of either subunit result in increased APP misprocessing and elevated Aβ production.

A prominent hypothesis in AD research suggests that elevated Aβ drives NFT formation [18]; however the development of an animal model that recapitulates the sufficiency of FAD mutations in initiating the pathological cascade remains elusive. The first mice to develop an AD-associated phenotype expressed the APP Indiana mutation, a single amino acid substitution (phenylalanine for valine) at residue 717 (APP_{F717V}) [11]. Mice developed Aβ deposits and plaques, synaptic loss, and gliosis, but they failed to show signs of cognitive impairment, NFTs, or neuronal loss [19]. Shortly after, a transgenic mouse line was engineered to express the APP Swedish variant, APP_{SWE} [20,21] discovered in a large Swedish family with AD containing two mutations, lysine to asparagine at 670 and methionine to leucine at 671 [13]. The APP_{SWE} mice were the first to show signs of memory impairment associated with elevated Aβ [20,21], but neither NFT formation nor neuronal loss developed. Many other transgenic mouse models engineered to express APP, PS1, or PS2 gene variants followed; all consistently

failed to recapitulate NFT and neuron loss [22]. In order to simultaneously acquire both the plaque and tangle phenotypes associated with AD, mice must express mutant variants of both APP and the NFT-containing subunit, tau [23,24]. The inability to fully recapitulate AD pathology by elevating Aβ prompted researchers to critically evaluate tau's role in AD pathogenesis.

Scientists researching microtubule (MT) regulation discovered tau proteins. MTs are structural fibrous systems necessary for many fundamental cellular processes including mitosis, cell transport and motility. Due to the dynamic nature of MTs, signals instructing tubulin monomer polymerization and depolymerization are crucial. Studies focused on the discovery of such regulatory molecules discovered tau as a protein that co-purified with tubulin, and a necessary factor for tubulin polymerization into microtubules [25].

Tau belongs to the family of microtubule associated proteins, MAPs. All MAPs influence cytoskeletal stability and plasticity through MT interactions. Tau proteins limit the dynamic MT shrinking and elongation phases, known as catastrophe and rescue [26]. Primarily a neuronal protein restricted to the axonal compartment, tau influences neuronal morphogenesis, cytoarchitecture, and cellular transport within neuronal cells [27,28].

Tau's coding gene, microtubule associated protein tau (MAPT), is a single copy gene with 16 exons [29-33]. Alternative splicing produces six tau isoforms [29,30]. Differential inclusion of exons 2 and 3 at the N-terminus results in three different splice variants that contain zero, one, or two amino acid inserts (0N, 1N, 2N). The N-terminal

projection domain bundles MTs [34], regulates MT spacing [35], and helps link MTs with the plasma membrane [36]. The C-terminal exons 9-12 contain imperfect repeat sequences referred to as the microtubule-binding (MTB) domain. Inclusion of exon 10 produces isoforms with four repeat sequences (4R) (Figure 1.1), which bind MTs with higher affinity than 3R isoforms lacking exon 10 [31,37-39]. Adjacent to the MTB domain is the proline-rich (PR) domain, which enhances MT targeting and binding [40]. Post-translational modifications alter tau's MT affinity, most notably phosphorylation decreases MT stability [41-45].

Central nervous system (CNS) region and developmental age dictate the identity of tau isoform, the level of tau expression, and the level of phosphorylation. The developing CNS requires a fluid cytoskeleton necessary for axonal migration and neurite outgrowth and extension. To accommodate this dynamic cellular environment heavily phosphorylated 3R tau isoforms are expressed [46]. Fetal tau contains 7 moles of phosphate per mole of protein, while healthy adult brains contain 1-3 moles of phosphate per mole of tau [47]. The adult CNS consists of mostly static neuronal circuitry with stable cytoskeletons. Adult human brains contain a 1:1 ratio of primarily non-phosphorylated 3R and 4R tau [32,37]; adult rodent brains exclusively express 4R isoforms [30,32,48] (Table 1.1).

Tauopathy

While highly phosphorylated 3R fetal tau is functional and necessary for neurite outgrowth, improper phosphorylation in the adult CNS coincides with neuronal malfunction. Hyperphosphorylated tau in the adult brain destabilizes neuronal MTs with

established cytoskeletons. Phosphorylation, particularly within the MTB and PR domains is associated with decreased MT polymerization, enhanced tau self-aggregation [41-43,45], and NFT formation [49]. Upon acquiring heavy phosphorylation [50] and conformational changes [51], tau mislocalizes from axons to the somatodendritic compartment [52-55]. Destabilized MTs and insoluble tau aggregates disrupt cell trafficking and coincide with neuronal death [56]. Neurodegenerative dementing diseases arising from these tau-misprocessing events are termed tauopathies. Many tauopathy inducing mutations cluster around the MTB domain. These mutations induce tau pathology either by altering the splicing pattern which affects the 3R:4R tau isoform ratio, or by altering tau's ability to interact with MTs [57].

In physiologic conditions tau is a highly soluble protein with an undefined secondary structure appearing as a random coil [42,58]. In tauopathy patient brains, however, hyperphosphorylated tau forms oligomers of helically twisted ribbon structures with regular periodicity referred to as paired helical filaments (PHF) [59,60]. PHF-tau, originally referred to as A68, was identified as an antigen recognized by the Alz50 antibody, a monoclonal antibody raised against pooled Alzheimer's brain tissue. The Alz50 specific antigen was highly concentrated in AD brains compared to controls, and purification revealed a single protein with a molecular weight of 68 kDa (A68) [61]. A68 reacted to many anti-tau antibodies and sequencing revealed that it was tau protein [62,63]. It curiously displayed a much higher molecular weight than previously characterized tau [64], and some antibodies revealed a triplet of proteins with electrophoretic mobility different from normal brain tau [65]. Later experiments

determined that the electrophoretic mobility and solubility differences between normal tau and A68, now termed PHF-tau [66], were largely due to phosphorylation [67-73]. The three distinct bands represented different hyperphosphorylated isoforms; when treated with phosphatase, PHF-tau migrated with normal tau and became immunoreactive to Tau1 [64,69], an antibody that recognizes unphosphorylated tau residues Ser^{199}/Ser^{202} [74,75].

PHFs are comprised of PHF-tau and neurofilament proteins with an external pronase-sensitive fuzzy region and a pronase-resistant double-helical stacked core twisted into a left-handed ribbon-like structure [76,77]. The PHF core is comprised specifically of tau's repeat region [62,78]. PHFs form dense aggregates that develop into mature NFTs. The distribution and density of NFTs correlate well with disease severity [8,56] (Figure 1.2).

Mouse Models

The pathways and mechanisms of tauopathies are not completely characterized, but transgenic mice have significantly increased our understanding of tau's physiologic function as well as pathogenic properties. Transgenic mice engineered to express familial tauopathy mutant MAPT variants develop pathology similar to that seen in human disease. A cytosine-to-thymine mutation coding for a leucine instead of wild type proline at MAPT's amino acid 301, P301L, was found in two families with the tauopathy, frontotemporal dementia (FTD) [79,80]. The mutation disrupts a highly conserved region within the MTB domain of exon 10 therefore only affects 4R tau (adult) isoforms. Several transgenic mouse lines have been generated to study this mutation. The first

mouse model was engineered to express 4R0N-tau$_{P301L}$ throughout the CNS (brain and spinal cord) using the mouse prion promoter [23]. These mice developed motor disturbances with 50% reduced spinal cord motor neurons by 10 months of age. The motor impairment affected the mice before brain pathology could fully develop, which prevented memory testing, and necessitated other transgene expression strategies.

The calcium calmodulin kinase (CK) IIα promoter systems restrict expression to the forebrain [81-83] the region affected in human FTD [84,85]. The same 4R0N-tau$_{P301L}$ transgene was engineered into a regulatable system, which allowed for transgene suppression by the administration of doxycycline (Figure 1.3). These mice, rTg(tau$_{P301L}$)4510, were generated using a bigenic system of responder and activator transgenes [84,85]. The responder mouse line carried the modified human tau 4R0N DNA sequence downstream of a tetracycline-operon responsive element (TRE). A second mouse line carried the activator transgene consisting of the tetracycline-controlled transactivator open reading frame [86] downstream of the CKIIα promoter [81], restricting mRNA [83] and protein [82] expression to forebrain neurons. In principle, neither the activator nor responder mouse line can express transgenic human tau. To achieve transgene expression the tet-transactivator (tTA) protein, driven by CKIIα, must bind to the TRE upstream of the human tau transgene. Crossing the activator and responder mouse lines generated offspring containing both the CK-tTA activator and TRE responder transgenes. Only these mice overexpressed human tau$_{P301L}$ at a level 13-fold over endogenous mouse tau [85].

rTg(tau_{P301L})4510 mice developed biochemical, histological, and cognitive decline similar to that seen in human disease. The rTg(tau_{P301L})4510 mouse line has been well-characterized and pathology occurs through tau misprocessing events that follow Braak staging in human patients: transentorhinal cortical cells develop pathology prior to hippocampal cells. The development of numerous antibodies [87] that recognize specific phosphorylated epitopes allowed the characterization of disease progression in rTg(tau_{P301L})4510 mice. Phosphorylation of specific PR domain residues and conformational alterations occurred early in disease, referred to as "pre-tangle" phenotypes [51], and were followed by MTB domain and C-terminal residue phosphorylation, tau mislocalization to the somatodendritic compartment, and sarkosyl insoluble NFTs [84]. NFTs were visualized histologically with silver staining methods, or as a sarkosyl-insoluble higher molecular weight fraction with slower electrophoretic mobility immunoreactive to numerous phospho-tau antibodies [84,88].

Though the hyperphosphorylation pathway has been well characterized from 2.5 months of age and beyond [84], phosphorylation of the immature CNS has not yet been explored but likely would provide important information for early stages of tauopathy. Inappropriate tau phosphorylation during development can cause neurological abnormalities. Transgenic mice with disruptions in the developmental cortical migration Reelin/Dab1 pathway develop excessive phosphorylation at epitopes classically phosphorylated during cortical development as well as hyperphosphorylation of residues that typically remain unphosphorylated [89-92]. These events cause severe neurological impairments due to improper migration of cortical neurons in the developing cerebral

cortex. Other tauopathy mouse models display hypophosphorylated tau during development and early adulthood [93,94] but go on to develop tauopathy later in life. A better understanding of developmental phosphorylation in tauopathy models may provide important insight into disease pathogenesis

For over a decade a prevalent hypothesis has maintained that tau hyperphosphorylation and NFTs are the proximal cause of neuronal death in tauopathy [95,96]. Interestingly, at about the same time a computer simulation suggested an entirely different paradigm. A computer program designed to model NFT formation and CA1 neuronal degeneration proposed that CA1 hippocampal neurons may survive approximately 20 years with NFTs, and that NFTs may not signify inevitable neuronal death [97]. Recent data, largely gathered with the rTg(tau_{P301L})4510 mouse model, support the computer model. Pre-tangles coincident with neuron loss and cognitive decline occurred as early as 2.5 months in rTg(tau_{P301L})4510 mice; however transgene suppression with doxycycline treatment resulted in a recovery of memory function and stabilized neuron numbers in spite of continued NFT accumulation [85]. While the quantity of NFTs correlates with disease severity in human patients [8,56], increasing evidence suggests dissociation between NFT and neuronal death [98-100]. The growing body of evidence implicates other cellular phenomenon, such as caspase activation [99], and not NFTs as the degenerative agent.

Caspases, cysteine proteases traditionally recognized for their apoptotic role, cleave tau at aspartate 421 [101,102]. This truncated tau species reportedly changes conformation, assembles rapidly [101,102], co-localizes with tangles, and correlates with

degenerating neurons [99,103,104]. Neurons in rTg(tau_{P301L})4510 mice developed caspase activation hours to days prior to developing NFTs; after tangles formed, caspase activity was suppressed and the neurons seemed to survive indefinitely [99] as proposed by the computer model [97]. Cells that displayed caspase activation without forming NFTs died suggesting that NFT formation may occur through a separate, but simultaneous, pathway as neurodegeneration. The NFT containing cells may represent cells surviving a potential lethal insult. Perhaps only a subset of neurons is susceptible to caspase-induced death while others cope by forming NFTs.

While tau hyperphosphorylation remains a tauopathy hallmark, tau-associated neuronal loss can occur in its absence, resulting in the emergence of other hypotheses. Several disease-causing mutant tau variants are less phosphorylated than tau_{wt} in young mice of other tauopathy mouse models [93,94,105]. Transgenic mice that expressed pseudohyperphosphorylated tau, a tau variant that mimics constitutively phosphorylated tau with serine and threonine residues replaced by glutamate [106], did not develop tau aggregates, neuronal loss, or behavioral abnormalities [107]. In contrast, the tau_{R406W} tau variant remained hypophosphorylated in aged mice. The hypophosphorylation mutants developed age-dependent tau aggregates [108] and memory and behavioral abnormalities [109]. These data suggest that while tau misprocessing is a common theme, hyperphosphorylation may not be required for later neurodegeneration.

Mutations may carry out their effect instead by increasing the propensity for β-sheet formation [110,111]. The MTB domain repeat regions 2 and 3 (R2 and R3 Figure 1.1) contain hexapeptide motifs that are responsible for β-structure formation and

enhanced aggregation potential [110]. Tau protein digested to contain these motifs alone was sufficient for structural changes that caused tau to dissociate from MTs, aggregate, and lose solubility [110].

Beta-sheet conformation and aggregation, not hyperphosphorylation were sufficient for mice to develop tauopathy [112]. *In vitro* aggregation studies demonstrated that tau harboring the ΔK280, deletion of lysine at amino acid 280, developed a β-sheet conformation with enhanced aggregation properties [110,113]. Mice engineered to express ΔK280 developed hyperphosphorylated, conformationally altered tau that mislocalized to the synaptodendritic compartment, which coincided with reduced spine synapses [112]. "Anti-aggregation" mice were engineered to express the same mutant ΔK280 isoform with additional genetic modifications to prevent β-sheet formation. Proline encoding mutations introduced into the hexapeptide motifs inhibited tau β-structure [110]. "Anti-aggregation" mice developed hyperphosphorylated tau that mislocalized, but synaptic integrity remained. These data suggest that overexpressed tau is sufficient for hyperphosphorylation and mislocalization, but conformational changes may be necessary for neuronal insult.

An important factor to consider with mouse models is transgene expression level. When tau_{P301L} was knocked-in to the endogenous mouse tau gene, therefore expressed at endogenous levels, mice did not develop tau pathology [105]. In contrast to the rTg(tau_{P301L})4510 model overexpressing human tau_{P301L} that developed age-associated hyperphosphorylated tau, the tau_{P301L} knock-ins displayed hypophosphorylated tau with reduced MT-binding and age-dependent changes in axonal transport of mitochondria with

hyperactivity [105] emphasizing the importance of gene dosage/protein level in mouse-modeled tauopathy.

Wild Type Tau Overexpressors. The generation of transgenic mice overexpressing wild type tau isoforms has helped dissociate tau overexpression from mutant tau effects. As a human tau overexpressor control for rTg(tau_{P301L})4510 mouse model, the rTg(tau_{wt})21221 mouse model was created [114]. The construct for the responder TRE-tau_{wt} transgene was identical to that of TRE-(tau_{P301L})4510 except for the lack of the mutation. When crossed to the CK-tTA activator mouse line, progeny that carried both transgenes, rTg(tau_{wt})21221, expressed wild-type 4R0N-tau at comparable levels and brain regions as tau_{P301L} in rTg(tau_{P301L})4510 mice. Unlike rTg(tau_{P301L})4510 mice, rTg(tau_{wt})21221 mice did not develop progressive memory deficits or neurodegeneration [114]; thorough phospho-tau characterization was not reported.

A separate series of transgenic mice were generated to compare overexpression of wild type human 4R2N-tau to endogenous levels of human 4R2N-tau, and overexpressed 4R2N-tau_{P301L} [93]. The neuronally expressed transgenes (thy-1 promoter) resulted in different phenotypes. Mice overexpressing mutant tau developed tauopathy. The wild type tau overexpressors developed axonal dilations and spheroids, a disparate condition termed axonopathy, accompanied by motor impairment in the absence of NFTs or neuronal loss. The mice expressing human 4R2N-tau at endogenous levels lived normally. Interestingly, transgenic tau from wild type overexpressors was more phosphorylated than tau from tau_{P301L}-expressing mice, but only tau_{P301L} changed conformation [93]. Their results suggest that while overexpression of wild type tau can

cause hyperphosphorylated tau and axonal disruptions, mutant tau is required to develop tauopathy.

Several other wild type tau overexpressing transgenic mice have been characterized; none have developed full tauopathy, but axonopathy is common [115-121]. Wild type tau overexpressors acquired somatodendritic tau mislocalization and "pre-tangle" pathology accompanied by axonal disruption in the absence of neurodegeneration. Tau 3R:4R isoform disruptions in human brains are sufficient to cause a subset of human tauopathies [30,122-125]. However, the introduction of 3R isoform expression into the adult mouse brain did not result in tauopathy as seen in human patients. Transgenic mice engineered to express the shortest tau isoform, either ubiquitously with the HMG-CoA reductase promoter [116] or restricted to the CNS with the Prnp promoter [126], developed hyperphosphorylated tau with NFTs but not neuronal loss. Likewise overexpression of the longest tau isoform 4R2N in neuronal cells with the thy-1 promoter [115,118,119], or using a PAC [120] caused phosphorylation of some epitopes and axonopathy, but not tauopathy. The same pre-tangle phenotypes occurred when the entire *Mapt* gene, driven by a BAC transgene, was overexpressed from its endogenous promoter [121] indicating that neither wild type human nor mouse tau overexpression initiates overt pathology despite early signs of tau phosphorylation.

Mapt Knock-Outs. Somewhat counterintuitive, while tau misprocessing and dysfunction coincides with human dementia, presumably through loss of function, tau ablation has not produced dramatic phenotypes in mouse models [127-130]. *Mapt* null, $Mapt^{0/0}$, mice develop and live normally with subtle, sometimes undetected, neurological

abnormalities. The overall unaffected existence of *Mapt*$^{0/0}$ mice likely stems from functional redundancy between tau and other MAPs. Map1b and tau work in concert to regulate microtubule organization necessary for proper axonal elongation and neuronal migration [131-133]. Synapse formation and neurite stabilization involves map1a [134,135].

One notable phenotype exhibited by *Mapt*$^{0/0}$ mice was increased spontaneous locomotor activity and muscle weakness [127]. Interestingly, tau$_{P301L}$ knock-in mice [105] also displayed hyperactivity in the absence of overt pathology suggesting that tau$_{P301L}$ acts similar to *Mapt* ablation. The motor phenotypes of *Mapt*$^{0/0}$ and tau$_{P301L}$ mice may be caused by MT disorganization in cerebellar cells. The cerebellum is a region of the brain involved in motor control. Small-caliber axons of the cerebellar parallel fibers displayed decreased MT stability and altered MT organization in *Mapt*$^{0/0}$ mice [128]. Unlike large-caliber axons that contain an abundance of other MAPs, small-caliber axons primarily express tau. Large-caliber *Mapt*$^{0/0}$ axons with elevated map1a were functionally identical to wild type axons, suggesting that MAP redundancy can overcome tau insult [128]. Without compensatory expression of other MAPs, cerebellar parallel fibers are likely more susceptible to tau ablation than other axons.

While *Mapt*$^{0/0}$ mice live normally, stressful environments may necessitate tau function [136]. Recent evidence indicates a tau-specific role in MT-dependent autophagy [136,137]. Niemann pick disease type c, NPC, is a tauopathy caused by mutations that affect intracellular lipid and cholesterol trafficking proteins. NPC patients and mouse models develop an increased autophagic response. The absence of tau-dependent MT

stability impaired the autophagic pathway and enhanced overall pathology in *Npc1/Mapt* double knockout mice to suggest a tau-specific role in autophagic trafficking [136].

Human wild type tau overexpressing mice develop neurodegeneration when expressed on a $Mapt^{0/0}$ background [138]. The increased pathology in the absence of endogenous tau impelled a hypothesis suggesting a resistance or inhibition of endogenous mouse tau to form AD-like tau pathology. The hypothesis was supported by enhanced pathology in a separate tauopathy model when transgenic tau was expressed on a $Mapt^{0/0}$ background [139]. However, the nucleotide and protein sequences of the largest tau isoform, 4R2N, are 83% and 88% identical, respectively, between mouse and humans with 98% identity in the MTB domains and the carboxyl terminus, the regions most implicated in tau pathogenicity [140] (Figure 1.4). Furthermore endogenous mouse tau has the capacity to become hyperphosphorylated and forms aggregates *in vitro* with ATP and kinases [141], in the presence of polyanions such as heparin [142,143]; and *in vivo* due to hypothermic body temperatures due to starvation [144,145], anesthesia [146], cold water stress [147] or hibernation [148-150]. These results provide evidence for pre-tangle phenotypes and argue against the mouse tau resistance hypothesis. An alternate explanation is that mice do not suffer from *Mapt* ablation unless tau-specific function is required, as seen in the Niemann pick mouse model [136], and in cerebellar parallel fibers [128].

It remains unclear how endogenous mouse tau would decrease pathology, and recent studies suggest that endogenous tau may instead become pathogenic. Misfolded tau may recruit or alter the conformation of endogenous tau and trigger it to adopt a

pathogenic form [88,151,152]. Ultrastructural analyses of NFTs have revealed that filament length, structure, and periodic twist differ among the diseases [153]. Tau fibrillization experiments have demonstrated that conformationally altered mutant tau species can induce wild type tau to modify its fibril structure [154]. The resulting wild type fibrils more closely resembled the conformation of the mutant tau fibrils than their native wild type structure. The recruitment of wild type tau into pathogenic fibrils could transform endogenous tau into a deleterious molecule by providing additional template to convert into pathogenic forms as seen with prion diseases [155].

To appropriately assess mouse-modeled human tauopathies, including AD, it is imperative to understand the effects of endogenous mouse tau on disease pathogenesis. While the absence of endogenous tau enhances pathology, it remains unclear if the presence of wild type tau alleviates disease severity by maintaining normal function, or inhibits pathogenic phosphorylation, misfolding, or aggregation. If so, the specificity of mouse tau needs to be explored; other wild type tau proteins may have the same effect. These subjects warrant further investigation.

While mice have greatly enhanced our understanding of tauopathy, differences due to mouse genetic background, species differences between mice and humans, the vast number of patients that develop sporadic disease, and our inability to recreate Aβ-induced tauopathy has left many questions unanswered. The overall failure to recapitulate mouse-modeled AD necessitates the need for more appropriate models to study disease. Recently stem cell models have gained momentum in this area of research.

Stem Cells

In 1906 Russian histologist Alexander Maksimov proposed the idea that a single cell, a "stem cell (SC)," could give rise to all types of blood cells. He postulated that all blood cells had a common origin and that the surrounding environment (i.e. bone marrow stroma) provided local cues to induce differentiation [156]. Though not an embraced idea at the time, over half-century later the SC dogma gained momentum [157-159] and today they have seemingly endless potential and are hot topics of scientific and popular culture.

All SCs possess two inherent qualities: self-renewal and ability to differentiate into multiple cell types, however not all SCs are the same. The most primitive and versatile SCs are zygotic cells created by the fusion of germ cells. These first cells are capable of becoming all cell types of an organism; this potential is called totipotency. Totipotent SCs can develop into the three primary germ layers (ectoderm, mesoderm, endoderm) and they can form extra-embryonic tissue. Totipotency does not last long. After a phase of rapid cell division the embryo emerges as a dense ball of cells called the morula. Each of the moruli is pluripotent. They can form cells of the three primary germ layers, but have lost their capability to develop extra-embryonic tissue. The morula matures to the next stage of development called the blastocyst. At this stage the embryo begins to fill with fluid, which forces the cells to cluster into a tight mass called the inner cell mass (ICM). These "embryonic stem (ES) cells" are genetically identical and pluripotent [160,161]. As the developing organism continues to mature and form cell types with specific function, cell potency becomes increasingly limited.

Adult tissues contain multipotent progenitor cells, often called adult SCs, with limited differentiation potential restricted to cell types of their organ lineage. Adult SCs replenish their tissue's dying or damaged cells by activating regeneration pathways in response to injury [162,163]. This innate ability to regenerate and restore has made SCs popular targets of therapeutic investigation in areas such as transplantation and drug discovery/delivery [164]. A different application has recently emerged, their use as model systems to study disease pathogenesis. Our current understanding of disease mechanisms largely depends on postmortem tissue samples and surrogate model systems. While such studies have led to key understandings of many biological processes, postmortem tissues are snapshots of end stage disease, and species differences often prevent recapitulation of important disease pathology in animal models. SCs may provide clues to disease mechanisms unattainable with other systems. They represent the most primitive developmental state and can differentiate into mature cells. With a single culture system, one can investigate how external factors influence immature cells, cellular development, and mature cell types.

Mouse Stem Cell Disease Models

The use of SCs to study disease requires either their harvest from an affected individual, or introduction of genetic material into normal SCs. Both strategies were first tested using mouse material. The first attempts to explore neurodegenerative disease-specific SC models evolved from genetically engineering mouse ES cells designed to mimic Parkinson's disease (PD) [165] and amyotrophic lateral sclerosis (ALS) [166].

Parkinson's Disease Mouse ES Cell Model. The degeneration of a specific subset of brain cells, the dopaminergic substantia nigra neurons of the midbrain, causes motor impairments in PD patients. Like AD, the vast majority of PD patients do not have a defining genetic component. While the discovery of genes linked to familial forms have provided insight into pathogenesis, transgenic mice expressing these mutant genes fail to recapitulate key disease phenotypes [167-171]. In attempt to create an *in vitro* model that recapitulated neuronal loss of PD, the DJ-1 gene associated with familial PD [172] was retrovirally knocked out of a mouse ES model [165]. DJ-1 encodes a broadly expressed protein [173] believed to have a role in the cellular oxidative stress response, a pathway common to many diseases. Upon culture and differentiation of the DJ-1 knock-out ES cell line, dopaminergic neurons had a heightened susceptibility to oxidative stress. With the genetically modified ES cell line the previously unknown molecular function of DJ-1 was determined to be a redox-sensitive molecular chaperone [174].

Amyotrophic Lateral Sclerosis Mouse ES Cell Model. The same experimental approach was applied to study ALS, commonly referred to as Lou Gehrig's disease. ALS is a fatal disease that specifically targets motor neurons causing progressive paralysis and death [175]. Superoxide dismutase-1 (SOD1) mutations are responsible for 20% of autosomal dominant familial ALS. ES cells from mice carrying either a normal or mutant human SOD1 gene were cultured. While both control and ALS-mutant ES cells differentiated into motor neurons with similar efficiency and proportions, with time ALS-mutant motor neurons developed signs of distress including SOD1 protein mislocalization, ubiquitination, and activation of cell death markers [166]. Interesting

differences were observed when motor neurons were co-cultured with glia derived from either normal or mutant SOD1 mice. Neurons from either genotype could be maintained in long-term culture when co-cultured with glia expressing wild type SOD1, but glial cells from SOD1 mutant mice induced neurodegeneration of motor neurons in both wild type or mutant human SOD1 motor neurons. Their results therefore implicated glia as a neurodegenerative agent for ALS and introduced a new avenue of research.

Human Stem Cell Disease Models

While genetically engineered SCs may provide useful information, introducing a single gene mutation does not mimic diseases that have multiple, or unknown, genetic components. Obtaining patient-specific sources would provide insight into disease pathways that arise from complex mechanisms involving multiple genes. The development of somatic cell nuclear transfer (SCNT) and reprogramming techniques helped make this possible.

SCNT involves transferring the nucleus of a mature somatic cell to a de-nucleated oocyte or ES cell. In doing so the genetic material of the adult is maintained, while the extranuclear material maintains the cell's immature cell state and ability to self propagate. This methodology is applicable to mammalian cells [176] and saw the emergence of live mammalian offspring with an established cell line [177], "Dolly" the sheep with adult cells and a de-nucleated oocyte [178], and adult cells fused with ES cells [179,180].

The ability of a denucleated oocyte or ES cell to maintain SC properties with a nucleus from a differentiated cell suggested that these cells possess factors able to

convert somatic cells into a less defined cell state. To investigate the hypothesis, genes known for their importance in maintaining pluripotency in ES cells and embryos, and genes responsible for rapid proliferation in tumors were tested for their ability to revert differentiated fibroblasts to an undifferentiated state, and maintain self-renewal and pluripotency [181]. Through an elaborate antibiotic resistance screening method, 24 candidate genes were tested for their ability to reprogram fibroblasts to SCs. The candidate genes were introduced by retroviral transduction. Fibroblasts that received all 24 factors displayed ES cell phenotypes. Single factors were then slowly removed from the screen until 4 necessary factors: c-Myc, Oct3/4, SOX2, and Klf4 remained. This was the first established induced pluripotent stem **(**iPS) cell line from mouse embryonic fibroblasts. Later the method was successfully repeated with adult human fibroblasts [182]. The iPS cells were comparable to ES cells in morphology, proliferation rates, and differentiation potential as evidenced by teratoma formation [183]. While the first iPS cells differed from ES cells in their global gene expression patterns, and germline transmission was unsuccessful [181], eventually adult chimera mice were produced [184-186] demonstrating the full conversion to an early ES cell state.

Reports of human PD and ALS-specific iPS cell lines followed and dissipated concerns regarding patient age on reprogramming ability. Fibroblasts from five PD patients between the ages of 53-85 were reprogrammed with OCT4, SOX2, KLF4, plus or minus c-MYC [187,188]. All iPS cell lines were stably maintained for over 30 passages. Directed differentiation produced dopaminergic cells providing a patient-specific substrate for investigating mechanisms of PD. Skin fibroblasts from elderly

sisters, 82 and 89, with familial mutant SOD1 were successfully reprogrammed and differentiated into motor neurons and glia [189] providing a source of cells to study the mechanisms of motor neuron death in ALS. These studies validated the principle and methodology, and recently disease mechanisms and drug trials are starting to be incorporated into SCs studies.

Spinal Muscular Atrophy Human iPS Cell Line. Spinal muscular atrophy (SMA) is an autosomal recessive neurological disorder characterized by motor neuron degeneration and progressive muscle atrophy [190]. Mutations in the survival motor neuron 1 gene (SMN1) decrease full-length SMN protein expression [191,192], which results in selective degeneration of lower α-motor neurons [193]. The clinical spectrum of SMA ranges from early infant death to normal adult life with only mild weakness. Studies on patient fibroblasts are common to the field; however, fibroblasts are not useful to understand vulnerability of motor neurons. Using patient fibroblasts and iPS methodology with OCT4, SOX2, NANOG and LIN28, a patient-specific SMA line was developed [194]. iPS cells from the patient had decreased full-length SMA transcript compared to the patient's mother, the unaffected control. Both cultures differentiated into neurons with similar proportions. However, the SMA culture had fewer and smaller motor neurons after long-term culture. In healthy individuals, SMN protein is found in the cytoplasm and nuclear aggregate structures called "gems". Gem number and disease severity are inversely correlated [192]. SMA iPS cells displayed a lack of nuclear gems while control iPS cells contained normal gem levels. A potential treatment avenue for SMA patients is to increase the concentration of nuclear gems. Using two compounds

known to increase SMN protein levels, cultures derived from the SMA patient developed a significant increase in SMA gems in response to treatment [194].

Familial Dysautonomia Human iPS Cell Line. Familial dysautonomia (FD) is a hereditary sensory and autonomic neuropathy due to incomplete development and the progressive loss of unmyelinated sensory and autonomic neurons [195-197]. The resulting autonomic nervous system dysfunction causes a wide array of symptoms and lethality. Most patients carry a mutant IkB kinase complex-associated protein (IKBKAP) gene. The mutation causes a tissue-specific skipping of exon 20 resulting in a truncated protein, and low levels of normal protein synthesis [198]. iPS cells were derived from three FD patients and studied for gene and protein levels [199]. They saw tissue-specific mis-splicing of IKBKAP in the patient-specific iPS cells. Specifically, neural crest precursor cells expressed low levels of normal IKBKAP transcript. FD-iPS cells displayed a decreased rate of neurogenesis, and upon differentiation defects in migration were noticed. Three potential drug candidates were tested for their ability to reverse aberrant splicing, and improve neurogenesis and migration defects. One of the three drugs reduced the proportion of the mutant splice variant by increasing the normal IKBKAP level; the effect was specific to the mutant FD-iPS cell line as the level of normal transcript remained unaltered in control iPS cells. Low dose treatments were sufficient to increase normal IKBKAP expression levels, but continuous drug treatment was required to enhance neurogenesis. Drug treatment failed to improve neuronal migration defects.

Fragile X Mental Retardation Human ES Cell Line. Mutations in the fragile X mental retardation 1 (FMR1) gene blocks production of the FMR protein resulting in mental retardation [200-205]. Mouse models carrying mutant FMRI genes have not revealed the molecular processes of pathogenesis; however, a fragile X-specific ES cell line was discovered through genetic screening of pre-implantation embryos [206]. Studies on the human ES cell line carrying the genetic mutation for fragile X syndrome revealed that the mutated FMR1 gene functions normally until differentiation. Upon differentiation the levels of FMR1 mRNA and FMR protein decreased, recapitulating the phenotype of diseased individuals. The silencing mutation was caused by a post-translational methylation event. The protein involved in genetic silencing was unmethylated in undifferentiated SCs and then methylated upon differentiation causing condensed chromatin in the region of the FMR1 gene preventing its transcription. This model demonstrated the value of SCs models in uncovering biological events that occur early prior to, during, or after differentiation.

While SCs show great promise in expanding our knowledge of disease mechanisms and drug screening, harvesting ICM cells destroys a developing embryo making the issue ethically questionable. Inducing differentiated cells to a less committed state using growth factors is a far less controversial methodology; however the presence of viral vectors used to deliver the transcription factors can induce oncogenes [186,207]. Genetic engineering to splice out the transgenic DNA after induction is being conducted to elucidate small molecules that could replace the transcription factors [208]. Initial

experiments using transient transfection or adenoviral infection to deliver reprogramming factors to mouse somatic cells yield low efficiency and require further study [208].

Adult Neural Stem Cells—Neurospheres

An alternate approach is to harvest SC from adult tissues. Adult SCs can self renew, but have a more defined differentiation potential; their fate is restricted to cell types of their host organ. The use of adult progenitor cells is limited to organs with easily accessible sources of SCs. The nose contains a peripherally available pool of neural SCs [209,210]. The organ of smell, the olfactory mucosa, is a neural tissue containing neural SCs that continually replenish olfactory sensory neurons throughout life [211,212]. Culturing neural SCs from patients provides the opportunity to study neurological disorders.

The *in vitro* culture of neural SCs began twenty years ago, and while different techniques have emerged, the original neurosphere method remains a standard. Neurospheres made their debut when dissected, dissociated, adult and embryonic mouse brain tissue detached from the culture plate and developed into free-floating balls of cells exposing a perpetual neural SC culture system [213,214]. Initially upon culture, many individual cells adhered to the culture plate and within the first two days nearly all had died. The small percent of surviving cells underwent cell division for 2-3 days then detached and formed spheres with proliferative capacity and nestin, an intermediate filament found in neuroepithelial SCs, expression. Additional characterization of neurospheres revealed cell type heterogeneity. The multi-cellular aggregates contained

CNS-SCs, lineage-committed, and differentiated cells [215-217]. Differentiated cells arose due to the lack of growth factor exposure by cells deep in the neurosphere center.

Neurosphere Characteristics. The free-floating nature of the culture is permissive to cell-cell interactions. Individual cells within the neurospheres are tightly bound, and once merged, the rich surrounding extra-cellular matrix (ECM) keeps the neurosphere compact [217-219]. Minor disruption caused by handling the culture flask during routine maintenance increases the likelihood of cellular contact, aggregation and resultant sphere merging [220,221]. However even untouched cultures develop merged spheres. Time-lapse imaging has revealed motile cells with spontaneous locomotion and the combining of more than one neurosphere [222,223] especially in high-density culture conditions [221,222].

Though a heterogeneous cell population, clonality can be achieved by plating cells at very low densities (0.2-20 cells/μL) or culturing single cells [221,224,225]. The caveat of low plating densities is that sphere-forming efficiency significantly decreases due to the lack of autocrine/paracrine signals from other cells. However, if strict plating method densities are not followed, clonality is lost due to spontaneous locomotion and sphere merging. Plating neurospheres as adherent cultures, or in semi-solid matrices [226,227] circumvents these issues and decreases the differentiation that occurs in the center of large spheres [228,229].

Original experiments described neurosphere proliferation in chemically defined serum-free medium supplemented with EGF but not with other mitogenic factors [213,214], likely due their high expression of EGF-receptors [217]. Exposure to serum or

an adherent substrate inhibited proliferation. Plating mature spheres on coated substrates resulted in mass cellular migration from the center of the sphere. The migrating cells acquired morphologies and protein expression of neurons and glia. Further experiments revealed directed differentiation by growth factor withdrawal, serum addition, exposure to adhesive substrates [214], and addition of specific neurotrophins [230,231].

To achieve reliable reproducible results, strict adherence to methodology is necessary. However, once established, the neurosphere culture system provides a robust assay for studying effects of external factors on the development and differentiation of the CNS, and the genetic susceptibility to neurological disorders. They are appealing *in vitro* models for several reasons: they generate large quantities of genetically identical cells required for statistically relevant results; their genes are identical to host of origin allowing for investigation of disorders involving complex genetic pathways; they remain euploid; they proliferate in long-term culture, which may be important for slowly progressing neurodegenerative diseases; molecular biological techniques that are difficult to apply to whole animal models can be utilized *in vitro* as a means to screen small molecules and potential drugs; they begin as immature cells types yet have the capacity to differentiate into neurons or glia [213,215] allowing for the effects of transgene expression on differentiation, cell fate, and post-differentiation cell viability to be explored. They can be harvested from patients with complex genetic diseases thereby avoiding the need for genetic reprogramming.

Recently, adult mouse neural SCs have been used to generate iPS cells [232]. The expression of Oct3/4 alone reprogrammed neural SCs to a less defined ES state that

yielded adult chimeric mice. Accessible adult neural SCs may provide a template for the generation of iPS cells in humans to study diseases affecting various organ systems.

Patient-Derived Human Neurospheres. Recently neurosphere cultures have been generated from human patients [233]. Cells isolated from the olfactory mucosa contain neural SCs. This organ is affected in numerous diseases, resulting in a common symptom smell loss [210,234-237], indicating that these cells may provide disease-specific alterations. Olfactory mucosa biopsies obtained from patients with the neurodevelopmental psychiatric disorder, schizophrenia, or PD were cultured as neurospheres. They were compared to skin fibroblasts from the same patients and neurospheres and fibroblasts derived from unaffected individuals. Disease-specific protein expression and cell function differences were noted including dysregulated neurodevelopmental cell proliferation, neurogenesis, and cell adhesion pathways in schizophrenia and dysregulated mitochondrial function, xenobiotic metabolism, and oxidative stress in PD. The respective fibroblasts controls failed to show differences in these pathways.

With the emergence of numerous SC methodologies, there is a great need to understand the potential and limitations of the system. Specifically SC cultures need to be directly characterized against their *in vivo* counterparts to fully understand their usefulness. While preliminary studies have demonstrated proof-of-principal, more thorough analyses are necessary.

Thesis Objectives

Overview

Mutations in genes that affect amyloid precursor protein (APP) misprocessing cause Alzheimer's disease (AD) in human patients. AD-causing APP mutations directly affect APP processing to produce an excess of Aβ, a proteolytic cleavage fragment of the APP holoprotein. Aβ monomers aggregate to form senile plaques, a major hallmark of AD. Concurrently, neurofibrillary tangles (NFTs) comprised of misprocessed tau protein accumulate. These findings led to the Aβ hypothesis which suggests that elevated Aβ induces tau pathology, and is sufficient to cause AD. However, transgenic mice that express human gene variants that cause AD develop Aβ plaques and synaptic loss, but fail to develop significant tau pathology and neurodegeneration. While human AD patients carry wild type tau genes, modeling tau pathology in mice requires overexpression of abnormal human tau isoforms. The incongruities between human patients and transgenic mice spawned the hypothesis that mouse tau resists or inhibits tau misprocessing. To explore this hypothesis we will exploit the rTg(tau_{P301L})4510 mouse model of a related disease, frontotemporal dementia (FTD), and the recently created rTg(tau_{wt})21221 mice that express wild type human tau (tau_{wt}) at the same level and in the same brain region as rTg(tau_{P301L})4510.

A recent interest in patient-specific stem cell (SC) lines to study disease has emerged. SC lines that capture the genetics of disease susceptibility may be useful to study disease pathogenesis. The potential utility of SC-based systems has seen the development of several methodologies including the harvest of central nervous system

stem cell (CNS-SC)-containing neurospheres from human patients. Such studies necessitate the need to critically evaluate the culture system's relevance to appropriately recapitulate *in vivo* phenotypes and yield reproducible robust results. We will compare tau-associated phenotypes between rTg(tau_{P301L})4510 and rTg(tau_{wt})21221 adult mice and their neurosphere derivatives to directly assess the ability of SCs to maintain genotype-specific characteristics over extended cultures periods.

Specific Aims

Aim 1. Test the hypothesis that expression of endogenous mouse tau affects transgene-encoded human tau phosphorylation and NFT formation. The poor understanding of endogenous mouse tau's influence on tauopathy may affect our ability to appropriately model tau-associated human diseases. Here we will study the resistance or inhibition of endogenous mouse tau on tau-associated pathology. We will utilize a mouse model that develops well-characterized age associated tau pathology, rTg(tau_{P301L})4510, and rTg(tau_{wt})21221 mice as human tau overexpression controls. Both human tau_{wt} and human tau_{P301L} transgenes will be bred onto mouse tau null genetic backgrounds. To comprehensively examine the effects of wild type tau, mouse or human, on tau_{P301L}-pathology, we will compare tau phosphorylation and neurodegeneration in mice that express either, or both, tau_{wt} and the FTD tau_{P301L} mutation with or without mouse tau. A time course of biochemical and histological features will be monitored in aging mice. Experiments comparing rTg(tau_{wt})21221 mice with rTg(tau_{P301L})4510 mice will indicate whether all tau phosphorylation events are mutation specific, or might be due to human transgene overexpression. Comparing rTg(tau_{P301L})4510 mice that

concurrently express wild type tau, human or mouse, will help dissociate general wild type tau effects from species-specific effects of endogenous mouse tau.

Aim 2. Test the utility of mouse CNS-SC containing neurosphere cultures derived from mice expressing FTD-mutant tau to recapitulate mutation-specific tau phosphorylation observed in mice. To assess their utility for studying heritable neurodegenerative disease, CNS-SC containing neurosphere cultures will be established from rTg(tau_{P301L})4510 mice, and compared to neurospheres generated from rTg(tau_{wt})21221 mice. Transgene expression levels will be tracked and compared over time using immunofluorescence (IFA) intensity and Western blot densitometry. Mutation-specific changes in tau misprocessing as well as other neurosphere phenotypes with potential relevance to disease will be explored. Results from proliferation rate and differentiation experiments will determine whether mutant transgene expression affects inherent SC properties. Appearance of specific tau phosphorylation epitopes will be tracked in both neurospheres and differentiated mature CNS cells and compared to changes observed in the mice. Differentiated neuronal cells will be investigated for mutation-specific differences in neuron numbers, transgenic protein localization, and filopodia-spine density. The effects of endogenous mouse tau will be evaluated by comparing all results to neurosphere cultures that express human tau, but lack mouse tau.

Figure 1.1: Cartoon of the Longest Tau Isoform, 4R2N.
The longest tau isoform (4R2N) contains exons 2 and 3 which code for the N-terminal inserts, N1 and N2, and exon 10, which encodes for an additional MT binding domain, R2. 441: amino acid length. Alternative spicing of exons 2, 3, and 10 yield the six isoforms expressed by mice and humans. PRD: proline rich domain.

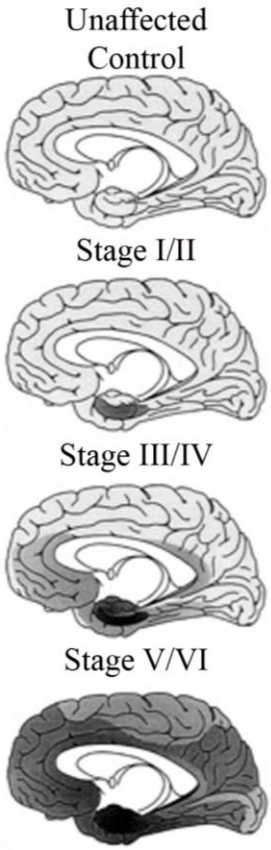

Transentorhinal Stages: Temporal Lobe NFTs
Cognitively normal
No brain atrophy

Limbic Stages: Temporal Lobe + Hippocampal NFTs
Noticeable personality changes and cognitive impairments
No brain atrophy

Neocortical Stages: Temporal + Hippocampal + Neocortical NFTs
Moderate to severe dementia and cognitive impairment
Severe neocortical destruction
Apparent brain atrophy

Figure 1.2: Braak Stages of NFT Progression.

During the earliest stages, Braak stage I/II, specific projection cells within the brain's memory relay between cortical and hippocampal cells, the transentorhinal region, begin developing pathology. Patients with these changes do not display clinical signs and may be unremarkable for decades, but the changes are irreversible and will progress to later stages. The transition into stages III/IV is marked by hippocampal and temporal neocortical cell pathology. Patients start to experience memory impairment due to increasing neuronal death. Patients in Braak stages V/VI experience significant memory and cognitive impairment with mild dementia. Brain atrophy occurs during these stages which correlates with prominent NFT load and neuronal loss. Patients diagnosed at Braak stage V exhibit moderate to severe dementia. All patients reaching Braak stage VI suffer with severe dementia and are unable to care for themselves due to extensive neuronal death.

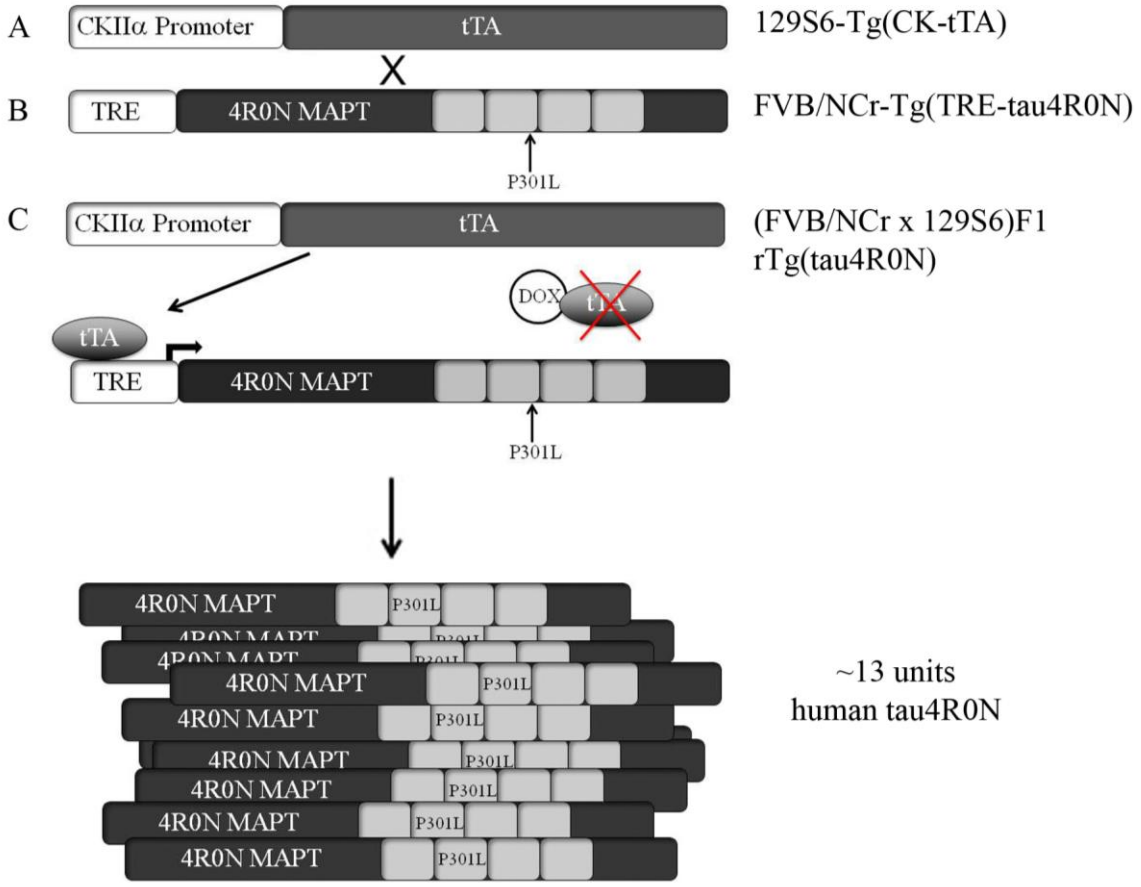

Figure 1.3: Regulatable Bigenic Transgene System to Drive Tau 4R0N.
Regulatable Tg(tau_{P301L})4510 [rTg(tau_{P301L})4510] mice were generated using a bigenic system of activator and responder transgenes. (A) The activator mouse line carried a tet-transactivator transgene driven by the forebrain specific CKIIα promoter, Tg(CK-tTA). Tg(CK-tTA) mice were maintained hemizygous on a126S6 genetic background. (B) The responder mouse line carried human tau4R0N downstream of the tet-responsive element (TRE), Tg(TRE-tau4R0N). Tg(TRE-tau4R0N) mice were maintained hemizygous on an FVB/NCr genetic background. (C) Transgene expressing rTg(tau4R0N)4510 F1 hybrid mice were produced by crossing the activator and responder mouse lines. Forebrain driven tTA protein binds the TRE to induce transgene expression. Transgene expression is regulatable and can be suppressed by the administered of doxycycline (DOX), which binds tTA and prevents it from interacting with the TRE.

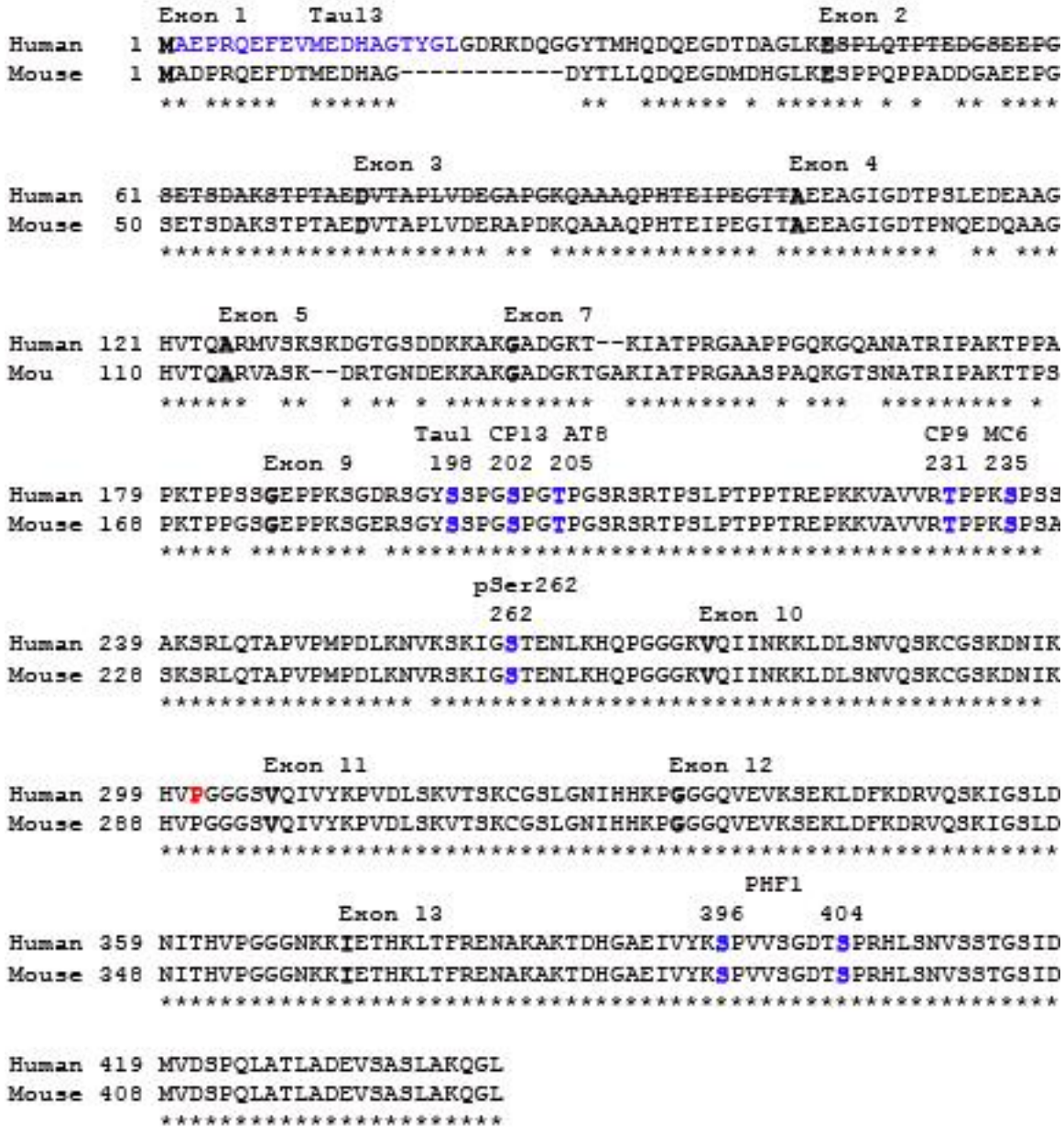

Figure 1.4: Mouse and Human Tau Protein Alignment.
The longest tau isoform, 4R2N, is 88% identical between mouse and human. Exons 2 and 3 are spliced out of the 4R0N isoform expressed in rTg(tau_{P301L})4510 mice. *: Identical amino acids, -: gap between species; blue: antibody recognition epitopes; red: P301L mutation; bold: exon border; strikethrough: exons spliced in the 4R0N tau isoform.

Table 1.1: Tau Isoform and Phosphorylation Levels Are Developmentally Regulated.

	Mouse	Human
Fetal Brain	Heavily phosphorylated 3R isoforms[238]	Heavily phosphorylated 3R isoforms 7 moles phosphate/mole tau protein [47]
Adult Brain	Non phosphorylated 4R isoforms [32,48,239]	Non phosphorylated 3R and 4R isoforms; 1:1 ratio 1 mole phosphate per mole tau protein [72,240]
AD Brain	N/A	Heavily phosphorylated 3R and 4R isoforms 8 mole phosphate per mole tau protein [72,240]

THE PRESENCE OF WILD TYPE TAU, MOUSE OR HUMAN, DECREASED PATHOLOGY IN THE rTg(tau_{P301L})4510 FRONTOTEMPORAL DEMENTIA MOUSE MODEL

Introduction

Alzheimer's disease (AD) patient brains contain senile plaques comprised of Aβ proteins and neurofibrillary tangles (NFTs) comprised of tau proteins. These protein aggregates are associated with neuronal death, brain atrophy, and dementia. Specifically, NFT density correlates with disease severity. Genes coding for Aβ and tau have been identified as amyloid precursor protein (APP) and microtubule associated protein tau (MAPT), respectively. Mutant APP is sufficient to cause genetic forms of AD, known as familial AD (FAD), but mice engineered to express the same FAD gene variants develop Aβ plaques without NFTs or neuronal loss. Mutant MAPT expression is required for mice to develop tauopathy, a finding that has impelled great interest in tau proteins and MAPT.

Tau belongs to the family of microtubule associated proteins (MAPs). All MAPs influence cytoskeletal stability and plasticity through microtubule (MT) interactions. Tau proteins regulate the assembly of tubulin monomers into MTs in neuronal cells. Alternative splicing of the single copy MAPT gene produces six tau isoforms [29,30]. Isoforms containing four imperfect repeat sequences (4R) bind MTs with higher affinity than their 3R counterparts that lack one of the repeats [38,39].

Central nervous system (CNS) region and developmental age dictate tau isoform and expression levels. The developing CNS requires a fluid cytoskeleton necessary for

axonal outgrowth, migration, and extension. To accommodate such a dynamic cellular environment, heavily phosphorylated 3R tau isoforms are expressed during development [46]. Conversely, the adult CNS consists of mostly static neuronal circuitry with stable cytoskeletons. Adult humans express a 1:1 3R:4R ratio of primarily non-phosphorylated tau [32,37]; adult rodent brains exclusively express 4R isoforms [30,32,48].

Tau post-translational modifications, primarily phosphorylation, alter MT binding affinity. Heavy phosphorylation, especially at or near the MT-binding (MTB) domain, decreases MT polymerization by reducing tau's MT affinity [41-43,45]. Neurodegeneration and dementia can arise from mutations that alter the 3R:4R tau isoform ratio, affinity for microtubules, or conformation [57]. Brains of affected patients develop hyperphosphorylated tau aggregates and NFTs, which coincide with neuronal loss and dementia. These diseases are collectively called tauopathies. Unlike most tauopathies, AD emerges without MAPT genetic insult, but instead hereditary forms are caused by mutations that alter misprocessing APP. Mice that express FAD gene variants consistently fail to develop tau pathology. To achieve tauopathy in mice, overexpression of mutant tau variants is required [241]. Interestingly, ablating mouse tau in tauopathy models enhances pathology [139,242]. The hypothesis emerging from these studies suggests a resistance or inhibition of endogenous mouse tau on tau-associated pathology.

The poor understanding of endogenous mouse tau's influence on tauopathy, and wild type tau in general, could impact our ability to appropriately model human disease. To help elucidate the effect of endogenous mouse tau on tauopathy, we used the frontotemporal dementia (FTD) mouse model, rTg(tau_{P301L})4510. rTg(tau_{P301L}) mice have

tet-regulatable 4R0N human tau_{P301L} driven by the calcium/calmodulin-dependent protein kinase IIα-tTA (CK-tTA) with the bulk of the expression in forebrain cells, the specific brain region affected by FTD [84,85]. Transgene expression can be suppressed by the administration of doxycycline.

This well-characterized mouse model develops age-related hyperphosphorylated, aggregated tau and NFTs associated with neuronal loss and memory decline [84,85]. We compared rTg(tau_{P301L}) mice with and without endogenous mouse tau to determine the effects of mouse tau ablation. Since the nucleotide and protein sequences of the largest tau isoform are highly similar (83% and 88% identical, respectively) between mouse and humans [140], we wanted to determine if the presence of human tau_{wt} affected tau_{P301L} pathology in a similar manner as mouse tau. We compared mice expressing human tau_{wt} with tau_{P301L} to mice expressing endogenous mouse tau with tau_{P301L} to determine if species-specific tau_{wt} effects occurred. The recently created rTg(tau_{wt}) mice [114] with and without mouse tau served as wild type tau overexpression controls to discriminate mutation specific from general tau overexpression effects.

All 1.5 month-old human tau-expressing mice acquired phosphorylation at residues associated with CNS development [46,243,244]. Interestingly, young human tau_{wt}-expressing mice contained a tau species more phosphorylated than rTg(tau_{P301L}) mice. With age, however, only tau_{P301L}-expressing mice acquired disease-associated hyperphosphorylation and conformational changes with manifest pathology and neurodegeneration. Though all aged tau_{P301L}-expressing mice developed tauopathy, the presence of wild type tau, mouse or human, delayed the overall pathology. We present a

hypothesis separate from the mouse tau interference hypothesis. We suggest that tau_{P301L}-expressing mice lacking endogenous mouse tau developed more severe pathology due to dual genetic insults: *Mapt* ablation resulted in the loss of normal tau function which was coupled with a toxic tau_{P301L} gain-of-function. We suggest that the presence of wild type tau, mouse or human, may have alleviated loss-of-function effects and reduced the overall pathology.

Materials and Methods

Generating Mice

rTg(tau_{P301L}) [84] and rTg(tau_{wt}) [114] mice were generated using a system of responder and activator transgenes (Figure 1.3). Tg(tau_{P301L}) mice were maintained hemizygous on an FVB/NCr background and Tg(tau_{wt}) mice were maintained homozygous on an FVB/NCr background. Mice were screened by PCR using primer pairs forward: 5` AAGATCGGCTCCACTGAGAA 3', reverse: 5` GGCGAGTCTACCATGTCGAT 3` which flanked the P301L mutation in the human tau4R0N gene. Mice expressing the activator transgene, Tg(CK-tTA), were maintained hemizygous on a 129S6 genetic background and have been described previously [81,85]. FVB/129 F1 hybrid rTg(tau_{P301L}) mice expressed ~13 units of tau_{P301L} where one unit is equivalent to endogenous mouse tau [85]. rTg(tau_{wt}) mice expressed human tau_{wt} at levels comparable to rTg(tau_{P301L}) [114].

Original $Mapt^{tm1(GFP)Klt}$ Tg(MAPT)8cPdav/J, referred to as $Mapt^{0/0}$, have been described previously [129,242]. $Mapt^{0/0}$ with EGFP cDNA disrupting exon1 of the *Mapt* locus mice were created on a mixed C57Bl/6 and 129/SvJae background. They were

crossed to mice that expressed the entire human MAPT transgene derived from a human PAC, H1 haplotype, known as 8c [120] and maintained on a mixed Swiss Webster/129/SvJae/C57Bl/6 background [242]. For these experiments, we genetically bred out the 8c human tau transgene to produce mice lacking endogenous mouse tau. This was accomplished by backcrossing the mice to both FVB/NCr and 129S6 mouse lines. We selected against MAPT, and kept only mice with the disrupted *Mapt* allele. Mice were genotyped by PCR using primer sets that amplified endogenous *Mapt*: (forward: 5-CTCAGCATCCCACCTGTAAC-3) and (reverse: 5-CCAGTTGTGTATGTCCACCC-3), and the disrupted *Mapt* (forward: 5-AAGTTCATCTGCACCACC-3) and (reverse: 5-TGCTCAGGTAGTGGTTGTCG-3). We selected for mice containing only the disrupted *Mapt* allele.

These mixed background $Mapt^{0/0}$ mice were mated with Tg(TRE-tau): Tg(tau_{wt}) and Tg(tau_{P301L}), or Tg(CK-tTA) mice. Mice hemizygous for activator or responder transgenes and heterozygous for endogenous *Mapt* were backcrossed to the $Mapt^{0/0}$ line to produce Tg(tau_{wt})$Mapt^{0/0}$, Tg(tau_{P301L})$Mapt^{0/0}$, and Tg(CK-tTA)$Mapt^{0/0}$ mouse lines on a mixed genetic background. To minimize genetic diversity due to the mixed genetics in these mice, we intercrossed Tg(TRE-tau) mouse lines homozygous for the $Mapt^{0/0}$ allele, Tg(tau_{P301L})4510$Mapt^{0/0}$ and Tg(tau_{wt})21221$Mapt^{0/0}$, and kept mice with both mutant and wild type alleles, Tg(tau_{P301L}/tau_{wt})$Mapt^{0/0}$. The various Tg(TRE-tau) pups were identified by SmaI restriction enzyme digestion of the PCR amplified gene product. The tau_{P301L} mutation disrupts the SmaI recognition sequence, 5`-C CCGG G-3`, by replacing a cytosine with a thymine. Tau_{wt} was digested into two distinct fragments, and amplified

tau_{P301L} remained uncut. Tg(tau_{P301L}/tau_{wt}) pups were identified by the presence of both the uncut tau_{P301L} band and the digested tau_{wt} bands. These Tg(tau_{P301L}/tau_{wt})*Mapt*$^{0/0}$ responder mice were crossed to Tg(CK-tTA)*Mapt*$^{+/0}$ activator mice. Offspring were genotyped for human tau (tau_{wt}, tau_{P301L}, or tau_{P301L}/tau_{wt}), endogenous mouse tau (*Mapt*$^{0/0}$ or *Mapt*$^{+/0}$) and CK-tTA. All mice were housed randomly to avoid caging effects.

Tissue Harvest

The mice were Avertin anesthetized, weighed, and transcardially perfused with filter sterile heparin containing 1x PBS (20-40 mLs). Whole brains were harvested, weighed, and sagittally bisected. The right hemisphere was drop fixed in 10% formalin for 24-48 hours at room temperature then transferred to 80% ethanol. Right hemispheres were paraffin embedded at the University of Minnesota. The left hemisphere was placed on a weigh boat and snap frozen in dry ice/ethanol slurry for later biochemistry. Tail snips were taken for genotyping confirmation.

Immunoblotting

Adult mouse hemibrains for Western blot analysis were prepared as described previously [85]. Mouse brains were homogenized in ice-cold buffer consisting of 10mM Tris-HCl, 1mM EGTA, 0.8M NaCl, 10% sucrose, pH 7.4, Complete Protease Inhibitor Cocktail (Roche), and Phosphatase Inhibitor Cocktail II (Calbiochem). Brain homogenate protein concentrations were determined via BCA BSA assay (Pierce). 10μg protein equivalent from adult brain homogenates, was electrophoresed on 10% Tris-Glycine (Invitrogen) and electro-blotted onto PVDF membranes (Millipore). We used the

following anti-tau antibodies: Tau13 at 1:5000 (Covance); Tau1 at 1:200 (Chemicon); CP13, AT8, PHF-1, MC6, TG3, Alz50, MC1 and DA9 (provided courtesy of Dr. Peter Davies) at 1:200; pSer262 and pSer356 (MBL International) 1:1000. The specificity of these antibodies is summarized in Table 3.1. Loading control anti-GAPDH was used at 1:5000 (Chemicon). Goat anti-mouse HRP-conjugated IgG (Biorad) secondary antibody was diluted 1:10,000. SuperSignal West Pico reagent (Pierce) was used for membranes probed with Tau13, Tau1, PHF-1, and DA9; the ECL Plus substrate (Amersham) was used for membranes probed with phospho-tau antibodies MC6, TG3, Alz50, MC1, CP13, and AT8. For both chemiluminesence systems, membranes were incubated with substrate for 3 minutes. Chemiluminescence was detected using a Biorad VersaDoc at 3-5 minute exposures. Tau levels were normalized to GAPDH levels to correct for loading and transfer differences.

Dilution Series Blots

To accurately assess the amount of human tau expressed in the brains of each genotype, three different protein concentrations (2μg, 4μg, 8μg) were immunoblotted. Three mice of each genotype were analyzed. Each blot was imaged at three different exposures (30 seconds to 5 minutes). Chemiluminescence was detected using a Biorad VersaDoc. Tau13 levels were normalized to GAPDH. Three samples from each mouse were averaged. Due to the large number of mice, all samples could not be compared on the same blot. To control for differences in immunoblotting, the same rTg(tau_{P301L}) mouse sample was loaded on each blot as the control standard.

Sarkosyl Extraction

Extraction of sarkosyl-insoluble Tau (Protocol adapted from [245-248]. Hemibrains were weighed and homogenized in 10 volumes of ice-cold buffer H (10mM Tris-HCl, 1mM EGTA, 0.8M NaCl, 10% sucrose, pH 7.4) and ultracentrifuged (Type 42.2 Ti rotor) 27,200 x g (15K x g) 20 min at 4°C. The supernatant (S1) was saved, and the pellet (P2) was re-homogenized using 22 and 27 gauge syringe/needles in 10 volumes cold buffer H. Centrifugation was repeated (15K x g for 15 min at 4°C). The supernatant (S2) was combined with S1 and adjusted to 1% (w/v) *N*-lauroylsarcosine, and incubated at 37°C with shaking 60-90 min. The combined S1/S2 fraction was centrifuged at 150,000xg (36,000rpm) for 35 min at 20°C. Both the sarkosyl soluble supernatant (S3) and sarkosyl insoluble pellet (P3) were kept. The P3 was resuspended in 50mM Tris-HCl, pH 7.4, using 0.5μL buffer for each mg of initial weight of brain tissue. For Western blotting a 1:2 ratio between volume of supernatant and sarkosyl-insoluble pellet was loaded in 10% Tris-Glycine gels.

Immunohistochemistry (IHC)

Prior to sectioning, paraffin embedded brain blocks were hydrated in a rocking soapy water bath at 37°C for one hour. After the water bath they were placed facedown on a gauze-covered ice block and allowed to cool for 15 minutes. Paraffin sections were then cut at 5μm and mounted onto charged slides and dried overnight. The following day the slides were baked at 60°C for 15 minutes prior to the de-waxing procedure.

To dewax the slides they were placed in three sequential xylene baths, 10 minutes each for a total of 30 minutes. Tissues were rehydrated with sequential ethanol baths for 5

minutes each. The first steps were in 100% ethanol, followed by 95%, and 80%. The slides were then placed in running tap water for 5 minutes. For antigen retrieval the slides were placed in ReVeal Buffer (Biocare) and steamed for 30 minutes, followed by a 20 minute cooling period. They were then rinsed in running tap water for 5 minutes. At this point a hydrophobic pen (Vector) was used to draw borders around each tissue section to create a hydrophobic barrier. The slides were then rinsed in rinsing buffer (0.1% Triton-X in PBS) for 5 minutes. The tissues were blocked with Sniper Blocking Sera (Sniper) for 10 minutes then placed in primary antibody overnight at 4°C. Primary antibody dilutions: Tau13 (1:8,000, Covance); MC1 (1:8000, P. Davies); Alz-50 (1:50, P. Davies); CP13 (1:2000, P. Davies); TG3 (1:200, P Davies); AT8 (1:4000; Thermo Scientific); PHF1 (1:3000, P. Davies); TauC3 (1:1000, Invitrogen) NeuN (1:4000, Chemicon); GFAP (1:20,000; Dako). The primary antibody diluent was 1:5 Sniper Blocker Sera in PBS. The following day the slides were rinsed for 5 minutes (rinsing buffer) then placed in a biotinylated-secondary antibody for 30 minutes. They were rinsed for 5 minutes and placed in a peroxidase block (3% H_2O_2 diluted in rinsing buffer) to neutralize any endogenous peroxidase activity consisting of for 10 minutes then rinsed with tap water for 5 minutes, followed by 5 minutes in rinsing buffer. They were then placed in peroxidase labeled streptavidin for 30minutes. They were rinsed in tap water for 5 minutes, PBS five minutes, and developed with DAB chromogen (Signet) using the microscope. Chromogen activity was neutralized when staining on positive controls became prominent and negative controls remained blank. Developed slides were rinsed in tap water for 5 minutes then dipped in Mayer's hematoxylin (Fisher Scientific) for 2-5

minutes. The slides were placed in running tap water until it ran clear. The slides were dehydrated with sequential steps of increasing concentrations of ethanol for 1 minute each: one 80%, two 95%, and two 100% ethanol baths. They were then bathed in xylene twice for 2 minutes each. They were cover slipped with Permount (Fisher Scientific), and the slides were sealed with clear coat fingernail polish.

Hematoxylin and Eosin (H&E) Staining

The IHC protocol for sectioning and rehydrating were followed. After the 80% ethanol step, slides were placed in running tap water for 5 minutes. Next they were stained with Mayer's hematoxylin (Fisherbrand) for 5-15 minutes, rinsed in running tap water for 10 minutes. Then placed in eosin (0.1% eosin Y (Fisher) in 95% ethanol) for 3 minutes, and dehydrated, cover slipped, and sealed as in the IHC steps.

Bielschowsky Silver Stain

The sectioning and rehydrating steps described for IHC were followed. After the 80% ethanol step, slides were placed in distilled water for 5 minutes. Next they were placed in 20% silver nitrate (Sigma-Aldrich) and incubated in the dark for 15 minutes. They were rinsed in distilled water then placed in ammoniacal silver solution, again in the dark, for 10 minutes. Then they were placed in ammonia water and developed with ammoniacal silver solution. Once silver impregnation was observed the reaction was stopped with ammonia water. The slides were then rinsed with distilled water then dehydrated, cover slipped, and sealed as in the IHC protocol.

Histological Analyses

PHF1 and NFT Counts. To determine the number of cells positive for PHF1 stain of silver impregnation, individual positive cells were manually counted on 5x hippocampal images. Entire hemibrains were sectioned and stained. We used hippocampal morphology to choose sections from comparable brain depth/location. We counted 3-6 5μm sections that were approximately 60μm apart to encompass approximately 300μm brain region. PHF1 and NFTs from 4-6 mice of each genotype were counted (See Appendix A).

NeuN Cell Counts. The number of NeuN positive cells was counted from sections adjacent to those analyzed for PHF1 and NFT positive cells to evaluate the same brain regions. Four to six mice of each genotype were analyzed. PhotoShop was used to view images and count NeuN cells. Each 5x image was opened in PhotoShop and the hippocampal formation was selected using the Magic Wand. All pixels that fell within the predesignated tolerance range were selected, extracted, and copied onto a transparent background. The area stained was calculated using Area Measurement. To determine cell number, the total area stained was divided by the area of an average NeuN cell. NeuN cell size was calculated by selecting and measuring individual NeuN cells. The average of 20 cells was used as the NeuN size. See Appendix A for a more detailed description.

Statistical Analyses

ANOVA were performed using StatView 5 for Macintosh (SAS Institute, Inc.) and StatPlus:mac LE.2009 (AnalystSoft, Inc.) as a Microsoft Excel add-on application.

Results

Generation of rTg(tau_{wt}) and rTg(tau_{P301L})*Mapt*$^{0/0}$ and *Mapt*$^{0/+}$ Lines.

The mouse line we used to introduce the genetic perturbation of endogenous mouse tau was on a mixed genetic background, which added an additional level of complexity to the system. Though the responder mouse lines, Tg(tau_{P301L})4510 [84,85] and Tg(tau_{wt})21221 [114], and activator mouse line, Tg(CK-tTA) [81,85], were all inbred strains, therefore genetically identical, introducing the *Mapt*$^{0/0}$ gene created genetic background diversity. We devised a breeding scheme to avoid founder effects that would be inevitable if Tg(tau_{wt}) and Tg(tau_{P301L})*Mapt*$^{0/0}$ lines were made independently. While congenic lines would be preferable, the time involved for their production led us to proceed with the experiments outlined here while congenic lines, which are now complete, were being made.

We produced N2 backcross tau_{P301L} and tau_{wt} mice homozygous for the *Mapt* allele, Tg(tau_{P301L})4510*Mapt*$^{0/0}$ and Tg(tau_{wt})21221*Mapt*$^{0/0}$, then intercrossed to avoid null lines with distinct genetic backgrounds. We kept mice with both the tau_{P301L} and tau_{wt} responder alleles, Tg(tau_{P301L}/tau_{wt})*Mapt*$^{0/0}$ as the responder line. In order to identify the Tg(tau_{P301L}/tau_{wt}), pups, the amplified tau transgene was digested with the SmaI restriction enzyme. The tau_{P301L} mutation disrupts the SmaI recognition sequence. Amplified tau_{P301L} remained uncut (494 bps) while amplified tau_{wt} was digested into 126 and 368 base pair fragments. Pups of interest, those hemizygous for both transgenes, were identified by the presence of both the uncut tau_{P301L} band and the digested tau_{wt} bands (Figure 2.1A).

These new responder mice, Tg(tau_{P301L}/tau_{wt})*Mapt*$^{0/0}$ were crossed to Tg(CK-tTA)*Mapt*$^{+/0}$ activator mice. Offspring that inherited both the activator and responder alleles expressed human tau in forebrain cells (See Figure 1.3 for diagrammatic representation of the bigenic transgene system). We examined rTg(tau_{P301L})*Mapt*$^{+/0}$, rTg(tau_{P301L})*Mapt*$^{0/0}$, rTg(tau_{wt})*Mapt*$^{+/0}$, and rTg(tau_{wt})*Mapt*$^{0/0}$ to study the role of the different human/mouse gene combinations in developing tauopathy. We also aged rTg(tau_{P301L}/tau_{wt})*Mapt*$^{0/0}$ and rTg(tau_{P301L}/tau_{wt})*Mapt*$^{+/0}$ mice to determine the effect of human tau_{wt}, with or without endogenous mouse tau, on tau_{P301L} pathology. See Table 2.1 for mouse genotypes and corresponding *Mapt* and MAPT expression. The Tg(TRE-tau) lines: Tg(tau_{P301L}) and Tg(tau_{wt}) with and without endogenous mouse tau, were used to determine the effects of "leaky" transgene expression. Tg(CK-tTA)*Mapt*$^{0/0}$ were used as tau null controls.

Only rTg(tau_{P301L}) Mice Accumulated
Human Tau Protein With Age.

rTg(tau_{wt})212221 and rTg(tau_{P301L})4510 mice with the identical F1 background express comparable levels of human tau [114]. To compare transgene expression levels among genotypes of the mixed genetic backgrounds presented here, we quantified human tau protein expression in young, 1.5-month-old, and mature adult, 7.5-month-old, mouse brains using the human tau specific antibody, Tau13. Overall, 1.5 and 7.5 month-old rTg(tau_{wt}) mice expressed significantly less transgenic tau protein than age-matched rTg(tau_{P301L}/tau_{wt}) mice ($p<0.005$ (1.5 month old mice); $p<0.01$ (7.5 month-old mice). rTg(tau_{P301L}) transgenic protein expression levels were comparable to rTg(tau_{wt}) mice at

1.5 months of age, and comparable to rTg(tau_{P301L}/tau_{wt}) at 7.5 months of age (Figure 2.1B).

Young rTg(tau_{wt}) mice, with and without mouse tau, and rTg(tau_{P301L})*Mapt*$^{0/0}$ mice expressed human tau at similar levels (Figure 2.1B). Young rTg(tau_{P301L})*Mapt*$^{+/0}$ mice expressed about 16% less transgenic tau; of note, two of the three rTg(tau_{P301L})*Mapt*$^{0/0}$ mice had transgene expression comparable to rTg(tau_{P301L})*Mapt*$^{+/0}$ mice, one mouse with higher expression increased the overall average (Figure 2.1B). Brains from young rTg(tau_{P301L}/tau_{wt}) mice, with and without mouse tau, contained significantly more transgene-encoded tau than the other genotypes, (rTg(tau_{wt}) and rTg(tau_{P301L})*Mapt*$^{0/0}$ ($p<0.05$) and rTg(tau_{P301L})*Mapt*$^{+/0}$ ($p<0.005$)). With age, all rTg(tau_{P301L}) mice reached accumulation levels comparable to rTg(tau_{P301L}/tau_{wt}) mice. However, human tau protein levels in tau_{wt}-expressing mice remained constant throughout adulthood which resulted in levels significantly lower, 12% ($p<0.01$), in rTg(tau_{wt}) mice than tau_{P301L}-expressing mice at 7.5 months of age.

Immunoblotting with Tau13 allowed us to visualize the electrophoretic migration pattern of human tau species among the genotypes. All young and mature adult tau_{wt}-expressing mice contained human tau species migrating between 58 and 67 kDa. In contrast, rTg(tau_{P301L}) mice lacked a 67 kDa tau species until 7.5 months of age (Figure 2.1C). The presence of this higher molecular weight tau species coincided with the increase in tau accumulation, 13% in rTg(tau_{P301L})*Mapt*$^{0/0}$ mice, and 41% ($p<0.05$) in rTg(tau_{P301L})*Mapt*$^{+/0}$ mice. Age associated differences in tau accumulation is common to genetically uniform rTg(tau_{P301L})4510 mice as well [88].

Mutant Human Tau Was Less Phosphorylated Than Wild Type Human Tau in Young Mice.

To better characterize the tau species expressed by the different mouse genotypes, we looked for histological and electrophoretic changes associated with tau phosphorylation and conformation. The CP13, AT8, and PHF1 antibodies recognize disease-associated phosphorylated tau epitopes. Neuronal cells acquire transient phosphorylation at AT8 and CP13 epitopes during development [46,243,244] and correlates with cortical migration, neurite outgrowth, and synapse formation [244,249]. CP13 expression was widespread throughout the cortex and hippocampal regions of all human tau-expressing mice at 1.5 months of age (Figure 2.2A). The peripheral most cortical layers also contained AT8-immunoreactive cells at 1.5 months of age (Figure 2.2B). At 5 months of age, human tau_{wt}-expressing mice developed AT8 immunoreactivity in cortical layer 5 neurites; similar AT8 distribution has been reported in other human tau_{wt}-overexpressing mice [119]. rTg(tau_{P301L}) mice did not acquire cortical layer 5 staining, but instead developed hippocampal AT8-immunoreactivity (Figure 2.2B). rTg(tau_{P301L}/tau_{wt}) mice developed both phenotypes indicating protein expression of both tau isoforms, and isoform-specific cellular localization.

PHF1 immunoreactive cells first appeared at 5 months of age. All human tau-expressing mice contained PHF1-immunoreactive cells in cortical and subicular cells (Figure 2.3A). However, only tau_{P301L}-expressing mice developed hippocampal CA1 PHF1 immunoreactivity. Evidence of CA1 PHF1 immunoreactivity was first seen in 5 month-old mice (Figure 2.3A) and increased immunoreactivity by 7.5 months of age (Figure 2.3B). rTg(tau_{wt}) mice did not develop hippocampal PHF1 tau phosphorylation

until 17.5 months of age (Figure 2.6C). Despite 5 month-old rTg(tau_{P301L}) mice containing more cells with PHF1-immunoreactivity than rTg(tau_{wt}), electrophoresed protein revealed that human tau_{wt}-expressing mice contained a more heavily phosphorylated tau species than rTg(tau_{P301L}) mice (Figure 2.3C). Tau_{wt}-expressing mice displayed a heterogeneous CP13 and PHF1 immunoreactive protein smear with a 67 kDa tau species, but rTg(tau_{P301L}) mice did not acquire a 67 kDa tau species until 7.5 months of age (Figure 2.3C and Figure 2.4A). This age interval, between 5 and 7.5 months, marked the transition from tau_{P301L} hypo-to-hyperphosphorylation (Figure 2.4A).

Only Tau_{P301L}-Expressing Mice Developed Age-Associated Hyperphosphorylation and Sarkosyl Insoluble Tau.

In healthy adult brains, tau remains predominantly unphosphorylated [47] and highly soluble. However, aggregates of heavily phosphorylated, conformationally altered, sarkosyl insoluble tau are characteristic of tauopathy. Healthy adult brains contain 1-3 moles of phosphate per mole of tau, and AD patient brains contain 3-4 fold higher levels than age-matched control brains [72,240]. Between 2.5 and 5 months inbred rTg(tau_{P301L})4510 mice acquired heavy phosphorylation [84]; the mixed genetic background tau_{P301L}-expressing mice presented here displayed the same signs of tau-misprocessing but at a slightly older age. We noticed dramatic changes between 5 and 7.5 months of age (2.4A). All tau_{P301L}-expressing mice, but not rTg(tau_{wt}), developed phosphorylation in the proline rich domain, recognized by AT8 and CP9, and the MT-binding domain, recognized by $pSer^{262}$ (see Figure 2.4B for an illustration of approximate antibody epitope locations along the tau protein). The 67 kDa tau species contained

conformationally-altered tau as evidenced by TG3 and MC1 immunoreactivity. A heavy 72 kDa tau species, especially prominent with Tau13 (2.1B), also emerged at this age in tau_{P301L}-expressing mice. The Tau1 migration profile was comparable among genotypes. This antibody recognizes unphosphorylated $Ser^{198/202}$ indicating that all genotypes contained this non-phosphorylated tau species.

Simultaneous with tau phosphorylation and the presence of 67 kDa tau in 7.5 month-old tau_{P301L}-expressing mice (Figure 2.4A) was the appearance of sarkosyl insoluble tau (Figure 2.5A) and NFTs (Figure 2.5B) absent in younger mice. All human tau-expressing mice contained soluble tau species, but only tau_{P301L}-expressing mice developed sarkosyl insoluble tau at 7.5 months of age (2.5A). Mature NFTs, visualized by Bielschowsky silver staining, were first seen in forebrain cells at this same age (2.5B). Of note, immunoblotting of sarkosyl insoluble fractions showed insoluble tau species in only one 7.5 month-old rTg(tau_{P301L}/tau_{wt})$Mapt^{0/0}$ mouse (Figure 2.5A) and histological silver staining revealed very few, if any, tau aggregates in rTg(tau_{P301L}/tau_{wt})$Mapt^{0/0}$ mice until 12.5 months of age (Figure 2.5A and 2.6A, B).

Greater Age-Associated Tau Phosphorylation and NFT Density Occurred in the Absence of Wild Type Tau.

The number of cells containing phosphorylated tau and NFTs increased with age in all tau_{P301L}-expressing mice. At 12.5 months of age, histological staining revealed numerous PHF1 and silver stained cells throughout the hippocampal formation with the highest concentration in CA1 (Figure 2.6A). The number of cells containing PHF1 immunoreactivity and silver deposits were counted and compared among genotypes.

Interestingly, the presence of wild type tau, mouse or human, resulted in fewer PHF1 positive and silver impregnated cells (Figure 2.6A, B) which suggests a universal effect of wild type tau, and not a mouse tau-specific resistance as previously hypothesized. Human tau_{wt} appeared to decrease pathology more dramatically than endogenous mouse tau, as evidenced by less severe pathology in rTg(tau_{P301L}/tau_{wt})$Mapt^{0/0}$ mice than rTg(tau_{P301L})$Mapt^{+/0}$ mice. We suspect that differences in the amount of wild type tau protein, i.e. overexpressed human tau_{wt} compared to one copy of endogenous mouse tau in $Mapt^{+/0}$, account for the discrepancy.

None of the rTg(tau_{wt}) mice developed sarkosyl insoluble tau or brain atrophy; however, in the absence of obvious neurodegeneration, one of the thirteen >12.5 month-old rTg(tau_{wt}) mice developed cortical NFT lesions (Figure 2.6C). We examined whole hemibrains with sections spaced approximately 60μm apart, and only visualized two NFTs. The remaining rTg(tau_{wt}) mice were devoid of NFTs but they acquired hippocampal CA1 and locus coeruleus PHF1 immunoreactivity at 17.5 months of age (Figure 2.6C). The locus coeruleus is a hindbrain structure indicating leaky, not forebrain promoter-driven, expression was sufficient for PHF1 tau phosphorylation in these cells.

Greater Neuronal Loss and Brain Atrophy Occurred in the Absence of Wild Type Tau.

Brain atrophy, determined by whole brain mass, started to occur in tau_{P301L}-expressing mice between 5 and 7.5 months of age. Tg(CK-tTA), Tg(TRE-tau), and rTg(tau_{wt}) brains did not atrophy with age, but became slightly larger with age (Figure 2.7A). All 12.5 month-old tau_{P301L}-expressing mouse brains were significantly smaller

than age-matched rTg(tau_{wt})*Mapt*$^{0/0}$ mouse brains (Figure 2.7B). Since control brains showed a trend for age-associated increase in mass (Figure 2.7A) we compared different ages within the same genotype to better assess brain atrophy. When compared to younger mice of the same genotype, only 12.5 month-old rTg(tau_{P301L})*Mapt*$^{0/0}$ mouse brains were significantly smaller than their 7.5 month-old counterparts (Figure 2.7A, C). Interestingly, brain mass of tau_{P301L}-expressing mice with wild type tau, mouse or human, did not reach atrophy mass of rTg(tau_{P301L})*Mapt*$^{0/0}$ mice until 17.5 months of age (Figure 2.7A). This result suggests that the presence of wild type tau, mouse or human, delays brain atrophy.

Forebrain-specific atrophy was obvious at the macroscopic level in 12.5 month-old mice (Figure 2.7D). To better assess neuronal loss, brain sections were stained with the neuronal antibody, NeuN. The number of NeuN positive cells in the CA1, CA3, DG, and whole hippocampus were counted and analyzed. Analyses revealed that the most significant neuronal loss occurred in the CA1 subdivision (with wild type tau, $p<0.05$; without wild type tau, $p<0.005$) (Figure 2.7E-F), which is consistent with inbred rTg(tau_{P301L}) mice [84].

Human Wild Type Tau Expressing Mice Acquired Transentorhinal Cortical GFAP Immunoreactivity Before Mutant Human Tau Expressing Mice.

Astrogliosis is common to many neurodegenerative disorders, and prominent in tauopathies with upregulated 4R tau [250]. To visualize astrocytic presence, we conducted IHC with the GFAP, glial fibrillary acidic protein, antibody. GFAP is an intermediate filament protein expressed by astrocytes. Only human tau_{wt}-expressing mice

contained GFAP positive cells in the cortical cells overlying the hippocampus, transentorhinal cortex, at 5 months of age. With age tau_{P301L}-expressing mice acquired the staining but Tg(CK-tTA) controls did not (Figure 2.8).

Mice Expressing Activator or Responder Transgenes
Alone Developed Subtle Histological Abnormalities.

We assessed the effects of each control transgene alone, Tg(CK-tTA) without Tg(TRE-tau), and Tg(TRE-tau) without Tg(CK-tTA). Macroscopic brain weights revealed that young Tg(CK-tTA) mouse brains were smaller than age-matched Tg(TRE-tau) mouse brains (Figure 2.7A). Interestingly, we saw evidence of delayed dentate gyrus (DG) development in Tg(CK-tTA) mice (Figure 2.9A). Histological analyses with hematoxylin nuclei stain revealed that Tg(CK-tTA) mouse DGs were much smaller than Tg(TRE-tau) DGs at 1.5 and 5 months of age, but were comparable by 12.5 months of age (Figure 2.9A).

Leaky transgene expression occurs in many tet-based models [251]. We observed transgene expression in the Tg(TRE-tau) responder mice in the absence of the CKIIα-driven tet-transactivator transgene. Many cells displayed Tau13 immunoreactivity (Figure 2.9A, B); human tau antibody specificity was confirmed by the lack of positive immunoreactivity in either Tg(CK-tTA) mouse brains or rTg sections treated with secondary antibody alone (Figure 2.9D).

Leaky expression began early in development, at least by E14, and was observed in CNS-stem cell containing neurosphere cultures generated from fetal mouse brains (Figure 2.9A and Chapter 3 Figure 3.2, 3.3). Strong leaky expression was observed in the

hippocampus at all ages. Of note, positive staining was observed throughout the axonal projections in 12.5 month-old Tg(tau_{P301L}) mice indicating that low level expression was not sufficient for tau mislocalization as seen in age-matched rTg mice (Figure 2.9B).

To determine if leaky expression induced pathological tau changes, we analyzed Tg(TRE-tau) brains for PHF1 immunoreactivity. Forebrain cells with leaky transgene expression did not acquire pathological tau phosphorylation (Figure 2.9C). Cells of the locus coeruleus, a hindbrain structure, however did display PHF1 immunoreactivity in 70% (12/17) of the 12.5-17.5 month-old mice examined. This result demonstrated that leaky expression occurred outside the forebrain and was sufficient for tau misprocessing.

rTg(tau_{wt}) Mice Were Significantly Larger Than All Other Genotypes.

We compared body weights of all 12.5 month-old mice. Tg(CK-tTA) and Tg(TRE-tau) control mice were significantly larger than rTg(tau_{P301L}/tau_{wt}) mice ($p<0.05$), but not rTg(tau_{P301L}) mice (Figure 2.10A). Surprisingly the non-transgene expressing control mice were significantly smaller than rTg(tau_{wt}) mice ($p<0.01$). rTg(tau_{wt}) mice were significantly larger than all other mice, rTg(tau_{P301L}) ($p<0.001$) and rTg(tau_{P301L}/tau_{wt}) ($p<0.00001$).

Human Wild Type Tau Did Not Delay Tau_{P301L}-Induced Brain Atrophy When Expressed on a *Mapt*$^{+/0}$ Background.

We compared brain masses of all 12.5 month-old mice. Strikingly, rTg(tau_{P301L}/tau_{wt})*Mapt*$^{+/0}$ mouse brain mass was comparable to age-matched rTg(tau_{P301L})*Mapt*$^{0/0}$. (Figure 2.10B) This result suggests that expressing both wild type

tau species, mouse and human, does not improve pathology more than when each are expressed separately. Instead they seem to negate each other and develop brain atrophy similar to rTg(tau_{P301L})$Mapt^{0/0}$ mice.

Discussion

Wild type tau, mouse and human, decreased mutant tau-related pathology and delayed brain atrophy in the rTg(tau_{P301L})4510 mouse model of FTD. Our data provides evidence against a mouse-specific inhibitory action on tauopathy, but instead suggests a general effect of wild type tau. One possibility is that wild type tau may partially restore loss of function associated with mutant tau isoforms [127,139].

Evidence of tau_{P301L} misprocessing was observed as early as 1.5 months of age. Contrary to the canonical tau hyperphosphorylation seen in rTg(tau_{P301L})4510 mice and FTD patient brains, brains from 1.5 month-old rTg(tau_{P301L}) mice contained less phosphorylated tau than age-matched tau_{wt}-expressing mice. Hypophosphorylated tau_{P301L} occurred as early as embryonic day 14 as seen in neurosphere cultures harvested from E14 fetal brains (Chapter 3). Such early misprocessing suggests an inherent or early-acquired protein malady, possibly one of protein conformation. Young transgenic mice that express other exon 10 variants reportedly displayed hypophosphorylated tau as well [94,105,252]. To determine if hypophosphorylated tau correlates with adult onset tauopathy, we plan to utilize the genetically engineered tet-off system to suppress transgene expression, [84,85], through development until the age of heavy tau misprocessing. The mixed genetic mice presented here developed these changes between 5 and 7.5 months of age, however we plan to conduct these experiments on inbred

rTg(tau_{P301L}) mice which developed pathology earlier, between 2.5 and 5 months of age [84,85].

Transgenic tau_{P301L}-expression levels correlated with disease onset in genetically identical rTg(tau_{P301L}) mice [85]. However, in the mice presented here, rTg(tau_{P301L}) mice developed more extreme pathology than rTg(tau_{P301L}/tau_{wt})$Mapt^{0/0}$ mice despite lower transgenic protein expression levels. The majority of rTg(tau_{P301L}/tau_{wt})$Mapt^{0/0}$ mice had less severe disease phenotypes but expressed 22% more human tau than rTg(tau_{P301L}) mice at 1.5 months of age. Preliminary experiments with a P301L-sepcific antibody revealed that soluble tau_{P301L} levels were comparable among all tau_{P301L}-expressing mouse genotypes at 1.5 and 7.5 months of age. This suggests that elevated soluble tau_{P301L} alone was insufficient to initiate disease, and that the presence of wild type tau, mouse or human, delayed disease onset.

Interestingly, only rTg(tau_{P301L}), but not rTg(tau_{P301L}/tau_{wt}), mice exhibited an age-associated increase in tau protein, which suggests a potentially limiting, or saturating, amount of transactivator protein. Fewer TRE-tau transgene copies increased human tau protein levels in rTg(tau_{P301L})4510 [84], presumably through similar mechanisms.

By 7.5 months of age, all tau_{P301L}-expressing mice displayed phosphorylation at residues within or adjacent to the microtubule-binding domain. Phosphorylation at these residues permits dimerization and PHF formation [44], and occurred simultaneously with the appearance of NFTs and sarkosyl insoluble tau. Tau_{P301L}-expressing mice also contained tau species immunoreactive to disease-specific conformations. Recent evidence suggests that misfolded tau may recruit/alter the conformation of endogenous tau and

trigger it to adopt a pathogenic form [88,151]. While tau_{P301L} acquired disease-associated conformations, we did not see evidence of endogenous mouse tau or human tau_{wt} recruitment. rTg(tau_{P301L}) mice without endogenous tau developed more severe tauopathy than those with widespread endogenous tau expression. While our study, and others [139], failed to demonstrate enhanced tau pathology in the presence of endogenous mouse tau, misprocessing of mouse tau in separate mouse models [88,151], and mouse tau assembly into PHFs [143] provides evidence that mouse tau is not resistant to pathogenic changes. One possibility is that different disease mechanisms ensue depending on the specific to tau isoform. Tau aggregate conformations vary among tauopathies, and may be specific to isoform [153]. When mutant and wild type were co-fibrillized, a novel fibril structure formed [154]. The hybrid fibril structure more closely resembled that of pure mutant fibrils than pure wild type fibrils. One possibility is that pathogenic rates may be unique to tau isoform and conformation as seen in prion disease incubation studies [253-256].

The quantity of NFTs correlates with disease severity in human patients [56]. However, recent evidence suggests dissociation between NFT and neuronal death [98-100]. Likewise, our data did not indicate a direct parallel between NFT number and neuronal loss as assessed by NeuN and NFT counts. We counted more hippocampal NFTs in rTg(tau_{P301L})$Mapt^{0/0}$ than all other tau_{P301L} genotypes, but all retained similar numbers of NeuN positive cells. A growing body of evidence implicates other cellular phenomenon, perhaps caspase activation [99], and not NFTs, as the degenerative agent. Interestingly, while the electrophoretic migration profile of tau from rTg(tau_{wt}) mice mirrored that of tau4R0N expressed *in vitro,* the tau banding pattern of young

rTg(tau_{P301L}) mice resembled the accumulation of 52 and 54 kDa 4R0N tau species associated with calpain and/or caspase activation caused by proteasomal inhibition [257]. The heavy 72 kDa tau species that developed in older mice, coincident with the first signs of NFT formation, could correspond to the accumulation of transgenic tau oligomers consisting of smaller truncated caspase-cleaved tau species. Preliminary experiments with the caspase-cleaved tau specific antibody, TauC3, revealed that 6/8 rTg(tau_{P301L}) 12.5 month-old mice contained caspase-cleaved tau in cortical cells. Only 2/4 age-matched rTg(tau_{P301L}/tau_{wt})$Mapt^{0/0}$ displayed TauC3 immunoreactivity. Future experiments will examine TauC3 immunoreactivity in younger and older mice to determine if more cells accumulate caspase cleaved tau, and when the first insult occurs.

Two NFT containing cells were found in one of six 17.5 month-old rTg(tau_{wt}) mice, but we did not see gross tau pathology or neuronal loss as described in other human tau_{wt}-overexpressing mice [117,138]. The spontaneous tauopathy observed in previous mouse models likely arose from altered 3R:4R tau isoform ratios, a phenomenon that causes a subset of human tauopathies [122-125,258]. The biochemical and immunohistochemical profile of the rTg(tau_{wt})$Mapt^{0/0}$ mice presented here resembled that of the mTau mouse line, a mouse line that overexpresses endogenous mouse tau_{wt} from its endogenous promoter [121]. The entire *Mapt* gene driven by a BAC transgene allowed for appropriate exon splicing; 4R tau comprised >95% of total tau in mTau brains. Likewise, our rTg(tau_{wt}) mice solely expressed 4R tau. Similar to our findings, mouse tau overexpression in mTau brains did not result in overt pathology despite CP13 and PHF1 immunoreactive cells. The comparable effects of human and mouse tau overexpression,

as demonstrated by similarities between rTg(tau_{wt}) and mTau mice, provides evidence against an anti-tauopathy property exclusive to mouse tau; instead we attribute these similarities to close functional conservation of tau proteins between species [140].

The finding that rTg(tau_{wt}) and rTg(tau_{P301L}/tau_{wt}) mice acquired transentorhinal cortical GFAP immunoreactivity prior to rTg(tau_{P301L}) suggests an effect of overexpressed tau_{wt}. Interestingly, human tauopathies that arise from disproportionate amounts of 4R tau over 3R tau also develop prominent astrogliosis [250]. Wild type tau is expressed in these diseases. The delayed astroglial phenotype in rTg(tau_{P301L}) mice may indicate that the 4R0N-tau_{P301L} is more similar to a loss of function *Mapt*$^{0/0}$ insult than overexpressed 4R0N. Supporting this hypothesis are behavioral similarities, i.e. hyperactivity between tau_{P301L} and *Mapt*$^{0/0}$ mice [105,127]. Alternatively, astroglial differences may correspond to different cellular localizations of each tau species as seen in 5 month-old forebrains where only phosphorylated tau_{wt} was present in cortical neuritic projections. We plan to co-stain brain sections with GFAP and Tau13 and compare them to brain sections co-stained with NeuN and Tau13 to determine if specific tau isoforms are more prominent in either glia or neurons.

Tg(CK-tTA) and Tg(TRE-tau) non-transgene expressing control mice were not thoroughly characterized in the original experiments [84,85]. We evaluated phenotypes associated with the activator or responder transgene alone. Our data suggest that Tg(CK-tTA) may affect the brain mass of young mice. Our brain mass data indicated that 5 month-old Tg(TRE-tau) mouse brains were larger than brains of age-matched Tg(CK-tTA) mice. Furthermore, hematoxylin staining revealed smaller DGs in Tg(CK-tTA) than

Tg(TRE-tau) mice until 12.5 months of age. Decreased brain mass in rTg mice may be a result of a developmental Tg(CK-tTA) effect combined with age-associated tau_{P301L} pathology. Newly born cortical neurons migrate out of the ventricular zone to form cortical layers 2-6 between E11-E18. Developmentally, *CKIIα,* thus tTA protein, expression occurs in the deep neocortical cell layers bordering the ventricles (see Chapter 3 Figure 3.11 for CKIIα spatial expression pattern at embryonic day 15.5 (E15.5), Allen Brain Atlas [259]) spatially similar to Sox1 expression, a marker of radial glia that reside in the ventricular zone. Transgene insertion site, or tTA protein, may slightly alter cortical development. Subtle effects of the tTA transgene should be considered when using brain mass as a parameter to assess the effects of CK-tTA driven transgenes.

We observed leaky transgene expression in regions outside and in the forebrain in all mice carrying a TRE-tau transgene. Locus coeruleus cells of all rTg and several Tg(TRE-tau) mice acquired PHF1-immunoreactivity due to low-level transgene expression. The ability of low-level tau to induce locus coeruleus PHF1 immunoreactivity suggests an extreme sensitivity of these cells to tau misprocessing. Interestingly, a recent study on human brain samples indicated tau pathology in the noradrenergic coeruleus/subcoeruleus complex decades prior to Alzheimer's disease onset [260].

Tg(TRE-tau) mice lacking the CK-tTA transgene expressed leaky levels of transgenic tau in forebrain cells as well; however they retained axonal tau_{P301L} compartmentalization and did not develop forebrain tau pathology. Tau mislocalization to the somatodendritic compartment is common to human tauopathy patients and mouse models [57], and occurred in the rTg(tau_{P301L}) mice presented here. The inability of low-

level human tau_{P301L} to induce disease-associated phenomenon parallels a separate study where endogenous levels of mouse tau_{P301L} did not induce tauopathy [105]. Collectively the data indicate mutation alone is insufficient to drive tauopathy, and expression level is a critical parameter. We saw hippocampal PHF1 immunoreactivity in 17.5 month-old rTg(tau_{wt})$Mapt^{0/0}$ mice, which may suggest a more detrimental effect of abundant tau_{wt} than low-level tau_{P301L}.

Despite understanding the genetic components of AD, the development of a proper mouse model remains elusive. While the prominent hypothesis attributes the repeated failures to mouse tau's resistance to tauopathy, our data, and those showing incorporation of mouse tau into the sarkosyl insoluble fraction, indicate otherwise. We suggest that species differences, distinct from endogenous mouse tau, in combination with temporal factors prevent tau pathology from developing in mice harboring AD gene variants. Additionally, we suspect that mouse tau ablation creates an environment more susceptible to neuropathogenic insults. $Mapt^{0/0}$ mice live normally with subtle, sometimes undetected, neurological abnormalities [127,128]. However, $Mapt^{0/0}$ mice exhibit increased spontaneous locomotor activity [127], as do mice harboring mutant tau [139], suggestive of a phenotype common to tau loss of function. The overall unaffected existence of $Mapt^{0/0}$ mice likely stems from functional redundancy between tau and other MAPs. While map1b and tau work in concert to regulate microtubule organization necessary for proper axonal elongation and neuronal migration [132], stressful environments may necessitate tau function [136].

Future Directions

We propose that endogenous mouse tau's previously hypothesized inhibitory role on tauopathy has been mistaken for a general effect of wild type tau. In our studies the presence of wild type tau, mouse or human, significantly decreased tau_{P301L}-induced tauopathy. While the mechanism remains unknown, we suggest that mice expressing tau_{P301L} in the absence of wild type tau suffer from two genetic insults, loss of *Mapt* function, and gain of toxic tau_{P301L} function. Recent evidence indicates a tau-specific role in MT-dependent autophagy [136,137]. Niemann pick disease type c, NPC, is a tauopathy caused by mutations that affect intracellular lipid and cholesterol trafficking proteins. NPC patients and mouse models develop an increased autophagic response. The absence of tau-dependent MT stability impaired the autophagic pathway and enhanced overall pathology in *Npc1/Mapt* double knockout mice to suggest a tau-specific role in autophagic trafficking [136]. While the effects of *Mapt* ablation are often overlooked due to the lack of overt phenotype in $Mapt^{0/0}$ mice, we suggest the possibility of unknown, non-redundant tau functions, exposed only under certain stressful conditions. Crossing $Mapt^{0/0}$ mice to other neurodegenerative mouse models expressing non-tau transgenes such as progranulin, TDP-43, Parkin, and CHMP2B, may provide additional insight into non-redundant tau function.

Our results suggest that human tau_{wt} had a greater, though non-significant, effect on dampening tau_{P301L} pathology than endogenous mouse tau. However, the level of human tau expression was much greater than endogenous mouse tau. To directly assess the effects of mouse and human wild type tau, expression levels should be comparable.

Additionally, more comprehensive quantification of tau_{wt} and tau_{P301L} protein levels with antibodies specific to each protein species will be important to make more conclusive claims regarding wild type tau's ability to delay pathology.

The inability of human tau_{wt} to decrease tau_{P301L}-associated pathology when expressed on a *Mapt*$^{+/0}$ background may be a dosage effect. While 7.5 month-old rTg(tau_{P301L}/tau_{wt}) mice, with or without endogenous mouse tau, expressed comparable levels of total tau, quantification of older mice has not been determined. When neuronal loss, NFT, and PHF1 pathology are compared between rTg(tau_{P301L}/tau_{wt}) mice, with or without endogenous mouse tau, all phenotypes were less severe on a *Mapt*$^{0/0}$ background, but significance was not reached. The use of genetically identical mice will help determine if mouse genetic background is a factor. Regardless, the increased phenotype on a *Mapt*$^{+/0}$ background argues against a tauopathy-inhibiting property of endogenous mouse tau.

The transition of developmental tau hypo-to-hyperphosphorylation of tau_{P301L} coincided with conformational alterations and insolubility. Tau hypophosphorylation may be a crucial pre-disease phenotype that requires further investigation. The regulatable mouse system provides the opportunity to suppress transgenic expression during development and early adulthood thereby avoid this stage and allow the dissociation of hypophosphorylation from age-associated tauopathy.

The potential DG developmental delay in mice carrying the activator transgene, Tg(CK-tTA), alone requires further attention. Subtle effects may be important to various model systems using the Tg(CK-tTA) system. DG developmental delay would especially

impact studies focusing on learning and memory, and behavioral phenotypes in mice. We did not conduct behavioral studies on these mice, but future experiments on genetically identical mice should take this into consideration. The amount of leaky transgene expression in Tg(TRE-tau) mice was quite surprising. Fortuitously, they served as an additional experimental group in these studies. They demonstrated that constant low-level tau_{P301L} was not sufficient to drive disease. However, complete absence of transgene expression is an important control. Future experiments should compare FVB/129 F1 mice lacking both responder and activator transgenes to single transgene expressing activator, Tg(CK-tTA), responder Tg(TRE-tau), and rTg mice to fully evaluate subtle effects of individual transgenes alone. Additionally, results from the mixed genetic background mice developed some subtle genotype-specific phenotypes, such as ventricle size, that did not reach significance. Future experiments using genetically identical mice will likely generate more robust and easily interpretable results.

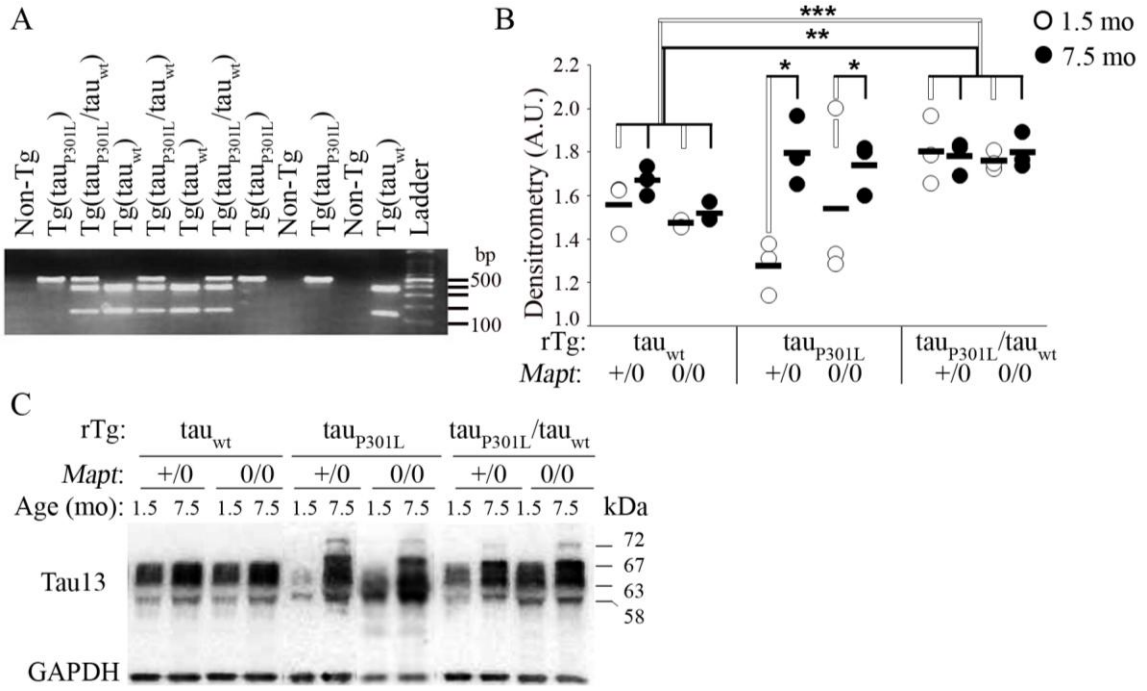

Figure 2.1: Human Tau Genotyping and Protein Expression Levels.
(A) The P301L single base pair mutation disrupted the SmaI restriction enzyme sequence and allowed genotyping of the otherwise identical constructs. Amplified DNA that contained tau_{P301L} remained as an uncut 594 base pair (bp) band while SmaI cleaved tau_{wt} DNA into 126 and 368 base pair bands. DNA from mice carrying both tau_{P301L} and tau_{wt} presented as three distinct bands after SmaI digestion. (B) To distinguish levels of total transgenic human tau protein expression among genotypes, adult mouse brains were analyzed by Western blot with the human tau specific antibody, Tau13. Three mice of each genotype were evaluated at 1.5 and 7.5 months of age. Densitometric normalization to the GAPDH loading control revealed that rTg(tau_{P301L}/tau_{wt}) mice expressed significantly more, 22%, transgenic protein than single transgene-expressing mice at 1.5 months of age. Transgenic protein levels of all tau_{wt}-expressing mice maintained with age, whereas 7.5 month-old rTg(tau_{P301L}) mouse brains contained significantly more transgenic tau than 1.5-month-old rTg(tau_{P301L}) mice. Overall, 1.5 month-old rTg(tau_{P301L}) Tau13 expression was comparable to rTg(tau_{wt}) mice but 7.5 month-old rTg(tau_{P301L}) Tau13 expression was comparable to rTg(tau_{P301L}/tau_{wt}) mice). All tau_{P301L}-expressing mice expressed significantly greater protein levels, 12%, than rTg(tau_{wt}) at 7.5 months of age. (***: ANOVA, $p<0.005$; **: $p<0.01$; *: $p<0.05$. Open lines indicate comparison of 1.5 month-old mice. Solid lines indicate comparison of 7.5 month-old mice). (C) 1.5 month-old and 7.5 month-old human tau_{wt}-expressing mice contained tau migrating from 58-67 kDa whereas rTg(tau_{P301L}) mice, with and without endogenous mouse tau, did not display the higher MW 67 kDa protein until 7.5 months of age. All tau_{P301L}-expressing mice acquired a heavy MW 72 kDa tau species at 7.5 months of age. Mo: months.

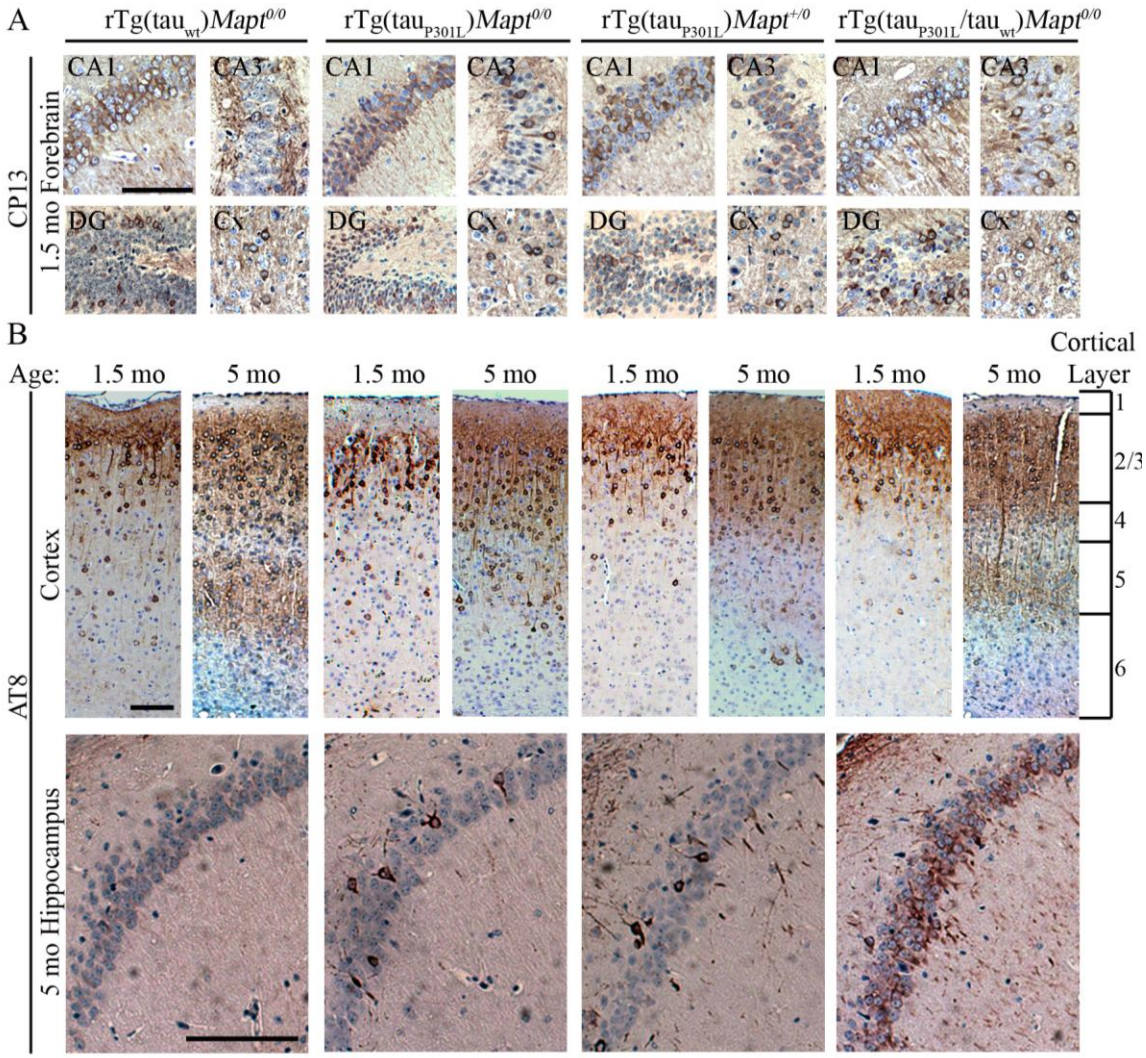

Figure 2.2: All Young Mice Displayed Tau Phosphorylation in Forebrain Cells.
(A) Histological analyses of 1.5 month-old mouse brains revealed CP13 phosphorylation in hippocampal CA1, CA3, and DG; and cortical cells in all human tau-expressing mice. (B) All 1.5 month-old mice displayed AT8 immunoreactivity in peripheral cortical layers 1-3. At 5 months of age, human tau$_{wt}$-expressing mice developed neuritic AT8 staining in cortical cell layer 5 whereas tau$_{P301L}$-expressing mice developed hippocampal AT8 staining. rTg(tau$_{P301L}$/tau$_{wt}$) mice developed both. DG: dentate gyrus; Cx: cortex; mo: month. Scale bar: 100μm.

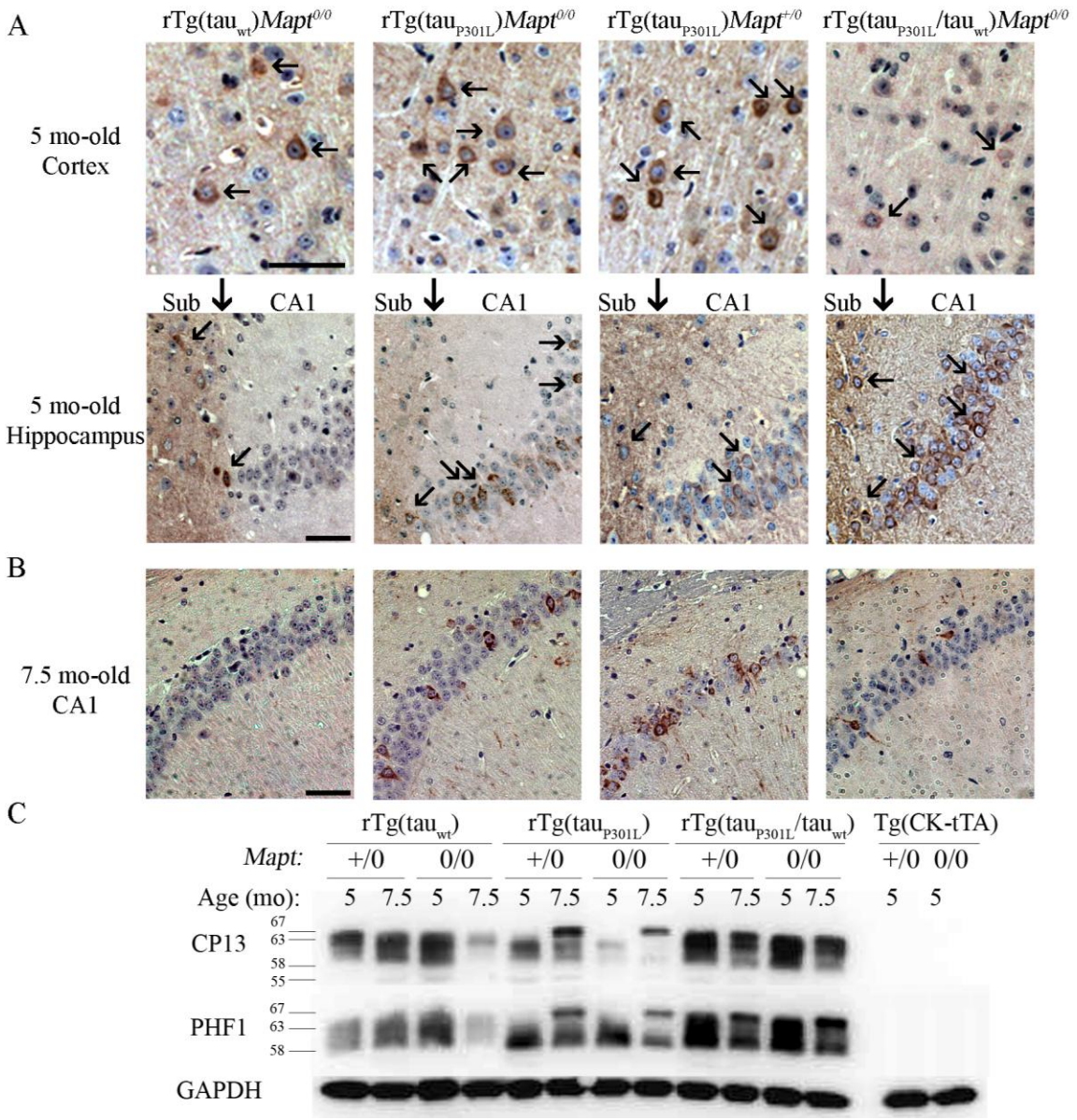

Figure 2.3: Tau$_{wt}$ Was More Heavily Phosphorylated Than Tau$_{P301L}$ in Young Mice.
Prior to overt disease, human tau$_{wt}$–expressing mice contained a more heavily phosphorylated tau species than rTg(tau$_{P301L}$) mice. (A) All genotypes contained PHF1-immunoreactive cortical and subicular cells at 5 months of age. Tau$_{P301L}$-expressing mice developed some CA1 PHF1 immunoreactivity at this age (arrows). (B) By 7.5 months of age PHF1-immunoreactivity had spread throughout the CA1 in all tau$_{P301L}$-expressing mice, but not rTg(tau$_{wt}$) mice. (C) The electrophoretic profile revealed that all 5 month-old tau$_{wt}$-expressing mice contained a more heavily phosphorylated 67 kDa CP13 and PHF1-immunoreactive tau species than 5 month-old rTg(tau$_{P301L}$) mice. rTg(tau$_{P301L}$) mice did not acquire the 67 kDa tau species until 7.5 months of age. Sub: subiculum; arrow indicates subiculum/CA1 border; mo: months. Scale bar: 50μm.

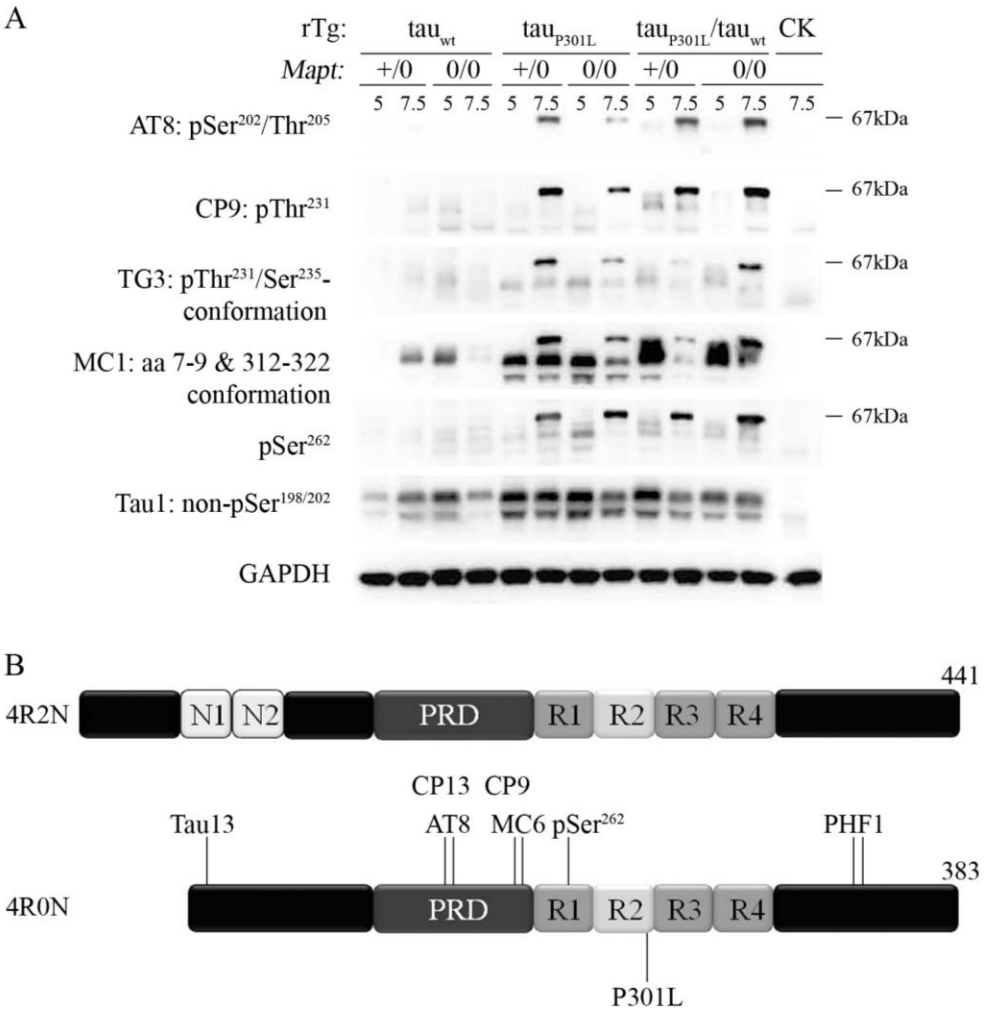

Figure 2.4: Tau_{P301L} Hypo-to-Hyperphosphorylation Transition.
Only tau_{P301L}-expressing mice developed conformational changes associated with phosphorylation at multiple epitopes. (A) Between 5 and 7.5 months of age tau_{P301L}-expressing mice acquired phosphorylation at numerous epitopes coincident with conformational alterations and the appearance of a 67 kDa tau species. All 7.5 month-old tau_{P301L}-expressing mice developed phosphorylation in the PR domain, recognized by AT8, CP9, and MC6; and MTB domain recognized by $pSer^{262}$; and MC1 and TG3 conformation changes. rTg(tau_{wt}) mouse brains were immunoreactive to Tau1 only. All human tau-expressing mice displayed the same Tau1 migration profile indicating the presence of a non-phosphorylated $Ser^{198/202}$ tau species in all genotypes. GAPDH control illustrates comparable loading. (B) The phospho-tau antibody epitopes are based on the longest tau isoform, 4R2N (441 amino acids). 4R2N contains both N-terminal inserts (N1 and N2) and an additional repeat (R2) in the MTB domain. Approximate antibody epitopes and P301L mutation are labeled on the 4R0N transgenic tau isoform expressed in the mice presented here. Antibody sites are labeled above the cartoon; below is the approximate location of the P301L mutation. PRD: proline rich domain.

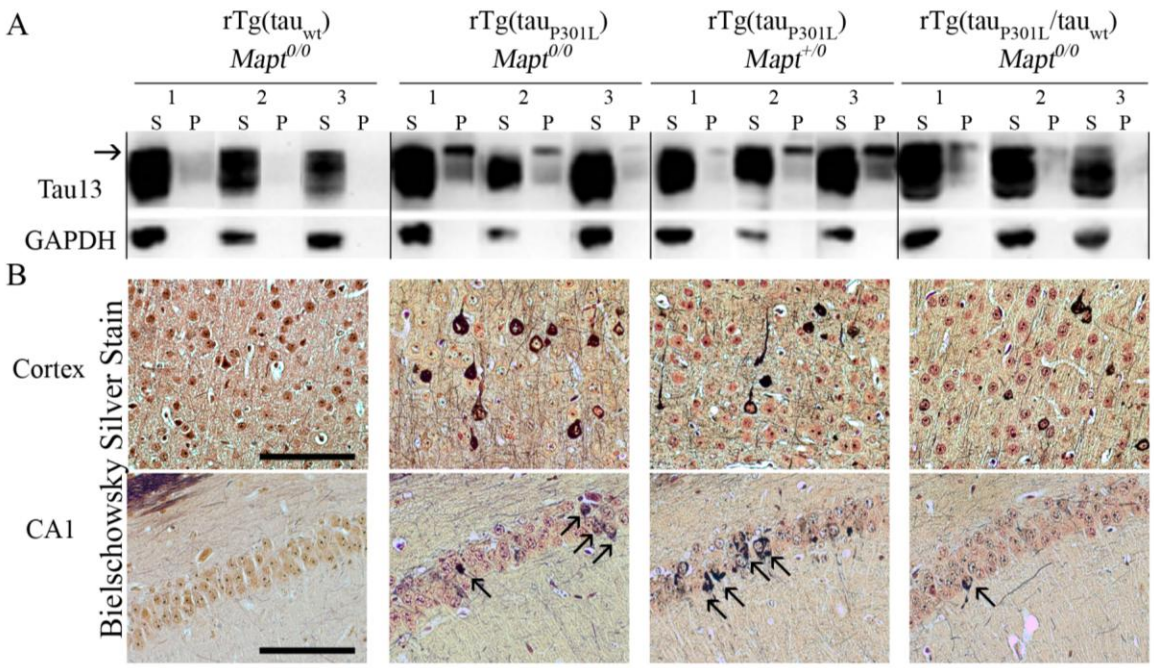

Figure 2.5: Human Tau$_{wt}$ Decreased Tau Aggregate Formation in 7.5 Month-Old Mice. (A) All 7.5 month-old tau-expressing mice contained soluble (S) human tau. Sarkosyl extraction yielded insoluble tau pellets (P) from tau$_{P301L}$-expressing mice. Arrow points to the Tau13-immunoreactive sarkosyl-insoluble pellet present only in tau$_{P301L}$-expressing brain homogenates. (B) The first evidence of cortical and hippocampal NFT lesions, visualized by Bielschowsky silver staining, occurred at 7.5 months of age. Of note, only one rTg(tau$_{P301L}$/tau$_{wt}$) mouse contained an insoluble tau species (A) with very few argyrophilic cells (arrows) (B). rTg(tau$_{wt}$) mice did not contain sarkosyl insoluble tau or silver impregnated cells. Scale bar: 100μm.

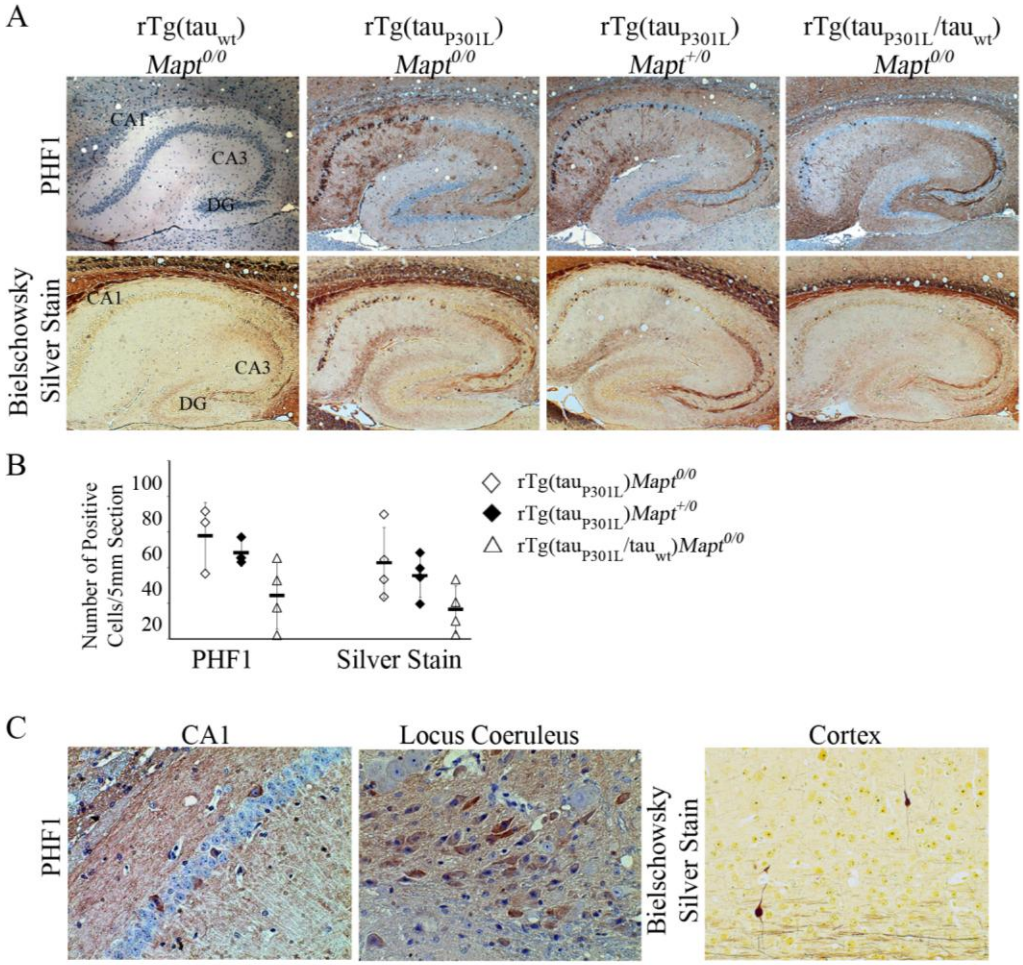

Figure 2.6: Wild Type Tau, Mouse or Human, Decreased PHF1 and NFTs in 12.5 Month-Old Mice.

(A) 12.5 month-old tau$_{P301L}$-expressing mice acquired numerous PHF1 positive cells and argyrophilic cells stained with the Bielschowsky method. Hippocampal CA1 contained the highest density of cells with misprocessed tau. rTg(tau$_{wt}$) brains did not develop these changes (n=7). (B) The number of individual PHF1 and argyrophilic cells in 12.5 month-old mouse brains were counted, plotted, and compared among genotypes. rTg(tau$_{P301L}$)*Mapt*$^{0/0}$ mice contained more cells with pathologically altered tau than age-matched tau$_{P301L}$-expressing mice with wild type tau, mouse or human. (C) 17.5 month-old rTg(tau$_{wt}$) mice displayed pronounced locus coeruleus and hippocampal PHF1 immunoreactivity. Of the 13 aged rTg(tau$_{wt}$) mice (>12.5 months of age) examined, only one contained cortical NFT lesions.

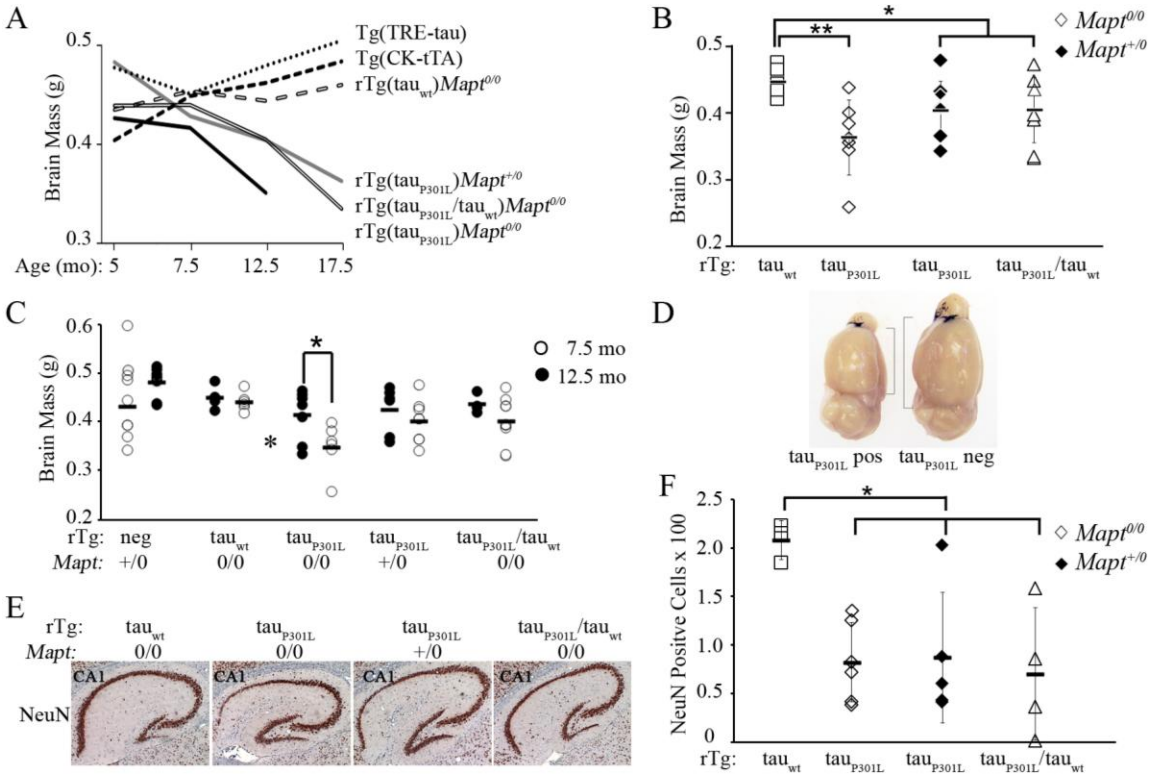

Figure 2.7: Wild Type Tau, Mouse or Human, Delayed Tau_{P301L}-Associated Brain Atrophy.

(A) Average brain weights of 5-17.5 month-old mice were plotted. rTg(tau_{P301L}) mice started to lose brain mass at 7.5 months of age and were significantly atrophied by 12.5 months of age. Tau_{P301L}-expressing mice with wild type tau, mouse or human, had delayed brain atrophy and did not reach the low level brain mass of 12.5 month-old rTg(tau_{P301L})$Mapt^{0/0}$ mice until 17.5 months of age. (n=3-9 for each 5-12.5 month-old genotype; 17.5 month-old points: n=6 rTg(tau_{wt})$Mapt^{0/0}$, n=1 rTg(tau_{P301L})$Mapt^{0/0}$, n=2 rTg(tau_{P301L})$Mapt^{+/0}$, n=2 rTg(tau_{P301L}/tau_{wt})$Mapt^{0/0}$). (B) Plots of 12.5 month-old whole brain weights revealed that all tau_{P301L}-expressing mouse brains were significantly smaller than age-matched rTg(tau_{wt})$Mapt^{0/0}$ brains. The presence of wild type tau, mouse or human, decreased atrophy (**: ANOVA, $p<0.005$; *: $p<0.05$). (C) When compared to genotype-matched 7.5 month-old mice, only 12.5 month-old rTg(tau_{P301L})$Mapt^{0/0}$ mouse brains were significantly smaller than their younger cohorts (*: $p<0.05$). (D) Macroscopic visualization of a 12.5 month-old non-transgene expressing mouse brain (PCR negative for activator and responder transgenes) next to an age matched rTg(tau_{P301L}/tau_{wt}) mouse brain illustrated severe atrophy restricted to the forebrain (area surrounded by brackets). (E) NeuN staining of 12.5 month-old mouse hippocampi illustrated a decrease in the number of NeuN positive hippocampal cells, especially in CA1. (F) NeuN positive CA1 cells were counted and plotted from 5-6 mice of each tau_{P301L}-expressing genotype and compared to rTg(tau_{wt})$Mapt^{0/0}$ mice. 12.5 month-old rTg(tau_{wt})$Mapt^{0/0}$ mice contained significantly more CA1 NeuN positive cells than age-matched tau_{P301L}–expressing mice (*: ANOVA, $p<0.05$). Bars in B, C, and F scatter plots indicate the average value; mo: months.

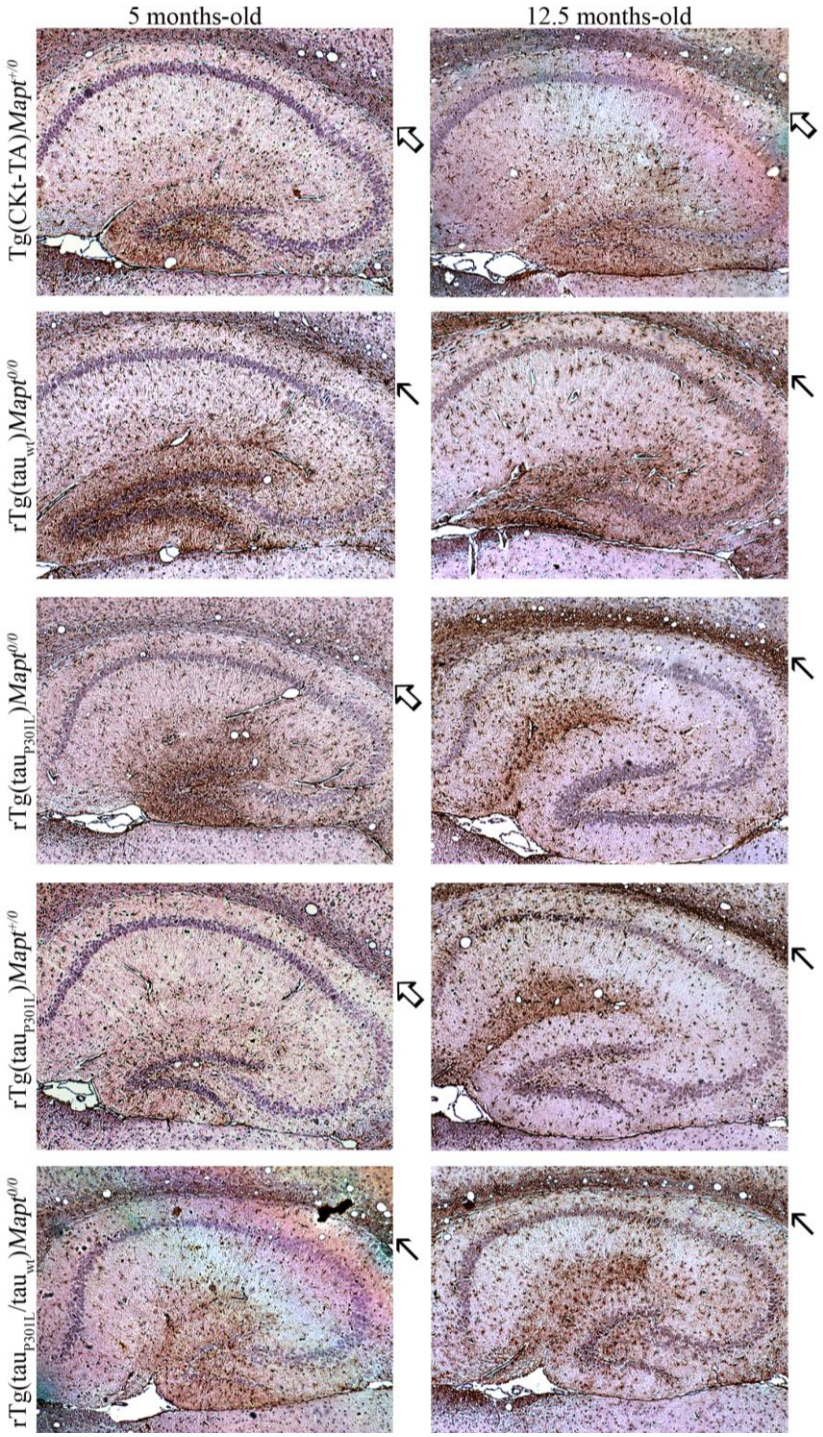

Figure 2.8: Human Tau_{wt} Overexpression-Associated GFAP Staining in 5 month-old Mice.

Immunostaining for the astrocytic GFAP protein revealed that tau_{wt}-expressing mice acquired GFAP-staining in cortical cells surrounding the hippocampus by 5 months of age (closed arrow). rTg(tau_{P301L}) mice did not develop GFAP immunostaining in this region (open arrow) until 12.5 months of age.

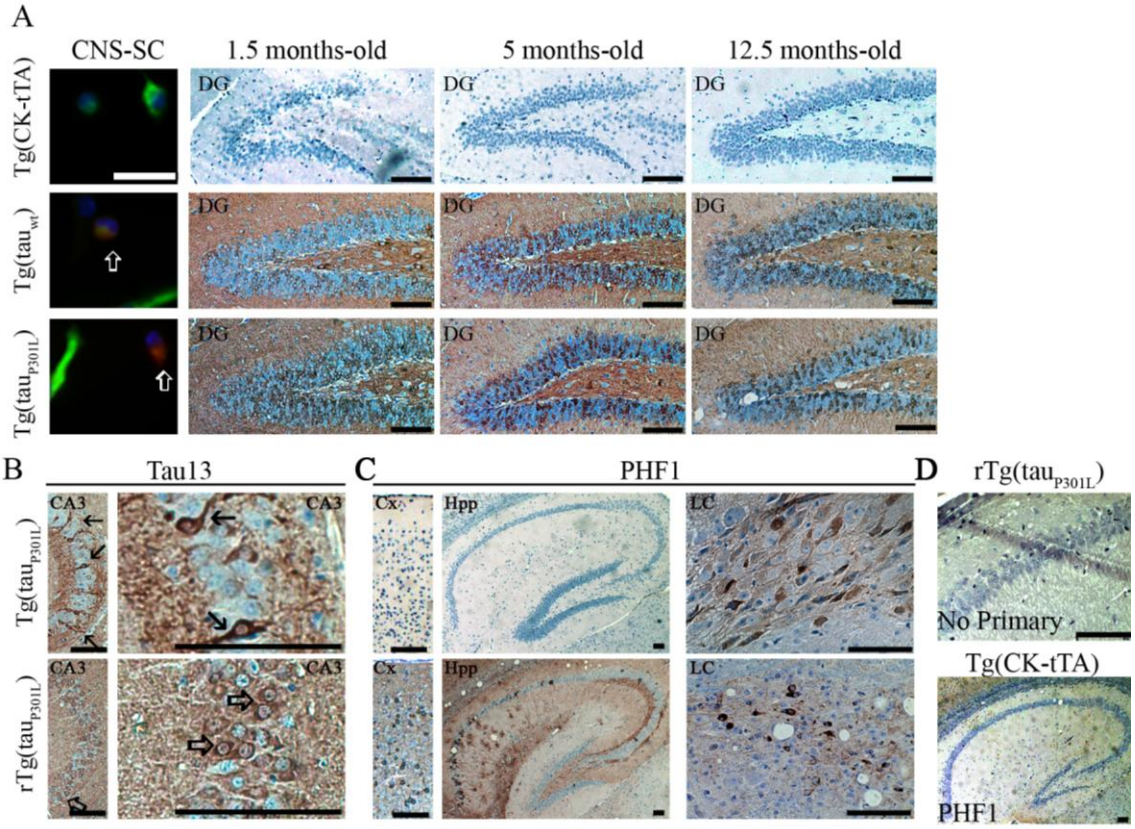

Figure 2.9: Subtle Histological Effects in Control Tg(CK-tTA) and Tg(TRE-tau) Mouse Brains.

(A) Immunostaining with the human tau specific antibody, Tau13, illustrated that Tg(TRE-tau) mice lacking the CK-tTA transgene: Tg(tau_{wt}) and Tg(tau_{P301L}), displayed considerable human tau expression at all ages. Leaky expression occurred early in development and was visible in CNS-SC containing neurosphere cultures harvested from E14 fetuses. Tg(CK-tTA) mice lacking the TRE-tau transgene did not express human tau, but blue hematoxylin nuclei staining indicated they had smaller DGs than age matched Tg(TRE-tau) mice until 12.5 months of age. IFA: Green: nestin neural stem cell intermediate filament; Red: Tau13; Blue: DAPI nuclear stain; Scale bar: 25μm. IHC: Brown chromogen: Tau13; Blue: hematoxylin; Scale bar: 250 μm. (B-C) 12.5 month-old Tg(TRE-tau) mice were compared to age-matched rTg mice to investigate CK-driven human tau overexpression effects. (B) rTg mice contained more Tau13 positive cells than Tg(TRE-tau) mice. Notably, Tau13 staining occurred throughout the axonal projections in Tg(TRE-tau) mice (closed arrow) while it was restricted to the soma in rTg mice (open arrow) Scale bar: 100μm. (C) Leaky human tau protein expression in the forebrain did not result in PHF1-tau phosphorylation; however, hindbrain locus coeruleus cells acquired PHF1-immunoreactivity. (D) Antibody specificity was confirmed. rTg(tau_{P301L}) samples receiving secondary antibody only did not develop immunostaining. Tg(CK-tTA) mice did not develop PHF1 immunoreactivity. Cx: cortex; DG: dentate gyrus; Hpp: hippocampus; LC: locus coeruleus. Scale bar: 100μm.

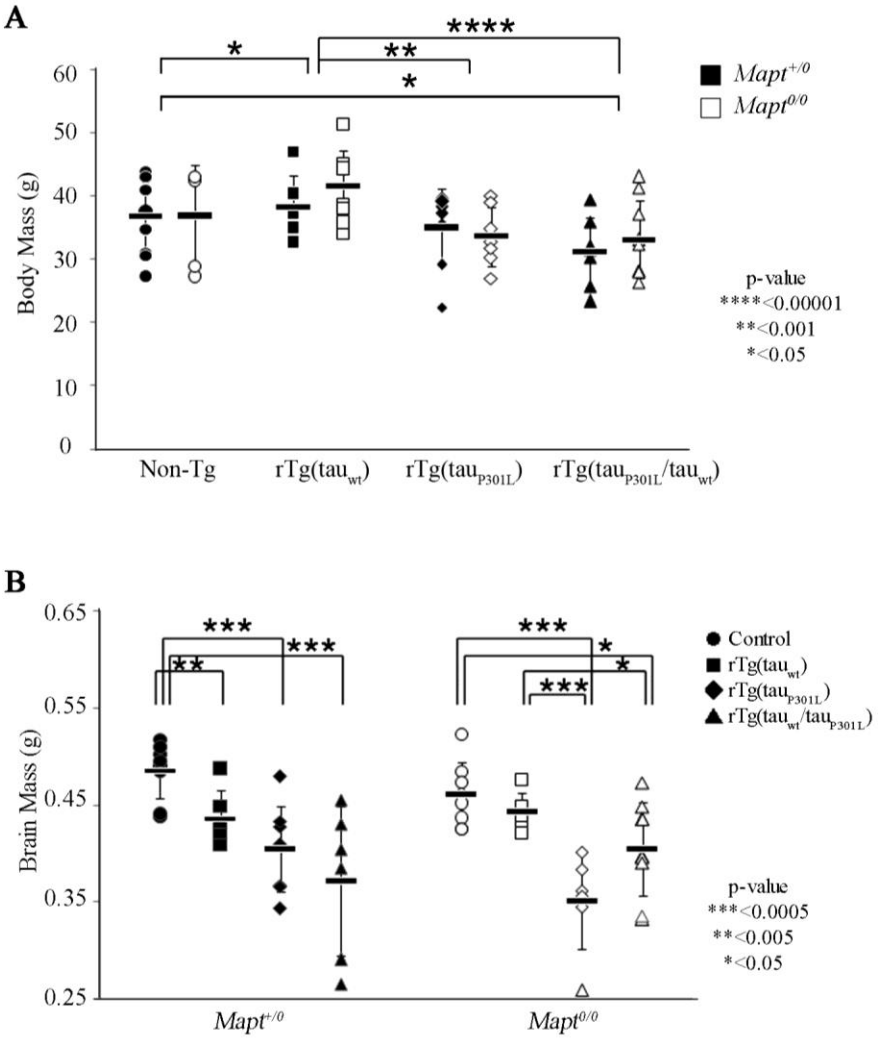

Figure 2.10: Brain and Body Masses of All 12.5 Month-Old Mice.
(A) 12.5 month-old non-transgene expressing control mice were significantly larger than age-matched rTg(tau_{P301L}/tau_{wt}) mice only, and significantly smaller than rTg(tau_{wt}) mice which were significantly larger than all other mice. (B) Comparison of brain mass data from all genotypes revealed that human tau_{wt} only dampened brain atrophy when expressed on a *Mapt*$^{0/0}$ background. rTg(tau_{P301L}/tau_{wt})*Mapt*$^{+/0}$ mouse brains were comparable in size to rTg(tau_{P301L})*Mapt*$^{0/0}$ mouse brains.

Table 2.1: Mouse Genotype and Corresponding Tau Protein Expression.

Genotype	**Human Tau**	**Endogenous Mouse Tau**
rTg(tau_{wt})*Mapt*$^{0/0}$	Wild type	Null
rTg(tau_{wt})*Mapt*$^{+/0}$	Wild type	Heterozygous
rTg(tau_{P301L})*Mapt*$^{0/0}$	Mutant P301L	Null
rTg(tau_{P301L})*Mapt*$^{+/0}$	Mutant P301L	Heterozygous
rTg(tau_{P301L}/tau_{wt})*Mapt*$^{0/0}$	Wild type & Mutant P301L	Null
rTg(tau_{P301L}/tau_{wt})*Mapt*$^{+/0}$	Wild type & Mutant P301L	Heterozygous

GENOTYPE-SPECIFIC DIFFERENCES BETWEEN MOUSE CNS STEM CELL LINES EXPRESSING FRONTOTEMPORAL DEMENTIA MUTANT OR WILD TYPE HUMAN TAU

Introduction

The ability to generate human embryonic stem cell lines by somatic cell nuclear transfer [179] or to produce induced pluripotent stem cells by reprogramming [181] provides the opportunity to capture the genetics of diseased patients. The availability of patient-specific SC lines offers the possibility of transplantation for cell replacement or the delivery of therapeutic agents, and patient-tailored drug therapy. Use of disease-specific SC lines to dissect cellular disease processes is a burgeoning field yielding promising results [165,166,174,187,188,194,199,206, 209,233,261-263].

While our goals are to develop and validate approaches that can be applied to patient-specific cell lines, mouse models offer important advantages for experimental analysis. Each human patient is unique, but members of inbred mouse strains are genetically homogeneous. Inbred mice allow discrimination of variation inherent to SC isolation from genetic effects. Mouse models also allow tracking the subtle biochemical, histological, and behavioral changes that occur long before clinical signs appear. By exploiting SC lines from well-characterized mouse models, we hope to relate cell culture phenotypes to pre-clinical pathogenic events.

Frontotemporal dementia (FTD) is a neurodegenerative disorder in which aggregates comprised of microtubule associated protein tau (MAPT) form in neurons. FTD, like other tauopathies, including Alzheimer's disease (AD), is characterized by tau

phosphorylation and aggregation events associated with neuronal death and dementia. Transgenic mouse lines expressing human MAPT with the FTD proline to leucine mutation at amino acid 301 (P301L) recapitulate aspects of familial FTD [23,80,84,85]. Ashe and colleagues [84,85] developed a regulatable bigenic transgenic line rTg(tau$_{P301L}$)4510 (herein referred to as rTg(tau$_{P301L}$) in which MAPT transgene expression is largely restricted to forebrain cells to avoid early spinal cord pathology that develops in mice with prion protein promoter driven mutant tau [23]. MAPT transgene expression can be suppressed with doxycycline.

Here we report the isolation and characterization of neurosphere lines from rTg(tau$_{P301L}$) mice and from recently created transgenic mice that express comparable levels of human tau$_{wt}$, rTg(tau$_{wt}$)21221, herein referred to as rTg(tau$_{wt}$) [114]. These multi-cellular aggregates consist of CNS-SCs, lineage-committed, and differentiated cells [213,215-217]. The effects of genetic alterations on cell proliferation, differentiation, and mature cell types can be assessed in neurosphere cultures [213,215]. We evaluated human tau$_{P301L}$ and human tau$_{wt}$ expressing mice and their SC derivatives for tau phosphorylation. Neurospheres recapitulated genotype-specific differences seen in mice, and we found cell line and genotype-dependent differences in the fraction of transgene expressing cells, the level of phosphorylation, and in filopodia-spine densities.

Materials and Methods

Generating Mice

rTg(tau$_{P301L}$) [85] and rTg(tau$_{wt}$) mice were generated using a bigenic system of responder and activator transgenes. Tg(tau$_{P301L}$) and Tg(tau$_{wt}$) mice carry their

corresponding tetO-tau4R0N responsive element (TRE) transgenes and were produced and maintained on the FVB/NCr background. Tg(CK-tTA) mice that express a calcium/calmodulin-dependent protein kinase IIα-driven tet transactivator transgene have been described previously and are congenic on a 129S6 genetic background [81,85]. The TRE-tau_{wt} construct was identical to that used to construct Tg(tau_{P301L})4510 mice except for the presence of a wild type proline codon at position 301. The rTg(tau_{wt})21221 line expressed human tau at levels comparable to rTg(tau_{P301L})4510 [114]. All rTg mice and their controls, which expressed either the CK-tTA or TRE-tau transgene alone, were genetically homogeneous (FVB x 129)F1 hybrid mice.

$Mapt^{tm1(GFP)Klt}$ Tg(MAPT)8cPdav/J mice, referred to as 8c$Mapt^{0/0}$, have a targeted disruption of mouse *Mapt* exon one and express a complete human MAPT transgene. They have been described previously [129,242]. Breeder pairs of mixed genetic background were obtained from the Jackson Laboratory. For these experiments, we genetically bred out the 8c human tau transgene to produce mice lacking endogenous mouse tau. These mixed background $Mapt^{0/0}$ mice were mated with Tg(tau_{wt}), Tg(tau_{P301L}), or Tg(CK-tTA). Mice hemizygous for activator or responder transgenes and heterozygous for endogenous *Mapt* were backcrossed to the $Mapt^{0/0}$ line to produce Tg(tau_{wt})$Mapt^{0/0}$, Tg(tau_{P301L})$Mapt^{0/0}$, and Tg(CK-tTA)$Mapt^{0/0}$ mouse lines on a mixed genetic background that were used to produce rTg mice with both the responder and transactivator transgenes.

Generation, Maintenance, and
Differentiation of Neurosphere Lines

Tg(tau_{wt}) or Tg(tau_{P301L}) females were mated with Tg(CK-tTA) males. Neurospheres were isolated from whole brains from individual E14 fetuses as described previously [215,264]. The cells were grown in "Complete" NeuroCult NSC Proliferation Medium comprised of NeuroCult NSC Basal Medium (Stem Cell Technologies (SCT)) supplemented with Proliferation Supplement (SCT), 20ng/mL rhEGF (SCT), and penicillin/streptomycin (GIBCO). The neurosphere sex was determined by PCR genotyping for the X and Y chromosome genes *Smcx* and *Smcy* [265]. For passage, neurospheres were enzymatically dissociated to single cells using the Papain Tissue Dissociation Kit as per the manufacturer's instructions (Worthington Biochemical Corporation). Dissociated cells were seeded at a concentration of 10^5 cells/mL in 15mLs "Complete" NeuroCult NSC medium (Stem Cell Technologies) and maintained in a humidified incubator at 37°C in 6% O_2 and 6% CO_2 (balance N2). Neurosphere lines were passaged every 5-7 days. Time of passage was determined by neurosphere density and media color change. Colorimetric cell proliferation assays (MTT) to assess neurosphere growth rates were conducted according to the manufacturer's recommendations (Cell Growth Determination Kit, Sigma).

For immunofluorescent analysis (IFA) or immunohistochemistry, undifferentiated single cells, $8x10^4$ cells/well, were plated on fibronectin (Invitrogen) coated 24-well glass bottom plates (Greiner) and placed in a humidified incubator at 37°C at 6% oxygen overnight.

To induce neural differentiation, dissociated cells were plated on laminin/poly-L-ornithine (15μg/mL poly-L-ornithine and 5μg/mL laminin) 24-well coated glass plates at a density of $12x10^4$ cells/well in complete NeuroCult medium (SCT). After overnight culture the growth factor-containing medium was removed and 0.3μmol retinoic acid was added every other day for seven days. Every other day, between days 8-25, cells were fed with B27-containing medium (Gibco). IFA was performed on day 21 or 25.

Immunoblots

Adult mouse hemibrains for Western blot analysis were prepared as described previously [85]. Mouse brains and neurospheres were homogenized in ice cold buffer consisting of 10mM Tris-HCl, 1mM EGTA, 0.8M NaCl, 10% sucrose, pH 7.4, Complete Protease Inhibitor Cocktail (Roche), and Phosphatase Inhibitor Cocktail II (Calbiochem). 20μg protein equivalent from adult brain homogenates, $3x10^6$ cells from neurosphere lysates, or 10μL from a 10% embryonic brain homogenate were electrophoresed on 12% Bis-Tris gels (Invitrogen) and electro-blotted onto PVDF membranes (Millipore). In some cases, neurosphere samples were treated with phosphatase prior to running; protein lysates were suspended in 0.5μg/10μL of NEBuffer 3 (New England Biolabs) and incubated with 10U/μL of calf intestinal phosphatase (CIP) (New England Biolabs) for 60 minutes at 37°C. We used the following anti-tau antibodies: Tau13 at 1:5000 (Covance); Tau1 at 1:200 (Chemicon); CP13, AT8, PHF-1, and DA9 (provided courtesy of Dr. Peter Davies) at 1:200. The specificity of these antibodies is summarized in Table 3.1. Loading control anti-GAPDH was used at 1:2000 (Chemicon). Goat anti-mouse HRP-conjugated IgG (Biorad) secondary antibody was diluted 1:10,000. SuperSignal

West Pico reagent (Pierce) was used for membranes probed with Tau13, Tau1, PHF-1, and DA9; the ECL Plus substrate (Amersham) was used for membranes probed with phospho-tau antibodies CP13 and AT8 and to detect immunoreactivity. For both chemiluminesence systems, membranes were incubated with substrate for 3 minutes. Chemiluminescence was detected using a Biorad VersaDoc at 3-5 minute exposures. Tau levels were normalized to GAPDH levels to correct for loading differences.

Immunofluorescence (IFA)

For whole neurosphere IFA, neurospheres were fixed in 4% phosphate buffered paraformaldehyde followed by 30% sucrose and equilibrated at 4°C overnight. Fixed neurospheres were placed in embedding medium (Sakura Tissue-Tek O.C.T.) and snap frozen in liquid nitrogen. Neurospheres were sectioned at -15ºC; 8µm sections were adhered to SuperFrost Plus microscope slides (Fisher) and stored at -20ºC for later IFA. Cryosectioned neurospheres were stained with the following primary antibodies: rabbit anti-Nestin at 1:200 (Covance); mouse anti-human Tau13 at 1:5000 (Covance); mouse anti-Tau46 at 1:600 (Cell Signaling). The secondary antibodies Alexa488-goat anti-mouse and Alexa546-goat anti-rabbit were used at 1:1500 dilution (Molecular Probes).

For analysis of individual undifferentiated cells plated on fibronectin substrate and differentiated cells plated on LPO substrate, cells were fixed at 37°C in PIPES fixative (0.1 M PIPES, 1.0mM EGTA, 3mM $MgSO_4$ and 3% PFA). Cells were permeabilized in 0.3% Triton X-100, placed in blocking buffer (5% normal goat serum, 5% glycerol, and 0.04% sodium azide in PBS), then incubated in primary antibody. Primary antibodies Tau13, Tau46, Tau1, CP13, AT8, PHF-1, and DA9 were used at

dilutions described above. Rabbit anti-β tubulin III at 1:2000 (Covance); chicken anti-MAP2 at 1:10,000 (Covance); and rabbit anti-GFAP at 1:1000 (Chemicon) also were used. The following secondary antibodies from Molecular Probes were diluted 1:1500: goat anti-mouse Alexa Fluor 546; goat anti-mouse Alexa Fluor 488; goat anti-rabbit Alexa Fluor 546; goat anti-rabbit Alexa Fluor 488; goat anti-rabbit Alexa Fluor 647. The goat anti-chicken Alexa Fluor 488 antibody was from Jackson ImmunoResearch, Inc. and used at 1:200. Cells were coverslipped with ProLong Gold antifade reagent containing DAPI (Invitrogen). Images were acquired with a Nikon Eclipse TE2000 microscope and analyzed with MetaMorph software. The proportion of total cells expressing human tau (Tau13 positive) was determined for each cell line. Fluorescence intensity and area stained, the threshold parameters, were based on Tg(CK-tTA) control cell fluorescence and fluorescence of cells incubated only with secondary antibody. All image acquisition and cell counts were conducted by an experimenter blind to genotype.

Immunohistochemistry (IHC)

Cryosectioned neurospheres were thawed overnight and the Vector M.O.M. peroxidase immunodetection kit was used to detect transgene expression (Vector Laboratories, Inc.) per manufacturer's instructions. Neurospheres were probed with Tau13 at a dilution of 1:5000.

Filopodia-Spine Counts

To determine filopodia-spines densities, total Map2 positive neurite lengths were measured 21 or 25 days post-differentiation; the experimenter was blind to genotype. All Map2-positive projections were measured using MetaMorph software and counted along

the Map2 positive neurites; projections >12μm were called neurites and <12μm were called filopodia-spines. The number of filopodia-spines/100μm was calculated. Between 75-100 total Map2 and TUJ-1 double positive cells were counted from each cell line. The average filopodia-spine density/cell was calculated for each cell line.

Statistical Analyses

ANOVA and paired t tests were performed using StatView 5 for Macintosh (SAS Institute, Inc.).

Results

CK-tTA-Driven TRE-Tau Transgenes Were Expressed in Neurospheres and Fetal Mice.

We previously generated a transgenic line, referred to as Tg(tau_{wt}), that harbors human wild type 4R0N tau transgenes driven by the same TRE, as Tg(tau_{P301L}). When crossed to Tg(CK-tTA) mice, the resulting rTg(tau_{wt}) mice express human wild type tau at levels comparable to those in rTg(tau_{P301L}) mice [114]. We refer to mice and cultures that carried both responder and activator transgenes as rTg, and refer to those that carried only the activator or responder transgene as Tg(CK-tTA) and Tg(TRE-tau) controls, respectively. Activator and responder mouse lines were maintained hemizygous for their respective transgenes, therefore one-fourth of all pups were expected to contain both the activator and responder transgenes and express the protein of interest.

Expression of *CKII*α is largely restricted to forebrain neurons [82]. CK mRNA [83] and CK-tTA-driven tau_{P301L} expression [84] have been reported to be absent in mice until postnatal day 3. In contrast, our WB analysis showed CK-driven expression of

human tau_{wt} and human tau_{P301L} as early as embryonic day 12 (E12) (Figure 3.1A-C). This verified transgene expression prior to E14, the developmental age that neurospheres are harvested.

rTg(tau_{wt}) and rTg(tau_{P301L}) Neurospheres
Expressed Human Tau at Comparable Levels.

Neurosphere cultures were generated from individual fetuses from Tg(CK-tTA) x Tg(tau_{wt}) and Tg(CK-tTA) x Tg(tau_{P301L}) matings, and were genotyped. All cultures grew as non-adherent free-floating aggregates characteristic of neurospheres (Figure 3.1D). Neurospheres were probed with antibody for nestin, an intermediate filament protein expressed by CNS-SCs, and were tested for human tau protein expression by IFA and WB with the Tau13 antibody. Nearly all cells in neurospheres were nestin-positive (Figure 3.1E-G). Neurospheres from rTg(tau_{P301L}) and rTg(tau_{wt}) cultures contained cells that also expressed human tau (Figure 3.1F-G), but Tg(CK-tTA) controls did not (Figure 3.1E). Western blot analyses on neurosphere lysates confirmed human tau expression in rTg(tau_{P301L}) and rTg(tau_{wt}) neurospheres, and showed that, as in mice, transgenic human tau was expressed at comparable levels in both genotypes (Figure 3.1H).

Tau Expression Variability Among Individual
Neurospheres and Independent Cell Lines.

Individual neurospheres in a single cell line varied in transgene expression. Cryosectioned neurospheres stained with Tau13 indicated that transgene-expressing cells were not preferentially located at the periphery or deep within most spheres (Figure 3.1F, G; 3.2G), but transgene expression within neurospheres varied within a single culture. Some neurospheres in a culture contained nearly 100% tau transgene expressing cells,

whereas other neurospheres from the same culture contained few, if any, human tau-expressing cells (Figure 3.2G).

At passages 3 and 6 we papain dissociated, fixed, and immunostained neurospheres (Figure 3.2). Individual cells within neurospheres are tightly bound with a rich extra-cellular matrix [217-219], which makes them difficult to dissociate without compromising cell integrity. Various protocols were evaluated for their ability to fully dissociate neurospheres into single cells, and cell viability was determined by Trypan blue exclusion. Mechanical dissociation with trituration, and enzymatic dissociation with blendzyme proved inefficient. Many cell aggregates remained, and both methods damaged cell integrity, 43% and 10% cell death, respectively. Papain successfully dissociated neurospheres into viable single cell cultures without compromising cell membranes and was used here.

We analyzed individual cells for human tau protein levels by measuring Tau13 fluorescence intensity (Figure 3.3). Total cell numbers were based on intermediate filament nestin and nuclear DAPI stains. The fraction of cells that expressed human tau was determined. A cell was considered positive for transgene expression if its Tau13 fluorescence was greater than the background fluorescence seen when incubated only with secondary antibody. Figure 3.2A and 3.2B show cells strongly positive with Tau13 in rTg cultures. Figures 3.2C and 3.2D indicate cells with very low level expression of human tau in Tg(TRE-tau) cultures carrying the responder transgene, but lacking the transactivator transgene; such minimally reactive cells were not seen in cultures positive only for the transactivator transgene (Figure 3.2E and 3.2H). Cell lines generated from

rTg(tau_{wt}) fetuses contained a higher proportion of cells expressing human tau than cultures harvested from rTg(tau_{P301L}) fetuses (Figure 3.3A). This was consistent among four independent experiments (ANOVA, $p<0.0001$). Each experiment was comprised of 2-4 independent rTg cell lines each produced from individual littermate pups harvested at the same time from Tg(CK-tTA) x Tg(tau_{wt}) and Tg(CK-tTA) x Tg(tau_{P301L}) matings. The percentage of cells expressing tau_{P301L} was less in each experiment that the percentage of cells expressing tau_{wt}, though comparison between lines derived from fetuses harvested at different times showed some overlap between mutant and wild type lines. The fraction of positive cells for each cell line persisted over passage.

We evaluated the Tau13 fluorescence intensity of transgene expressing cells. Transgene-positive cells were binned (1 to >10) based on fluorescence intensity (Figure 3.3B). The "dim" cells indicated by the open arrows in Figure 3.2C and 3.2D fall in bin 1, while the bright cells in Figure 3.2A and 3.2B are in bins 6 to >10. While the rTg(tau_{P301L}) cultures had a lower proportion of total cells expressing human tau (Figure 3.3A), they contained a greater proportion of cells that expressed higher levels of tau (brighter fluorescence intensity) (Figure 3.3B). We have shown the intensity histogram from one experiment (Experiment 3 from Figure 3.3A). Due to inherent variability with immunofluorescence not all independent experiments had the same fluorescence intensity scale therefore were not all plotted together. The Tg(TRE-tau) cultures, which expressed the responder transgene alone, contained a fraction of cells, approximately 41% of Tg(tau_{P301L}) cells and 19% of Tg(tau_{wt}) cells, that expressed human tau at very low levels consistent with the leaky expression reported previously [85,266].

Generation of Neurospheres From
Alternative Responder and Activator Lines.

In attempt to resolve whether or not the proportion of transgene expressing cells was due to transgene insertion site differences or due to the tau_{P301L} mutation, we generated neurospheres from alternative Tg(TRE-tau) responder lines, but used the same Tg(CK-tTA) activator mouse line. All responder lines carried the same human tau_{P301L} or tau_{wt} variants, but when crossed to Tg(CK-tTA) mice, the resulting rTg mice express lower levels of transgenic tau protein than rTg(tau_{P301L})4510 and rTg(tau_{wt})21221. We used the following alternative Tg(TRE-tau) responder lines: Tg(tau_{wt})14238, Tg(tau_{P301L})14718, and Tg(tau_{P301L})14319.

In a single experiment we looked for the percent of human tau expressing cells present in neurosphere cultures harvested from rTg fetuses derived from these alternative mouse lines. We paired rTg(tau_{wt})14238 with rTg(tau_{P301L})14718 mice. These two mouse lines express human tau at comparable levels to each other, which is 50% less than rTg(tau_{P301L})4510 and rTg(tau_{wt})21221. The neurosphere culture derived from rTg(tau_{wt})14238 mice expressed human tau in fewer cells (42.5%) than three neurosphere cultures derived from rTg(tau_{P301L})14718 neurospheres (46%, 45%, 71%) (Figure 3.4A); this result does not agree with rTg(tau_{wt})21221 which express tau in a greater proportion of cells than rTg(tau_{P301L})4510 (Figure 3.3). The third transgenic mouse line we investigated, rTg(tau_{P301L})14319, expresses human tau at approximately 75% the level as rTg(tau_{P301L})4510; we did not have a comparable tau_{wt} mouse to match. The neurosphere culture derived from rTg(tau_{P301L})14319 mice contained 60% human tau expressing cells (Figure 3.4A). In general, neurosphere cultures derived from different mouse lines

expressed human tau in proportions of cells unique to the founder mouse line. Interestingly, the tau_{P301L}-expressing cultures contained more similar proportions of human tau-expressing cells across mouse lines than tau_{wt}, whereas the alternative tau_{wt}-line expressed at a much lower level than rTg(tau_{wt})21221.

We also investigated tau_{P301L}-expression with different promoter systems. Tg(tau_{P301L}) mice were crossed to three distinct promoter-tTA mouse lines. Tg(CK-tTA) driven tau_{P301L} results were compared to tau_{P301L} driven by the prion promoter, Tg(Prnp-tTA), or neuropsin promoter for entorhinal cortex (EC) expression, Tg(EC-tTA) (Figure 3.4B, C). The forebrain specific promoter, Tg(CK-tTA) generated the largest proportion of transgene expressing cells: 64.1% and 62.7% (Figure 3.4B). However, this particular litter only yielded 2 rTg cultures so statistics could not be conducted with Tg(CK-tTA) driven tau_{P301L} expression. rTg(tau_{P301L}) from Tg(Prnp-tTA) cultures contained significantly more transgene-expressing cells, 51.6% +/- 1.8% (n=8), than rTg(tau_{P301L}) from the Tg(EC-tTA) cross which contained 46.1% +/- 7.6% (n=5) ($p<0.05$) (Figure 3.4B). However, when fluorescence intensity histograms were compared to Tg(TRE-tau) controls with leaky expression, only CK-tTA driven rTg(tau_{P301L}) cultures contained cells with fluorescence above leaky expression (Figure 3.4C) indicating that they were the only cell lines with promoter driven expression. The remaining experiments presented here were conducted on rTg(tau_{wt})21221 and rTg(tau_{P301L})4510 neurospheres with the CK-tTA promoter system only.

Mutant Human Tau Was Less
Phosphorylated Than Wild Type
Human Tau in Neurospheres and Mice.

Characteristic of tauopathy patients and the rTg(tau_{P301L})4510 FTD mouse model is adult onset of tau misprocessing, primarily phosphorylation. To determine if tau phosphorylation occurred in neurospheres, we used a battery of phospho-tau specific antibodies. Due to the numerous sites for phosphorylation and other post-translational modifications of the tau protein, immunoblotted tau most often does not resolve as distinct bands but instead as a heterogeneous protein smear. To discriminate distinct tau species within the total tau population, we used antibodies specific to total tau (DA9), human tau (Tau13), and phospho-tau epitopes (CP13, AT8, PHF-1, Tau1; see Table 3.1 for epitope specificity). Each antibody was probed on independent membranes simultaneous with GAPDH; the GAPDH blot presented is from the Tau1 blot.

Immunoblotting with DA9 allowed us to determine total tau (mouse and human) expression and visualize the electrophoretic migration pattern of tau from both species (Figure 3.5A.) Densitometric analysis with DA9 indicated that rTg neurospheres expressed over five-times the amount of total (mouse and human) tau protein than Tg(CK-tTA) control samples (Figure 3.5B). The migration profile revealed by DA9 showed a distinct band migrating at ~52 kDa cultures with mouse tau (Figure 3.5A). This band was absent in non-transgene expressing control samples from *Mapt*$^{0/0}$ neurospheres indicating that it was 3R mouse tau, the only tau isoform expressed in mice during development [267] (Table 1.1). Compared to non-transgene expressing controls (shown here: Tg(CK-tTA) and Tg(TRE-tau_{P301L}), rTg samples had additional DA9 signals that appeared as a dense series of diffuse bands up to ~60 kDa in rTg(tau_{wt}) samples and ~58

kDa in rTg(tau_{P301L}) samples. Strikingly, the diffuse band in tau_{wt}-expressing samples had a slower migrating component than tau_{P301L}-expressing samples.

To better characterize the tau species within the diffuse bands and the nature of the slower migrating tau_{wt} band, we used human-specific Tau13, phospho-tau specific antibodies, and alkaline phosphatase treatment. The diffuse series of bands in rTg samples and the slower migrating tau_{wt} species were observed with the Tau13 antibody confirming that they contained transgene-encoded human tau (Figure 3.5A). All control samples lacked Tau13 signal demonstrating human tau specificity. We analyzed the neurosphere lysates for phosphorylated epitopes using CP13, AT8, and PHF-1 (MC6 not shown) phospho-tau antibodies. The phospho-tau immunoreactivity in Tg(CK-tTA) and Tg(TRE-tau) control samples was endogenous mouse tau and appeared as distinct 52 and 53 kDa bands (Figure 3.5A). Human transgene expressing samples with mouse tau contained the 52 and 53 kDa bands with an additional protein smear up to ~60 kDa in rTg(tau_{wt}) samples and to ~58 kDa in rTg(tau_{P301L}) samples indicative of phosphorylated human tau. Strikingly, the slower migrating tau_{wt} band became more apparent with the phospho-tau antibodies providing evidence that it was a phosphorylated tau species. Densitometric normalization to GAPDH, showed that rTg samples had greater immunoreactivity to CP13 (2.9x), AT8 (1.9x), and PHF-1 (2.4x) than non-transgene expressing controls (Figure 3.5B). Significant differences between rTg(tau_{wt}) and rTg(tau_{P301L}) were not reached, though immunoreactivity was stronger in rTg(tau_{wt}) with all antibodies except with Tau1 (Figure 3.5B). The Tau1 antibody recognizes tau species that are not phosphorylated at or near $Ser^{198/202}$, and has decreased immunoreactivity

when tau is phosphorylated at these epitopes. Tau1 levels determined by densitometry was slightly greater in rTg(tau_{P301L}) expressing cultures indicating a larger proportion of non-phosphorylated tau species in tau_{P301L} cultures than in tau_{wt} cultures.

Tau1 immunoreactivity and phosphatase treatment revealed that the migration difference between tau_{wt} and tau_{P301L} was due to phosphorylation. Both tau_{wt} and tau_{P301L}-expressing cultures contained Tau1-immunoreactive non-phosphorylated tau with identical banding patterns migrating at ~53 and 52 kDa (Figure 3.5A). Tg(TRE-tau) and Tg(CK-tTA) samples displayed only the 52 kDa band with Tau1 representing non-phosphorylated mouse tau. We treated lysates with calf intestinal phosphatase (CIP); to examine human tau only, we analyzed neurosphere lysates from tau_{wt} and tau_{P301L} expressing cultures lacking endogenous mouse tau. Phosphatase treatment abolished the higher molecular weight bands (>52 kDa) providing evidence that they were phosphorylated human tau (Figure 3.5C). Only a single tau band migrating at ~52 kDa, the known molecular weight of recombinant human tau 4R0N [37], remained after phosphatase treatment in both samples (Figure 3.5C). Collectively, our data indicated that the difference between mutant and wild type tau protein migration was due to phosphorylation, and not other post-translational modifications. We did not recover sarkosyl insoluble tau indicating that insoluble tau aggregates did not form in undifferentiated cultures (data not shown).

Mapt$^{0/0}$ cultures have not been fully characterized. Here we used them to help distinguish between mouse and human tau bands. The wt_3 rTg(tau_{wt})*Mapt*$^{0/0}$ culture with low total tau (DA9) and human tau (Tau13) immunoreactivity (Figure 3.5A) may be due

to the low proportion of human tau expressing cells (42%) compared to the other rTg(tau_{wt})$Mapt^{0/0}$ culture, wt_4 with 62% tau-expressing cells.

Brain homogenates from E14, the developmental stage at which neurospheres were harvested, and adult 2.5 month-old mice were analyzed for tau phosphorylation. As seen in neurospheres, rTg(tau_{wt}) homogenates displayed a distinctly slower migrating tau species than rTg(tau_{P301L}) (Figure 3.5D) demonstrating that neurospheres reliably model several tau phosphorylation events that occur *in vivo*. The difference in electrophoretic motility between tau_{wt} and tau_{P301L} is seen in adult mice until 7.5 months of age (Chapter 2 Figure 2.1, 2.3, 2.4). Of note, a lower molecular weight tau isoform intensely stained with phospho-tau antibodies in E14 brains was absent in 2.5-month-old mice. During embryonic development, the vast majority of expressed tau is a low molecular weight (~48 kDa without modifications) [267] heavily phosphorylated 3R tau isoform [46,70]. By postnatal day 24 fetal tau isoforms have been replaced with larger, though less phosphorylated, tau isoforms [238,267,268]. The lower molecular weight tau species unique to E14 brains likely represents heavily phosphorylated fetal tau. Also of note, adult rTg(tau_{wt}) mice contained a higher molecular weight Tau1-immunoreactive tau species than adult rTg(tau_{P301L}), suggesting that young adult rTg(tau_{wt}) mice express a tau species not phosphorylated at $Ser^{198/202}$ that is either more heavily phosphorylated at other epitope(s), or has other post-translational modifications distinct from tau_{P301L}. Results from these analyses are summarized in Table 3.1.

To help discern the differences in tau phosphorylation we utilized IFA to analyze individual cells within each culture. We looked for tau phosphorylation in single cells

from dissociated neurospheres (Figure 3.6). Phospho-tau immunoreactivity was present throughout the cell body with all antibodies. Additionally, the AT8 antibody revealed focal staining in nuclei of all genotypes expressing mouse tau (Figure 3.6B). The staining was absent in *Mapt*$^{0/0}$ cells providing evidence that it was of mouse origin, and may represent binding of 3R pSer^{202}/Thr^{205} mouse tau to nucleolar organizing regions as reported previously [269-271]. Visualization of this nuclear mouse tau species indicated that overexpression of human tau likely does not compromise, or interfere with, endogenous mouse tau's physiological functions.

For each cell culture we determined the proportion of nestin stained cells also immunoreactive with phospho-tau antibodies (Figure 3.6C). There was no difference in the proportion of PHF-1 immunoreactive cells across genotypes. Nearly all cells in all genotypes contained PHF-1 immunoreactive tau. Both tau_{wt} and tau_{P301L}-expressing cultures contained a significantly higher proportion of CP13 (pSer^{202}) immunoreactive cells compared to Tg(CK-tTA) control cultures ($p<0.05$), but the difference between tau_{wt} and tau_{P301L} was not significant. While the proportions of cells with phospho-tau did not differ between tau_{wt} and tau_{P301L}, the fluorescence intensity histograms for CP13 (Figure 3.6D, G) and PHF-1 (Figure 3.6F, G) revealed that tau_{wt} cultures contained more cells with strong fluorescence intensity than tau_{P301L}. These cells containing intensely phospho-tau immunoreactivity may correlate with the slower migrating tau bands seen in WBs. The fluorescence intensity of AT8-positive cells was comparable among genotypes (Figure 3.6E), and only tau_{wt}-expressing cultures contained significantly more AT8 positive cells than control cultures ($p<0.01$) (Figure 3.6G).

Transgenic Human Tau Expression Did Not
Alter Stem or Progenitor Cell Properties.

Proliferation. We examined the variability of self-renewal and differentiation among independent cell lines. We found that CK-tTA-driven human tau transgene expression did not obviously interfere with their SC properties. Human tau transgene expression did not alter the proliferation rate of neurosphere lines; regardless of genotype, all cell lines required passaging every 5-7 days. We conducted quantitative cell proliferation assays between passages 2-3 and between passages 6-7 on cell lines of all genotypes. Independent cultures of all genotypes had similar doubling times ranging from 20 to 32 hours as reported for neural SCs [272]. Tau_{P301L}-expressing cultures had a shorter, though non-significant, doubling time of 23.3 +/- 4 hours (n=3), than controls and rTg(tau_{wt}) with 29.4 +/- 8.8 hours (n=5) and 29.3 +/- 5.5 hours (n=3) doubling times. Neurosphere sex did not influence transgene expression or growth rates.

Differentiation. To investigate the effects of transgene expression on neurosphere multipotency and differentiation, we plated dissociated neurosphere cells on laminin/poly-L-ornithine coated glass bottomed plates in basal medium supplemented with retinoic acid [273,274]. Various differentiation factors (NeuroCult Differentiation supplement, Millipore Rodent Neuron Differentiation kit, serum, retinoic acid, and B27), oxygen levels (6% and 20%) [275], and time exposed to differentiation conditions (5 days through 25 days) were examined. Cells were fixed, stained, and visualized with IFA using antibodies against neuronal and glial antigens following each condition. The greatest number of cells expressing neuronal proteins were observed in neurospheres

cultured in NeuroCult Basal medium supplemented with retinoic acid and B27, in 6% oxygen (significantly greater than 20% $p<0.05$ (Figure 3.7A)), and 21 days in culture (significantly greater than 5 days $p<0.01$ (Figure 3.7B)). These conditions were followed for all of the following experiments.

Differentiated rTg(tau_{P301L}), rTg(tau_{wt}), and Tg(CK-tTA) control neurospheres contained cells positive for neuronal proteins microtubule associated protein 2 (recognized by Map2 antibody) and β-tubulin III (recognized by TUJ-1 antibody) or the astrocytic protein, glial fibrillary acidic protein (GFAP) (Figure 3.7C-E). Though mature neurons restrict Map2 expression to dendritic spines, immature neurons express Map2 in developing axons as well as in developing dendrites [276-279]. Neuritic projections contained both β-tubulin III and Map2 expression, but in contrast to the smooth axonal TUJ-1 staining, Map2 staining had a spiny morphology indicative of developing dendritic-spines (Figure 3.7C-E, 3.9A).

The rTg cell lines contained cells that co-expressed neuronal proteins and human tau and cells that co-expressed GFAP and human tau (Figure 3.7A, B). All genotypes contained similar proportions of cells immunoreactive with both Map2 and TUJ-1, 3-5%, indicating that transgene expression did not alter neuronal cell differentiation. Compared to tau_{wt}-expressing cultures, tau_{P301L} cultures contained fewer neuronal protein expressing cells that also expressed human tau; the proportions mirrored that of undifferentiated cells co-expressing nestin and human tau (Figure 3.8).

Differentiated rTg(tau_{P301L}) neural cells developed more filopodia-spines than rTg(tau_{wt}) and controls. We observed a difference in filopodia-spine density between

tau_{P301L} and tau_{wt} differentiated cells. Mature dendritic spines develop from elongated filopodial projections [280-284]. Here we counted the density of these dendritic spine precursors, filopodia-spines, from differentiated cells derived from neurosphere cultures (Figure 3.9A). The filopodia-spine density among genotypes did not differ significantly at 21 days post-differentiation, but became statistically significant 4 days later (Figure 3.9B). The filopodia-spine density increased between days 21 and 25 in tau_{P301L} cultures; conversely, the filopodia-spine density in the tau_{wt} and control cultures slightly decreased during this interval. At 25 days post-differentiation, cells derived from tau_{P301L}-expressing neurospheres had a 23 ± 3% higher filopodia-spine density than neurons derived from tau_{wt}-expressing cultures, and 20 +/- 4% higher filopodia-spine density than non-Tg expressing controls ($p<0.0001$); rTg(tau_{P301L})$Mapt^{0/0}$ and rTg(tau_{wt})$Mapt^{0/0}$ cultures showed similar results (Figure 3.9D). Interestingly, we saw an association of cell culture genotype, but not the level of transgene expression in individual cells, with spine density. Within a single culture, cells expressing high levels of human tau had filopodia-spine densities similar to those in cells expressing low levels of human tau and cells in which transgene-encoded protein was not detectable (Figure 3.9C). We did not observe any genotype-specific differences in tau localization to spines in differentiated cells (Figure 3.9A); transgene-positive tau_{wt} and tau_{P301L} cells expressed human tau throughout their neuritic projections.

In addition to cell types with protein expression and morphology characteristic of neurons or astrocytes, a population of very large cells that, in some cases, had a diameter over 100μm emerged. These cells had a flattened appearance, some were elongated, and

they expressed low levels of nestin and GFAP but not Map2, β-tubulin III, or GABA; some expressed human tau. These cells first appeared in culture ~7 days after induction of differentiation and grew in size until the cultures reached confluence. Examples of these cells can be seen in Figure 3.7C-E. They appeared after growth factor withdrawal upon receiving differentiation stimuli and developed morphological phenotypes resembling senescent cells [285] and may indicate cells that did not receive the appropriate stimuli to complete differentiation and remained in a pseudo-stem cell state. While morphologically and antigenically distinct neural precursor cells have been identified in neurospheres, one of which is EGF-responsive and the other morphologically large EGF/FGF-2 responsive cells [286], we did not supplement cultures with FGF-2. Though neurospheres may have endogenously synthesized FGF-2 [217], the uncharacterized cells did not display strong nestin immunoreactivity typical of neural SCs. We looked for actin cytoskeletal differences using phalloidin and co-stained with Tau13. The large cells with irregular cytoskeletons were not specific to transgene expressing cells, or unique to a genotype. They were present in all cultures, and some co-expressed human tau indicating a possible artifact of the culture protocol (Figure 3.7C-E).

Modeling AD Using Neurosphere Cultures.

The long-term goal of this research is to identify the pathways and mechanisms by which Aβ elevating mutations in amyloid precursor protein (APP) induce NFT formation in AD. The lack of an appropriate model system has delayed progress in understanding AD pathogenesis. Neurospheres may be useful systems to investigate the effects of elevated Aβ on tau misprocessing.

AD patients carry normal MAPT genes. Mutant APP is sufficient to cause both Aβ plaques and NFTs in human patients. However, mice expressing the same mutant human APP gene variants develop elevated Aβ, but not tau pathology. Endogenous mouse tau may inhibit APP-induced tau changes. This hypothesis can be tested using neurospheres. rTg(tau_{wt})$Mapt^{0/0}$ neurosphere cultures express human wild type tau, which is known to become misprocessed in the presence of mutant APP in human patients. Importantly, they lack endogenous mouse tau, the hypothesized inhibitory agent for mouse modeled AD.

I conducted preliminary experiments to monitor proliferation and human tau electrophoretic mobility in human tau-expressing neurospheres co-cultured with APP neurospheres or neurospheres exposed to brain homogenates from adult mice with elevated Aβ. Neurospheres and adult brain homogenates were derived from either Tg(APP_{NLI})19959 mice or transgene-negative control mice. Tg(APP_{NLI})19959 overexpress mutant human APP_{NLI}, which contains both the Swedish and Indiana mutations. Adult mice expressing the mutant human APP_{NLI} acquire elevated Aβ, a sign of APP misprocessing.

Preliminary results suggested that co-culturing human tau and APP neurospheres for 2 passages did not affect the proliferation rate, and was insufficient to induce the tau_{wt} migration patterns to adopt that of tau_{P301L}. Culture immunoreactivity to Tau13 and APP indicated that both neurosphere genotypes were represented in the culture system (Figure 3.10A). Tau_{wt} retained the higher MW slower migrating band in the presence of control

or mutant APP_{NLI} neurospheres. DA9 revealed mouse tau species in APP_{NLI} and control cultures that migrated at approximately the same MW as endogenous tau.

Results from rTg(tau_{wt})*Mapt*$^{0/0}$ and rTg(tau_{P301L})*Mapt*$^{0/0}$ neurospheres exposed to brain homogenate from APP_{NLI} or non-transgenic mice showed that high concentrations (1:50) of brain homogenate resulted in a loss of DA9 expression (Figure 3.10B). This was true for both tau_{P301L} and tau_{wt}, and with both sources of brain homogenate. The decrease was more dramatic with FVB homogenate. Barely any signal was observed in rTg(tau_{P301L})*Mapt*$^{0/0}$ cultures with 1:50 FVB. The cultures that received 1:50 dilutions of either brain homogenate became adherent cultures. Cultures with $1:10^3$ brain homogenate were a mixture of adherent and free-floating spheres, while those that received $1:10^4$ brain homogenate remained non-adherent.

Discussion

Neurosphere cultures derived from the rTg(tau_{P301L})4510 mouse model of human FTD recapitulated several tau phosphorylation events that occur in adult mice. Neurospheres derived from tau_{wt}–expressing mice contained more heavily phosphorylated tau species with slower electrophoretic motility than tau_{P301L}. The phosphorylation differences between tau_{P301L} and tau_{wt} occurred in fetal mouse brains and persisted through young adulthood. Though hyperphosphorylated tau is a hallmark feature of tauopathy, several disease-causing mutant tau variants are less phosphorylated than tau_{wt} *in vitro* [287-290] and in young mice [93,94,105]. While abnormally phosphorylated tau in aged rTg(tau_{P301L})4510 mice coincides with memory and behavioral abnormalities [84,93], the hypophosphorylated tau_{P301L} seen in young mice

may have pre-clinical significance and deserves attention. Transgenic mice that expressed pseudohyperphosphorylated tau, a tau variant that mimics constitutively phosphorylated tau by replacing Ser/Thr residues with glutamate [106], did not develop tau aggregates, neuronal loss, or behavioral abnormalities [107]. In contrast, mice that expressed tau_{R406W}, a variant that remains hypophosphorylated compared to tau_{wt} even in aged mice, developed age-dependent tau aggregates [108] and memory and behavioral abnormalities [109].

The hypophosphorylated tau_{P301L} species in neurospheres and young mice may represent free tau not associated with microtubules (MT). Tau bound to MTs acquires more phosphorylation than free tau as demonstrated by *in vitro* phosphorylation of tau in the presence or absence of MTs [290,291]. Many of the MAPT exon 10 missense mutations that cause dementia, including P301L, reduce the ability of tau to interact with MT [95,96,292,293], and tau_{wt} displaces mutant tau from MTs [106,294]. The absence of tau_{P301L} aggregates or neurofibrillary tangles (NFTs) in neurospheres and young mice, despite phosphorylation at many sites most frequently phosphorylated in AD and FTD ($pSer^{202}$, $pSer^{396}$, $pSer^{235}$, $pSer^{404}$) [45,46,243,295,296], may also correspond to unbound tau as MT association has been implicated as an important step for tau nucleation [297,298]. The quantity of NFTs correlates with disease severity [299]. However, recent studies have dissociated NFTs from neuronal death [98-100] and decreased memory function [85], and instead suggest a deleterious effect of soluble tau.

The PHF-1 epitope is phosphorylated during mitosis [300-302], which likely explains the high proportions of cells containing PHF-1 immunoreactive tau among

genotypes including controls. rTg cultures with more CP13 positive cells than controls could indicate that human tau is being expressed in cells that typically do not express tau, or that overexpressed tau becomes preferentially phosphorylated over endogenous tau. The spatial expression patterns of *Mapt* and *CKII*α in the developing cortex between E13.5 and E15.5 suggest that they represent different cell populations [259] and provide evidence for the former explanation.

Between E13.5 and E15.5 *Mapt* expression is located in the most superficial layers of the dorsal pallium, the future forebrain [259] (Figure 3.11A). Conversely, *CKII*α, thus CK-tTA driven human tau, expression occurs in the deep neocortical cell layers bordering the ventricles [259]. The superficial layers with *Mapt* expression also express *Reln* [259]. During cortical migration, Cajal-Retzius cells of the superficial preplate secrete Reelin, encoded by *Reln*. Reelin is a glycoprotein that serves as a stop signal to migrating neurons [303]. On the opposing end, the deep ventricular layer, *Sox1* is expressed by radial glia. The deep neocortical layers lack endogenous *Mapt* expression until E18.5. Based on the spatial expression patterns it appears that CK-driven expression of human tau may prematurely induce tau expression in this subset of cells and could explain the increased proportion of cells with CP13 phosphorylation.

CKIIα, PKA, and GSK3β kinases phosphorylate tau at the CP13 epitope, Ser^{202}, and are expressed in these deep neocortical layers. Furthermore, after initial tau phosphorylation by CKIIα, GSK3 has enhanced kinase activity on 4R tau, but not 3R tau, at several epitopes including Ser^{202} [304]. While CP13 immunoreactivity is dependent only on $pSer^{202}$, AT8 immunoreactivity requires the simultaneous phosphorylation of

Thr^{205}. Even though both tau_{wt} and tau_{P301L} cultures contained more cells phosphorylated at Ser^{202}, only tau_{wt} contained more cells phosphorylated at Ser^{202} and Thr^{205}. The phosphorylation of both epitopes is increased by PKA primed GSK3β; these kinases are expressed at the developmental time period of neurosphere harvest [259], and tau_{wt} has been shown to be a better substrate for tau kinases than tau_{P301L} [93,290]. Alternatively, the increased proportion of AT8 immunoreactive cells in tau_{wt}-expressing compared to tau_{P301L} and controls may be a result of the higher proportion of human tau expressing cells in tau_{wt}-cultures compared to tau_{P301L} cultures. However, this was not observed with the CP13 or PHF-1 antibodies, so it seems specific to tau phosphorylation recognized by AT8.

We observed differences in filopodia-spine densities between tau_{wt} and tau_{P301L} differentiated cells. Developmentally, dendritic spine morphology evolves from long thin filopodia-spines to mature spines of various morphologies; during this transformation, filopodia-spine density decreases [280-284]. We observed a slightly higher filopodia-spine density in Map2 and TUJ-1 double-positive cells from tau_{P301L} cultures than those derived from tau_{wt} or cultures that did not express MAPT. While the level of transgene expression within individual cells did not affect filopodia-spine density, we have not ruled out an effect of the transgene insertion site. Interestingly, in a separate mouse line that harbored the P301L mutation in the longest mouse tau isoform, 4R2N, driven by the neuronal thy1 promoter, young mice with hypophosphorylated tau had enhanced learning and memory and increased long-term potentiation (LTP) in the dentate gyrus than controls [94]. Later, with age, the spine density of rTg(tau_{P301L})4510 mice reportedly

decreases and coincides with increased neuronal excitability [100]. Whether or not the greater filopodia-spine density we observed in differentiated tau_{P301L} cultures relates to enhanced LTP in young mice or neuronal vulnerability later in life in unknown, but warrants further exploration.

We did not observe tau mislocalization to dendritic spines specific to tau_{P301L} as reported in aging mice [93] or in transfected rat neuron cultures [114]. We saw high levels of transgenic tau protein throughout neuritic projections in differentiated neurospheres from both human tau transgene genotypes. The presence of tau in the filopodia-spines of developing cells [243,305] suggests that the phenomenon correlates with a dynamic morphology and does not necessarily indicate pathological injury.

Overall, when using the same mouse line, neurosphere cultures isolated from individual fetuses at different times proved highly similar in transgene expression, proliferation, and differentiation. Unlike clonal cultures, these neurospheres formed by aggregation which results in some culture heterogeneity [213,215-217]. During culture they merge and fuse as they proliferate [220,223] which likely resulted in the heterogeneous composition of transgene expressing and non-expressing cells within the same sphere. The minor transgene expression variability among neurosphere cultures generated from littermate fetuses possibly occurred during the initial brain harvest. We did not specifically dissect the forebrain from each fetus. Nestin expressing neural SCs in the developing midbrain [306] and hindbrain [307] may have contributed to the non-transgene expressing cell population since *CKIIα*, the promoter driving tTA-transgenic human tau expression, is expressed throughout the brain at this developmental age [259].

We saw more variability between independent experimental harvests than among cultures derived from littermate fetuses; we attribute this variation to inconsistencies inherent to IFA. Regardless, IFA consistently demonstrated that undifferentiated cells derived from rTg(tau_{wt}) expressing fetal brains expressed human tau in a higher proportion of cells than those derived from rTg(tau_{P301L}) expressing fetal brains.

Total brain homogenates [114] and cell lysates indicated that rTg(tau_{wt}) mice express comparable levels of transgenic tau as rTg(tau_{P301L}). While the rTg(tau_{P301L}) cultures had a lower proportion of total cells expressing human tau, they contained a greater proportion of cells that expressed higher levels of tau (brighter fluorescence intensity). This feature of some transgenes is caused by position-effect variegation [308-310]. Neurospheres, like the mice from which they were derived, may show this effect and could be useful models for screening transgene expression in founder lines. Consistent with the difference in transgene expression seen in undifferentiated neurospheres, differentiated cells derived from tau_{wt}-expressing neurospheres expressed human tau in a higher proportion of cells than those derived from tau_{P301L}-expressing neurospheres. Likely, non-transgene expressing progenitor cells gave rise to non-transgene expressing differentiated cells and transgene expressing progenitor cells differentiated into transgene expressing mature cells. Alternatively, tau_{P301L} transgene expression may have decreased neural precursor survival. Since neurospheres proliferated and differentiated over several passages in both genotypes, and differentiated transgene expressing cell proportions mirrored that of the undifferentiated condition, evidence favors the former explanation.

We investigated the proportion of human tau_{P301L}-expressing cells generated from three different tTA-driven promoter systems (i.e. CK, EC, Prnp). The prion protein is ubiquitously expressed through the nervous system, and Prnp-driven tTA was predicted to produce the greatest proportion of transgene positive cells. Previous experiments reported nearly 100% transgene positive cells in neurospheres with Prnp promoter driven expression of PrP [264]. Neuropsin, the EC gene driving tTA in the Tg(EC-tTA) mouse, expression is specific to the entorhinal cortex [311], and was predicted to yield the lowest proportion of transgene-expressing cells. Interestingly, only cells derived from the Tg(CK-tTA) promoter system expressed transgene above leaky levels. While Prnp is ubiquitously expressed throughout the nervous system, developmental expression is lower than CK between E13.5 and E15.5, the age at which neurosphere cultures are generated [259] (Figure 3.11B). To determine whether or not leaky expression results from cells with low-level tTA expression, or only in cells without tTA, we plan to stain with CKIIα and/or tTA antibodies simultaneous with Tau13 and look for co-expression.

We also investigated different responder lines to determine if neurosphere expression would mimic the expression levels seen in the mice from which they were derived. Interestingly, when we crossed the Tg(CK-tTA) activator line to different Tg(TRE-tau) responder lines, we saw a notable difference in proportion of human tau-expressing cells from the rTg(tau_{wt}) line, but not tau_{P301L} lines. rTg(tau_{wt})14238 neurospheres expressed human tau in approximately 50% fewer cells than typically seen in rTg(tau_{wt})21221 neurospheres, which mirrors that of adult mice. Adult rTg(tau_{wt})14238 mice express 50% less human tau than rTg(tau_{wt})21221. However, rTg(tau_{P301L}) cultures,

regardless of founder, expressed human tau at similar levels. This result argues for an effect of transgene insertion site as well as the tau mutation.

The preliminary data gathered from rTg(tau_{wt}) and rTg(tau_{P301L}) neurospheres exposed to high concentrations (1:50) APP_{NLI} and control mouse brain homogenates indicated a loss of total tau expression. Loss of transgene expression is one possibility, but total tau levels decreased. A more likely explanation is protein degradation. Also, high concentration of brain homogenate caused cultures, regardless of genotype, to become adherent. Soluble factor(s) in adult brains are likely not permissive to non-adherent culture conditions and may have induced differentiation or altered neurosphere cell adhesion protein expression. Further experiments should focus on dilutions between than $1:10^3$ and $1:10^4$ to permit neurosphere formation.

With the emergence of methodology to culture neurospheres from human patients [233], experiments evaluating the culture system's relevance and validity are crucial. Our data provide supporting evidence for neurospheres to reliably model phenotypes of their derived source over extended culture periods. The neurosphere culture system provides a robust assay for studying effects of external factors on the development and differentiation of the CNS. While it is unreasonable to expect that an *in vitro* system will fully recapitulate a complex disease process involving complex cell interactions, biologically relevant models that provide reproducible results are invaluable resources. This SC model shares the genetics of mice that model human FTD, and has shown the capacity to model pre-disease phenotypes. By using two distinct transgenic mice as the

source of SCs, we have established that neurosphere cultures maintain genotype specific characteristics.

Future Directions

Our results lend credence to the growing body of data supporting the development and use of patient-specific SC lines to study disease. We have already shown that these cells reproducibly mimic biological events of the mice from which they were derived, and that they express the appropriate molecules to modify tau as seen in advanced disease. Further characterization should focus on comparing neurosphere-differentiated neurons to primary neuronal cultures from mice at different ages. Results would indicate whether or not SC-differentiated cells mimic phenotypes of the developmental age from which they were derived, or if they can develop phenotypes associated with later disease stages. Filopodia-spine density and the tau hypo-to-hyperphosphorylation transition may be useful markers to assess disease stage.

Though APP:tau co-culture experiments did not reveal significant findings over two passages, longer culture periods may expose changes in tau phosphorylation. Additionally, differentiating these cultures may provide insight into their differentiation potential and post-differentiation cell types upon exposure to mutant APP. To determine if secreted factors are sufficient for changes in tau processing, or if cell-cell contact is required, neurosphere cultures can either be supplemented with media from APP cultures or co-cultured with APP neurospheres at different cell densities. High plating densities induce neurosphere fusion, which may be necessary for APP to carry out its effect.

We are also focusing on microarray analysis experiments to uncover differentially regulated genes between tau_{P301L} and tau_{wt} mice and neurosphere cultures. This will direct hypotheses about potential pathways targeted in cells that carry the tau_{P301L} gene. By extending this research to patient-specific SCs, high-throughput cell based genetic screening (cDNA or siRNA) assays could uncover small molecules and potential pathways involved in pathogenesis and, ideally, the genetic specificity of the system may lead to treatment therapies tailored to unique patient needs.

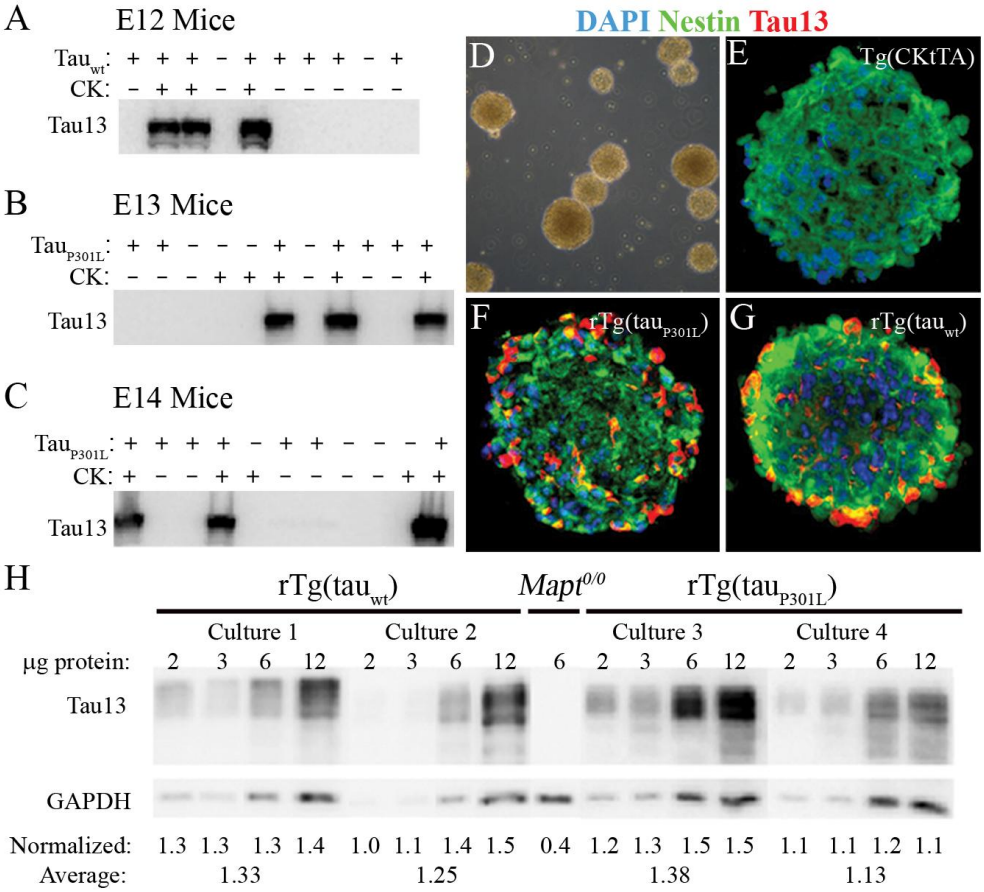

Figure 3.1: rTg Fetuses and Neurospheres Expressed Human Tau.
(A-C) Brains were taken from Tg(CK-tTA) x Tg(tau) pups at E12 (A) E13 (B) and E14 (C) for WB analysis with the human specific anti-tau antibody, Tau13. We saw immunoreactivity only in brain homogenates from pups that genotyped positive for both transgenes. None of the samples from pups with either the transactivator or responder transgene alone or with neither transgene were immunoreactive with Tau3. (D-G) Neurosphere cultures generated from E14 Tg(CK-tTA) x Tg(tau) mouse litters grew as non-adherent neurospheres and expressed human tau. (D) Representative phase contrast image of neurospheres in culture. (E-G) Fixed and cryosectioned neurospheres analyzed by fluorescence microscopy demonstrated that nearly all cells in Tg(CK-tTA) (E), rTg(tau_{P301L}) (F), and rTg(tau_{wt}) (G) expressed the CNS-SC protein, nestin (green). rTg(tau_{P301L}) (F) and rTg(tau_{wt}) (G) neurospheres contained cells that were strongly immunoreactive with Tau13 (red); control Tg(CK-tTA) (E) neurospheres did not. DAPI nuclear stain is blue in E-G. (H) Western blot analysis from two independent rTg(tau_{wt}) neurosphere cell lines (cultures 1 and 2) and two independent rTg(tau_{P301L}) neurosphere cell lines (cultures 3 and 4) showed comparable levels of human tau between genotypes. Tau13 immunoreactivity was normalized to GAPDH. The normalized values indicated that human tau levels were comparable between genotypes.

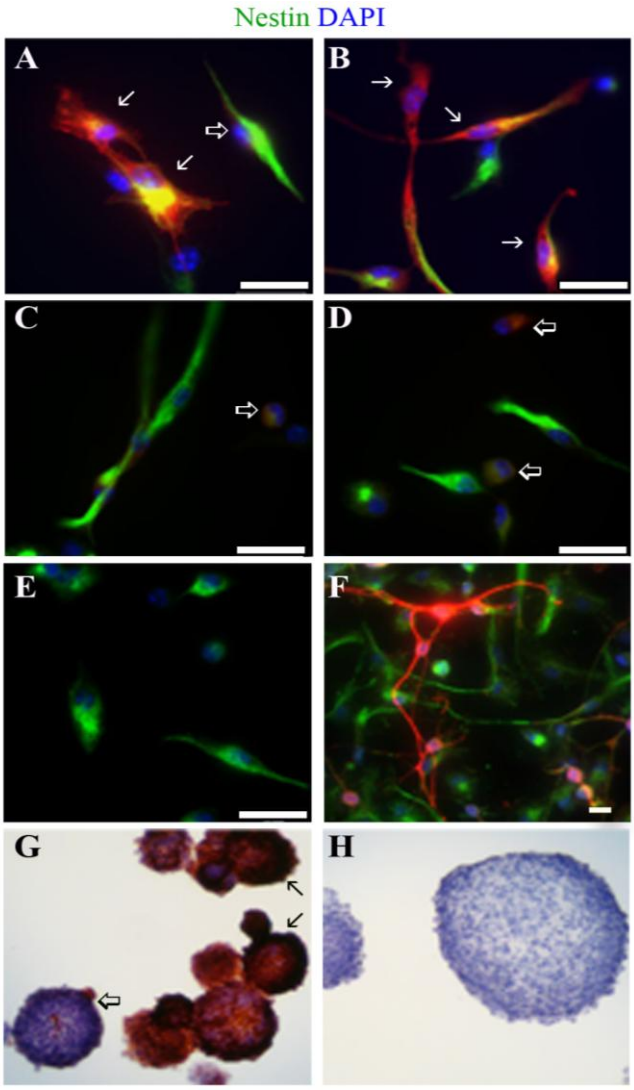

Figure 3.2: Human Tau Protein Expression Heterogeneity Among Individual Neurospheres and Single Cells.

A proportion of cells from rTg(tau_{wt}) (21-30%) (A) and rTg(tau_{P301L}) (38-44%) (B) cultures displayed strong immunoreactivity with Tau13 (solid arrow), while others were weakly immunoreactive (open arrow). Tg(tau_{wt}) (C) and Tg(tau_{P301L}) (D), did not contain any cells with strong Tau13 immunoreactivity, but they did contain cells with weak immunoreactivity indicative of leaky transgene expression. (E) Tg(CK-tTA) cultures did not express human tau but were immunoreactive with Tau46 (F) which recognizes mouse tau. Nearly all cells in all genotypes were immunoreactive with the anti-nestin antibody (green); DAPI nuclear stain is blue. Scale bar: 25μm. (G) Immunohistochemistry of cryosectioned neurospheres probed with Tau13 revealed that some neurospheres from rTg cultures, rTg(tau_{P301L}) shown here, contained a large proportion of transgene expressing cells (closed arrow), other neurospheres from the same culture contained very few transgene expressing cells (open arrow). (H) Control Tg(CK-tTA) neurospheres were not immunoreactive with Tau13. Red: Tau13 (A-E, G), Tau46 (F).

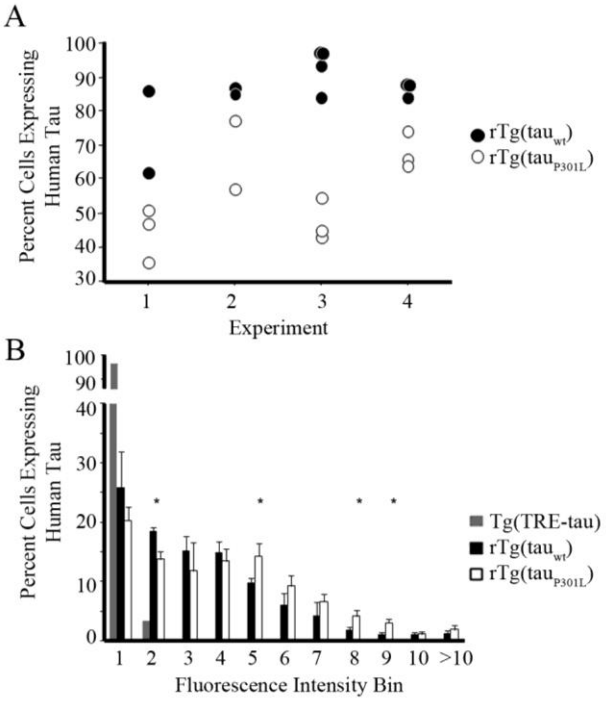

Figure 3.3: Human Tau_{wt} Was Expressed in More Cells, but at Lower Levels, Than Tau_{P301L}.

Undifferentiated single cells (shown in Figure 3.2) stained with DAPI and nestin were counted and the proportion co-expressing Tau13 was determined. (A) Consistently the proportion of cells co-expressing Tau13 was significantly higher in rTg(tau_{wt}) cultures than rTg(tau_{P301L}) cultures. Four independent experiments consisting of 11 independent rTg(tau_{wt}) cultures and 11 independent rTg(tau_{P301L}) cultures are shown here (ANOVA, p-value<0.0001). Closed circles represent tau_{wt}; open circles represent tau_{P301L}. (B) A fluorescence intensity histogram from Figure 3.3A's Experiment 3 cells revealed heterogeneity in transgene expressing cells. Transgene positive cells were binned (1 to >10) based on fluorescence intensity. "1" indicates a "dim" cell with low transgene expression (open arrow from Figure 3.2), and bins 6 through >10 indicated "bright" cells with high transgene expression (closed arrow from Figure 3.2); proportion of cells is on the y-axis. Though rTg(tau_{wt}) cultures contained a greater proportion of transgene expressing cells shown in (A), in this particular experiment rTg(tau_{P301L}) cultures contained a greater proportion of high transgene expressing cells. Bins 5, 8, and 9 contained a significantly higher proportion of rTg(tau_{P301L}) cells than rTg(tau_{wt}) cells (*: ANOVA, p<0.05). Tg(TRE-tau) cell lines, tau_{P301L} in this experiment, expressed human tau at low levels. All cells were in bins 1 and 2.

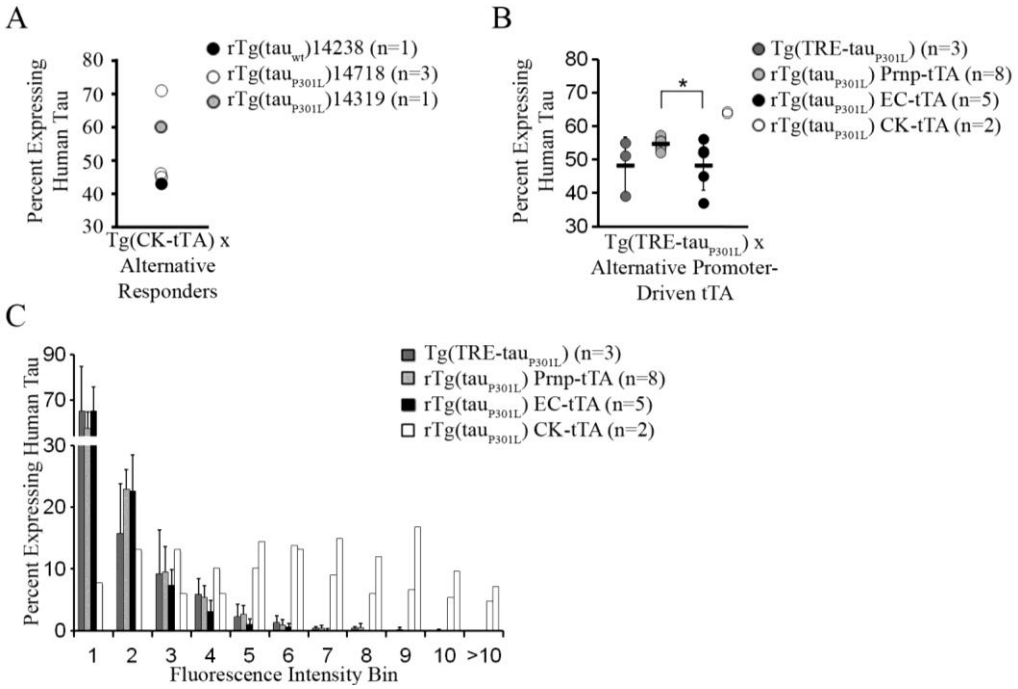

Figure 3.4: Human Tau Expression in Neurospheres Derived From Alternative Mouse Lines.

Neurosphere cultures harvested from rTg mice derived from alternative activator or responder lines indicated mutation and insertion site differences; only CK-tTA driven transgene expression was above leaky levels. We generated neurosphere cultures from alternative responder (A) or activator (B, C) lines. (A) rTg(tau_{wt})14238 and rTg(tau_{P301L})14718 mice express 50% less human tau than rTg(tau_{wt})21221 and rTg(tau_{P301L})4510 mice; rTg(tau_{P301L})14319 mice express 25% less human tau than rTg(tau_{P301L})4510 mice. Neurospheres harvested from the alternative-tau_{P301L} responder mice expressed human tau_{P301L} in similar proportions of cells typically seen in rTg(tau_{P301L})4510; however, tau_{wt} was expressed in fewer cells than in rTg(tau_{wt})21221. More notably, tau_{wt} was expressed in a lower proportion of cells than tau_{P301L}, which opposes rTg(tau_{wt})21221 and rTg(tau_{P301L})4510 expression patterns (Figure 3.3A). (B) Various promoter-driven tTA mouse lines were crossed to Tg(TRE-tau_{P301L})4510 mice to determine if other promoters could more effectively drive tau_{P301L} expression. CK driven tTA generated the highest proportion of human tau expressing cells. Prnp-tTA driven tau_{P301L} neurospheres expressed human tau in significantly more cells than EC-tTA neurospheres, but less than CK-tTA's. EC-tTA proportions were comparable to Tg(TRE-tau_{P301L}) alone (*: ANOVA, $p<0.05$). (C) Fluorescence intensity histograms from (B) revealed that only cells from Tg(CK-tTA) driven tau_{P301L}-cultures expressed human tau above leaky levels. Bins from Prnp-tTA and EC-tTA cultures mirrored Tg(TRE-tau_{P301L}) cultures indicating cells with leaky, not transgene-driven, expression. n: number of independent cultures harvested examined.

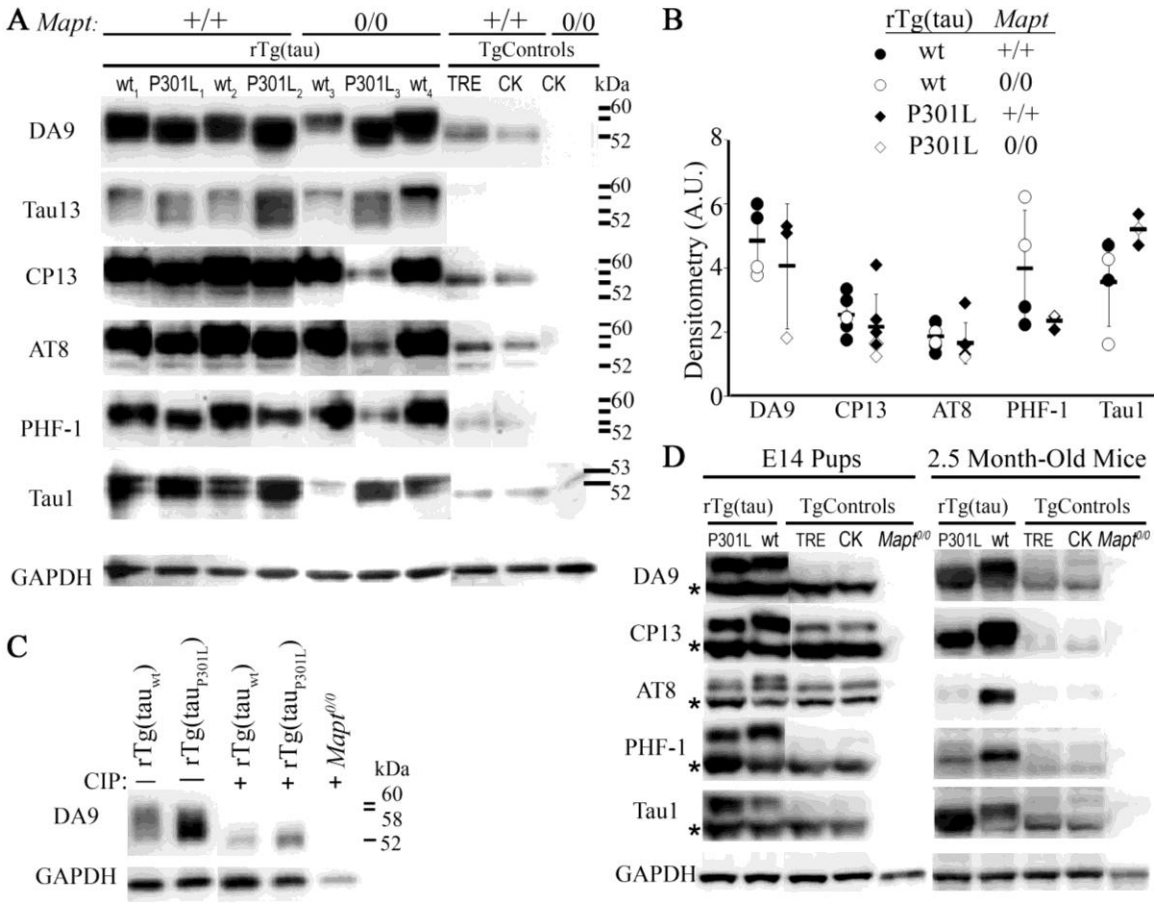

Figure 3.5: Human Tau_{wt} Was More Heavily Phosphorylated Than Tau_{P301L}.
(A) Electrophoresed and blotted neurosphere lysates were probed with anti-tau antibodies. In control samples, Tg(TRE-tau) (tau_{P301L} shown here) and Tg(CK-tTA), all antibodies, except Tau13, revealed a mouse tau band at ~52 kDa that was absent from *Mapt*$^{0/0}$ samples. Human tau from rTg samples migrated as a diffuse series of bands. Human tau_{wt}-expressing cells contained more slowly migrating tau species (~53 to 60 kDa) than tau_{P301L}-expressing cells (~53 to 58 kDa) with all anti-tau antibodies, except Tau1. In all blots (except Tau1), MW lines indicate 60, 58, 53, 52 kDa, respectively. (B) Western blot densitometry was calculated by normalizing phospho-tau antibody immunoreactivity to GAPDH. Tg(CK-tTA)*Mapt*$^{+/+}$ immunoreactivity corresponds to y=1. All rTg cultures contained significantly higher phospho-tau immunoreactivity than Tg(CK-tTA) (ANOVA, $p<0.05$). (C) Tau protein from rTg(tau_{wt})*Mapt*$^{0/0}$ and rTg(tau_{P301L})*Mapt*$^{0/0}$ neurosphere lysates had the same electrophoretic mobility after treatment with calf-intestinal phosphatase (CIP). Untreated samples (-) showed the characteristic slower migrating (~60 kDa) trailing edge for tau_{wt} compared to tau_{P301L} that was abolished upon CIP treatment (+). (D) Human tau from rTg(tau_{wt}) E14 and adult mice contained more slowly migrating phospho-tau species than rTg(tau_{P301L}) as seen in neurospheres; * = mouse tau. All samples blotted with the same antibody were probed on the same membrane simultaneous with GAPDH; the *Mapt*$^{0/0}$ and control samples were rearranged for presentation/labeling purposes in A and D.

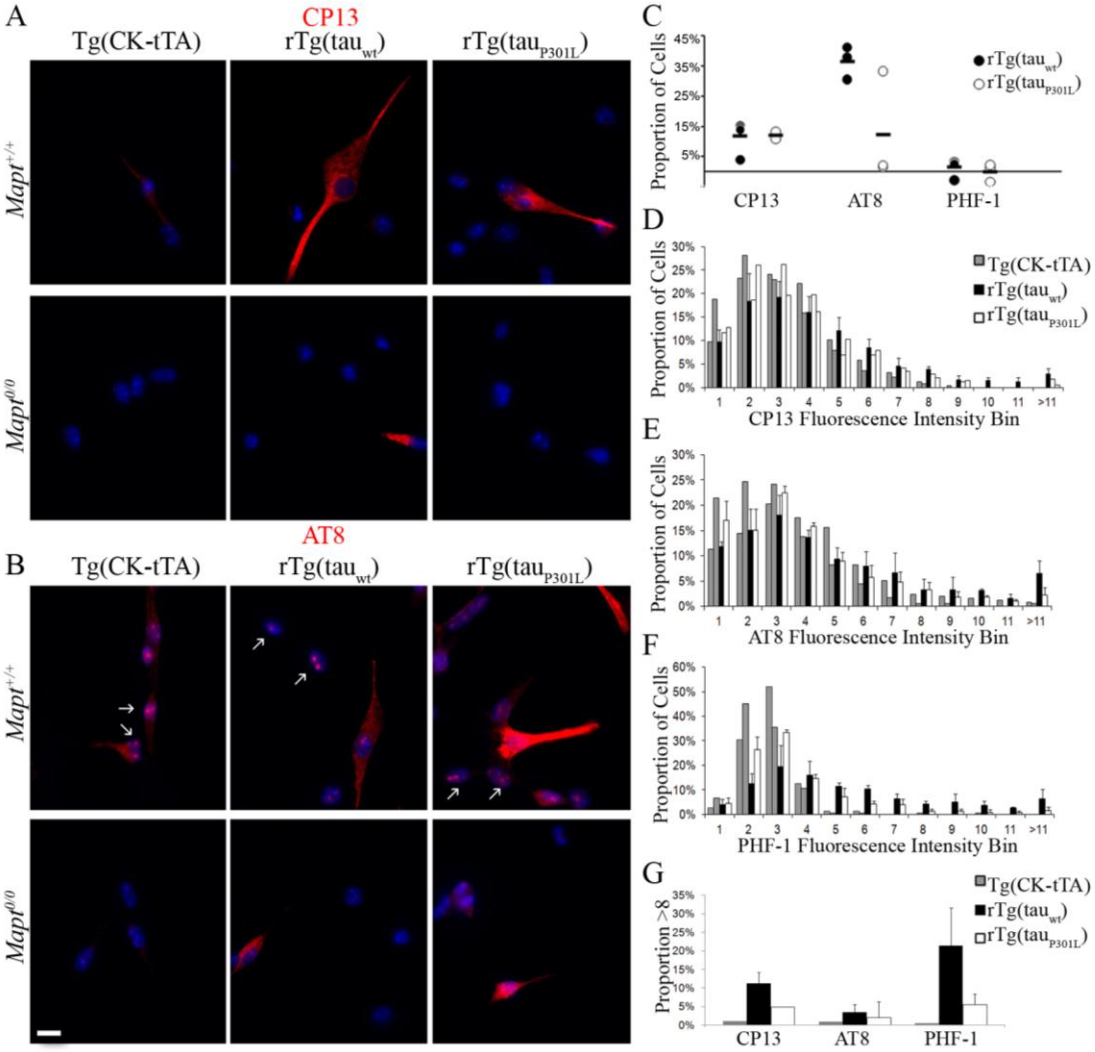

Figure 3.6: Phosphorylated Tau Localization and Level in Single Cells.
Phospho-tau immunoreactivity, CP13 (A) and AT8 (B), was observed throughout the cytoplasm in dissociated undifferentiated neurospheres. Specific to AT8 was punctate staining in the nucleus (arrows) only in genotypes expressing mouse tau, but absent in *Mapt*$^{0/0}$ cells, indicating that it was of mouse origin. Blue: DAPI nuclear stain. Scale bar: 25μm. (C-G) Tau$_{wt}$ cultures contained more cells with high phosphorylation levels than tau$_{P301L}$ cultures. (C) The number of CP13, AT8, and PHF-1 immunoreactive cells were counted and plotted as proportions greater than Tg(CK-tTA). Phospho-tau counts revealed significantly more CP13 immunoreactive cells in both rTg genotypes than Tg(CK-tTA) controls (ANOVA, $p<0.05$); only rTg(tau$_{wt}$) cultures contained significantly more AT8-immunoreactive cells (ANOVA, $p<0.01$); and PHF-1 was comparable among all genotypes. Fluorescence intensity histograms were generated for CP13 (D), AT8 (E), and PHF-1 (F) immunoreactive cells. Bright cells (fluorescence intensity bins greater than 8) were combined and compared. Tau$_{wt}$-expressing cultures contained higher proportions of bright CP13 and PHF-1 (ANOVA, $p<0.05$) cells than tau$_{P301L}$-expressing and Tg(CK-tTA) cells. AT8 fluorescence intensity was comparable among all genotypes.

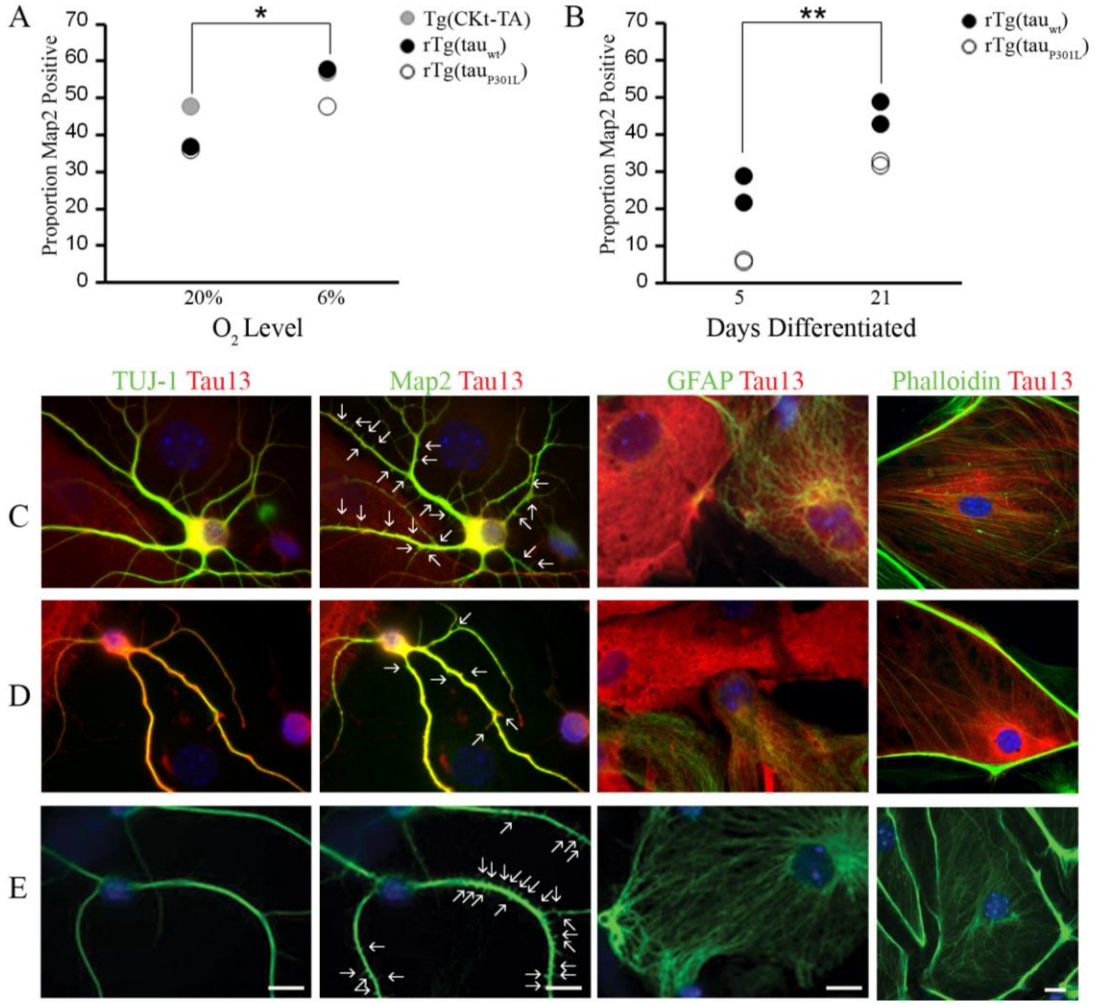

Figure 3.7: Neurospheres Differentiated Into CNS Cell Types.
Dissociated neurospheres stimulated with retinoic acid were cultured under different oxygen tension (A) and lengths of time (B) and analyzed for Map2 expression. (A) 6% oxygen yielded significantly more Map2 positive cells than cultures differentiated in 20% oxygen (*: ANOVA, $p<0.05$). (B) The number of cells expressing Map2 significantly increased between 5 and 21 days in culture (**: ANOVA, $p<0.01$). Cells differentiated for 21 days in 6% oxygen expressed neuronal or glial antigens. Each rTg(tau_{P301L}) (panel C) and rTg(tau_{wt}) (panel D) culture contained cells positive for Tau13 and TUJ-1, Tau13 and Map2, and Tau13 and GFAP; merged images of Tau13 (red) with TUJ-1, Map2, or GFAP (green) are presented; yellow color indicates overlapping expression. Tg(CK-tTA) control cells are shown in panel E. Arrows point to spiny projections labeled with Map2 staining. Phalloidin staining (green) revealed strong actin belts around large undefined Tau13 positive (red) cells in all culture genotypes. Scale bar: 10μm. Cells were simultaneously stained with three different secondary antibodies (Alexa 546 anti-mouse for Tau13; Alexa 647 anti-rabbit for TUJ-1; Alexa 488 anti-chicken for Map2) and each fluor was imaged separately. Alexa 546 was artificially colored red, and Alexa 647 and 488 were both artificially colored green for image color-combine with Tau13.

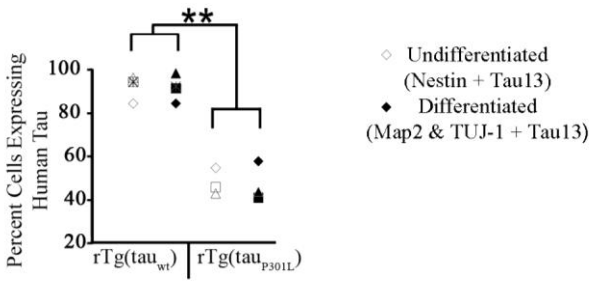

Figure 3.8: Transgene Expression Persisted Through Differentiation.
The proportion of differentiated cells that expressed human tau reflected that of undifferentiated neurospheres. Differentiated cells immunoreactive with both Map2 and TUJ-1 antibodies were counted; the proportion co-expressing Tau13 is presented here. Presented are results from five independent rTg(tau_{wt}) cultures and four independent rTg(tau_{P301L}) cultures generated from two litters of each CK-tTA x TRE-tau mating. The four litters were harvested, genotyped, and cultured simultaneous. They yielded five rTg(tau_{wt}) and four rTg(tau_{P301L}) pups for neurosphere culture shown here. The proportions of differentiated cells (closed symbols) did not differ from those of the neurospheres (open symbols) from which they were derived (**: ANOVA, $p<0.0001$).

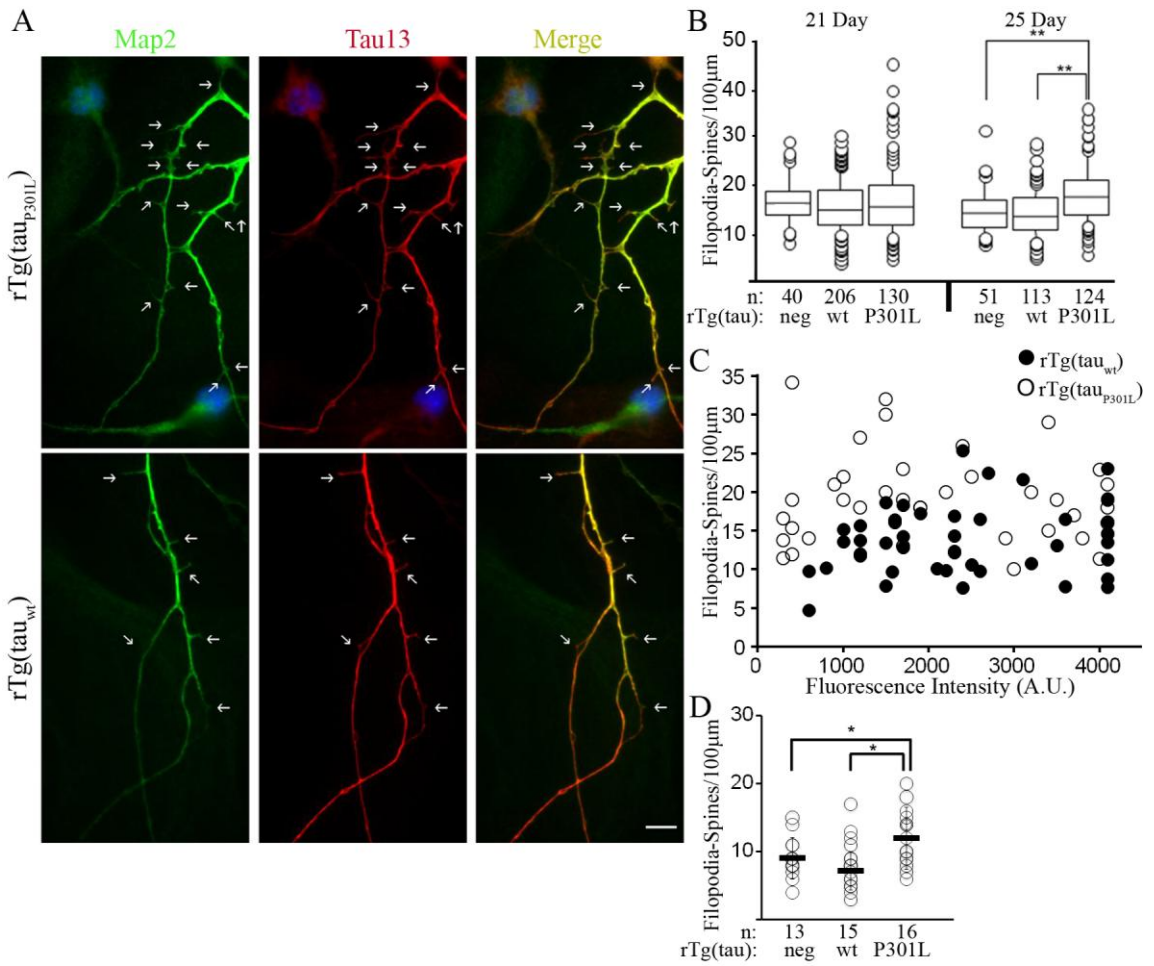

Figure 3.9: Differentiated rTg(tau$_{P301L}$) Cells Developed More Filopodia-spines Than rTg(tau$_{wt}$) and Controls.

(A) Cells differentiated for 21 or 25 days were evaluated for the number of Map2 positive filopodia-spines and tau localization. Shown here are data pooled from 3 independent rTg(tau$_{P301L}$) and 4 independent rTg(tau$_{wt}$) lines. We observed human tau expression (Tau13), throughout Map2 positive neurites and filopodia-spines (arrows) in tau$_{P301L}$ (top panel) and tau$_{wt}$ (bottom panel) expressing cells. Scale bar: 10µm. (B) The density, filopodia-spines/100µm, was plotted for each genotype (n indicates number of cells counted). Filopodia-spine density increased between 21 and 25 days in rTg(tau$_{P301L}$) cells resulting in significantly higher filopodia-spine densities (**: ANOVA, $p<0.0001$) than seen in rTg(tau$_{wt}$) or non-transgene expressing Tg(CK-tTA) cells (neg). Horizontal lines inside boxes: mean filopodia-spine densities; circles: outliers. (C) Plotting of spine density against fluorescence intensity revealed no correlation between protein expression level and filopodia-spine density. Closed circles: rTg(tau$_{wt}$) cells; open circles: rTg(tau$_{P301L}$) cells. (D) *Mapt*$^{0/0}$ neurosphere cultures were differentiated for 21 days and analyzed. As seen in *Mapt*$^{+/+}$ cultures, rTg(tau$_{P301L}$)*Mapt*$^{0/0}$ contained significantly more filopodia-spines than rTg(tau$_{wt}$)*Mapt*$^{0/0}$ or Tg(CK-tTA)*Mapt*$^{0/0}$ controls (*: ANOVA, $p<0.05$).

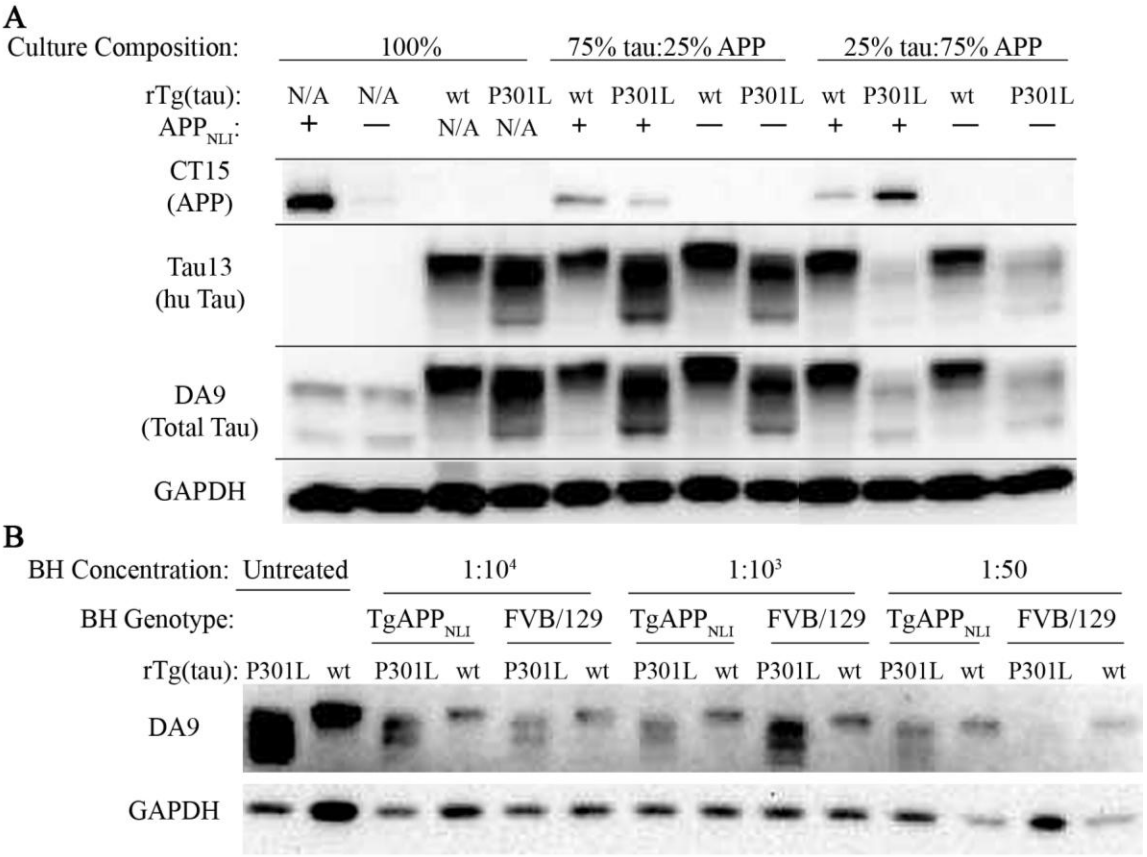

Figure 3.10: Short Term Exposure to Mutant APP Did Not Alter Neurosphere Expressed Human Tau.

(A) rTg(tau_{wt})*Mapt*$^{0/0}$ and rTg(tau_{P301L})*Mapt*$^{0/0}$ neurospheres were co-cultured with APP_{NLI} transgene positive (+) or transgene negative (-) cultures. After two passages cell lysates were monitored for APP-induced changes in tau migration by immunoblotting with human tau (Tau13) and total tau (DA9) antibodies. Pure cultures containing 100% of each genotype were compared to various culture compositions; 75% tau with 25% APP, and 25% tau with 75% APP are shown here. Immunoblotting with the APP antibody, CT15, detected APP protein in neurosphere lysates. APP co-culture did not alter the tau migration pattern. In all culture conditions tau_{wt} contained the canonical higher MW species than tau_{P301L}. DA9 detected endogenous mouse tau in APP neurospheres. N/A: cultures did not contain cells of that genotype. (B) rTg(tau_{wt})*Mapt*$^{0/0}$ cultures were exposed to brain homogenates from adult APP_{NLI} or FVB/129 mice. The tau migration pattern was compared to rTg(tau_{P301L})*Mapt*$^{0/0}$ cultures that received identical treatment. All cultures receiving brain homogenates displayed decreased DA9 immunoreactivity. Cultures that received the highest concentration of brain homogenate (1:50) showed the most profound decrease. DA9 signal was nearly absent in rTg(tau_{P301L})*Mapt*$^{0/0}$ cultures that received 1:50 FVB/129 brain homogenate. BH: brain homogenate.

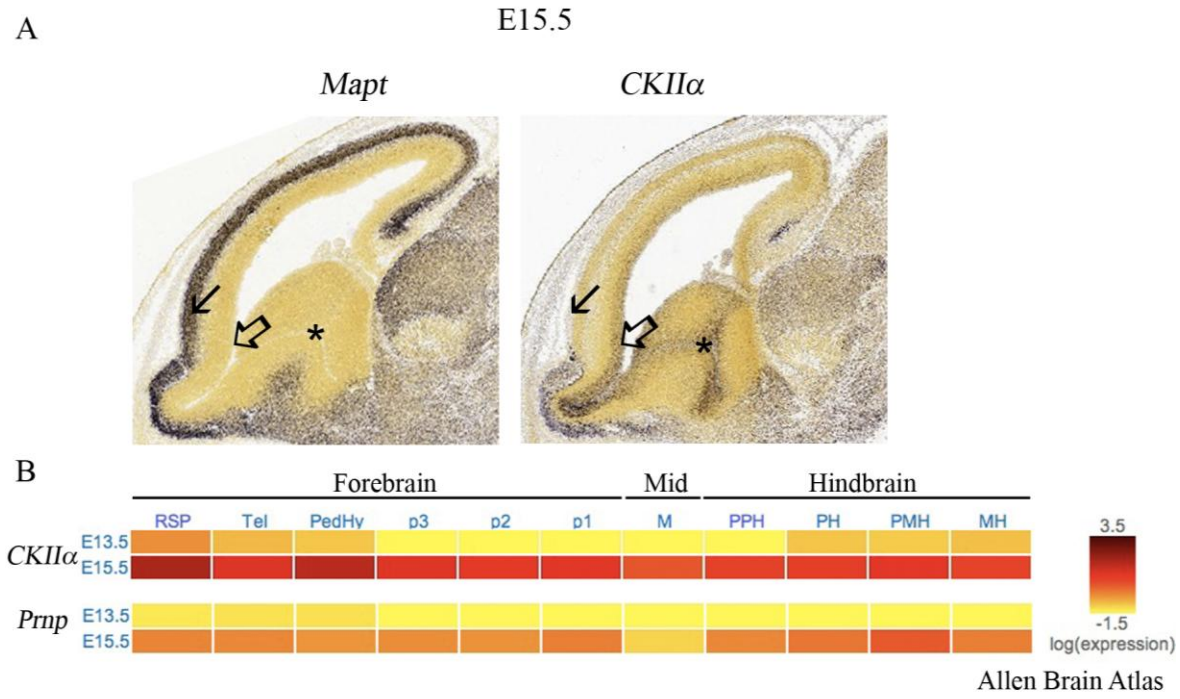

Figure 3.11: *Mapt, CKIIα,* and *Prnp In Situ* Hybridization From Allen Brain Atlas. Whole fetal brains are harvested at E14 for neurosphere culture. (A) *In situ* hybridization data illustrates that *Mapt* and *CKIIα* do not have overlapping expression patterns at E15.5. The developing outer forebrain cells display strong *Mapt* expression, but not *CKIIα* (closed arrow). *CKIIα* is expressed by cells in the innermost developing cortical layer adjacent to the ventricle; *Mapt* is not expressed in these cells (open arrow and *). (B) *CKIIα* expression is much stronger than *Prnp*, especially in the developing forebrain, during the developmental age that neurospheres were harvested. Allen Brain Atlas [259].

Table 3.1: Antibody Epitopes and Genotype-Associated Electrophoretic Migration.

Antibody	Relative Size			
	E14 mice	Neurospheres	2.5 - 5 mo-old mice	>/=7.5 mo-old mice
Tau13 (human residues 2-18)	tau_{wt}>tau_{P301L}	tau_{wt}>tau_{P301L}	tau_{wt}>tau_{P301L}	tau_{wt}=tau_{P301L}
CP13 ($pSer^{202}$)	tau_{wt}>tau_{P301L}	tau_{wt}>tau_{P301L}	tau_{wt}>tau_{P301L}	tau_{wt}=tau_{P301L}
AT8 ($pSer^{202}$/$pThr^{205}$)	tau_{wt}>tau_{P301L}	tau_{wt}>tau_{P301L}	tau_{wt}>tau_{P301L}	tau_{P301L} only
PHF-1 ($pSer^{396}$/$pSer^{404}$)	tau_{wt}>tau_{P301L}	tau_{wt}>tau_{P301L}	tau_{wt}>tau_{P301L}	tau_{wt}=tau_{P301L}
Tau1 (non-phospho Ser^{198}/Ser^{202})	tau_{wt}=tau_{P301L}	tau_{wt}=tau_{P301L}	tau_{wt}>/=tau_{P301L}	tau_{wt}=tau_{P301L}
CP9 ($pThr^{231}$)	N.D.	N.D.	Negative	tau_{P301L} only
$pSer^{262}$	N.D.	N.D.	Negative	tau_{P301L} only
MC6 ($pSer^{235}$)	N.D.	tau_{wt}>tau_{P301L}	Negative	tau_{P301L} only
TG3 ($pThr^{231}$associated conformation)	N.D.	N.D.	Negative	tau_{P301L} only
MC1 (aa 7-9 & 312-322)	N.D.	N.D.	Negative	tau_{P301L} only

Epitopes recognized by each antibody are shown in parentheses. The more slowly migrating, and hence higher apparent MW, band is to the left and separated from the smaller, more quickly migrating tau species by the symbol ">". The "=" symbol indicates no difference in apparent size of the tau species. Negative: no immunoreactivity above background; N.D.: not determined.

SUMMARY AND CONCLUSIONS

As the number of AD diagnoses continues to climb, the development of appropriate model systems to study disease pathogenesis becomes increasingly important. We developed and characterized two novel systems to study tau pathology, the phenotype lacking in current AD mouse models. To test the hypothesis that mouse tau inhibits tau pathology we exploited the well-characterized mouse model of a related disease, FTD, which develops tauopathy similar to human patients. By ablating mouse tau in the FTD mouse model we tracked pathological differences due to the presence of endogenous mouse tau. In addition, we utilized the rTg(tau_{wt})21221 human wild type tau overexpressing mouse to create transgenic mice that expressed novel MAPT and *Mapt* gene combinations. With these mice we studied endogenous mouse tau's influence on tau pathology, pre-disease tau phenotypes, dissociated endogenous mouse tau effects from universal wild type tau expression, tracked pathogenesis, and separated mutation specific effects from general tau overexpression phenotypes. Additionally, we examined CNS-SC containing neurosphere cultures derived from the mouse models. We investigated their reproducibility among independent harvests, their longevity, and ability to mimic phenotypes of their parent mouse strains.

We found that the transgenic protein level and mutation played distinct roles in pathology. Differentiated cells from rTg(tau_{wt}) and rTg(tau_{P301L}) neurospheres contained human tau throughout all cellular processes indicating a phenotype of general tau overexpression. Similarly, widespread cellular distribution of transgenic tau was observed in adult mouse brain cells that expressed either human transgene. However,

with age leaky levels of tau in Tg(TRE-tau) mice remained throughout cellular processes, but overexpressed tau became restricted to the somatic compartment *in vivo* indicating the sufficiency of overexpression, but not mutation for tau missorting. Sarkosyl insolubility and neuronal loss required both overexpression and the P301L mutation. Despite expressing constant high levels of human tau_{wt}, or low levels of tau_{P301L}, neither rTg(tau_{wt}) nor Tg(TRE-tau_{P301L}), respectively, developed neuronal loss.

While the human pan-tau antibody revealed transgenic protein expression throughout all cellular processes, phosphorylation specific antibodies revealed differences in cellular compartmentalization specific to wild type or mutant tau. In 5 month-old mouse brains only phosphorylated human tau_{wt} appeared in cortical layer 5 neuritic projections whereas only phosphorylated tau_{P301L} was found in hippocampal cells. Mice expressing both human transgenes, rTg(tau_{P301L}/tau_{wt}), contained phosphorylated tau in both cellular regions suggesting that each tau variant was expressed and sorted in an isoform-specific manner. Interestingly, rTg(tau_{P301L}/tau_{wt})$Mapt^{0/0}$ mice showed signs of decreased, possibly delayed, tau pathology compared to rTg(tau_{P301L})$Mapt^{0/0}$ despite their similarities in soluble tau expression, phosphorylation, and histological distribution, and was a key finding to these experiments. Wild type tau, mouse or human, reduced the pathogenic effects of mouse-expressed mutant human tau suggesting a general, not species, effect.

Patient-specific SC cultures hold promise for investigating disease mechanisms and drug treatments tailored to the individual. Such cultures must reliably retain their multipotency and proliferative capacity and simultaneously maintain patient-specific

gene expression and biochemical tendencies. We tested these parameters in neurospheres harvested from two genetically distinct transgenic mouse lines with well-known genotype-specific biochemical properties. Extensive characterization of over 30 independent neurosphere lines generated from rTg(tau_{P301L}) and rTg(tau_{wt}) fetuses demonstrated that they maintained *in vivo* characteristics specific to the mice from which they were derived, and retained SC qualities (i.e. proliferation and differentiation) for at least 10 passages.

Though rTg(tau_{P301L}) and rTg(tau_{wt}) cultures expressed comparable levels of total human tau, unexpectedly each experiment revealed a greater proportion of transgene-expressing cells in rTg(tau_{wt}) than rTg(tau_{P301L}) neurosphere cultures. While the rTg(tau_{P301L}) cultures contained a lower proportion of total cells expressing human tau, they contained a greater proportion of cells that expressed higher levels (brighter fluorescence intensity) of human tau protein. Transgenic mice are often matched to controls by total protein expression level. However, slight differences in transgene expression, as seen here, may be an important factor for diseases that arise from specific cell population degeneration. If distinct cell populations express transgenic protein at different levels, results could be misinterpreted. These subtle differences would have been difficult to detect *in vivo* and illustrate the importance of *in vitro* surrogate systems. Our results demonstrated the ability of neurospheres to recapitulate *in vivo* phenotypes and their utility as investigative models to uncover relevant biological phenotypes.

Tau_{wt}-expressing fetuses, neurospheres, and young mice contained more heavily phosphorylated tau species than those expressing tau_{P301L}. However, only adult

rTg(tau_{P301L}) mice developed tauopathy which suggests that tau phosphorylation does not necessarily drive pathology and that tau hypophosphorylation may be an important pre-disease phenotype. The transition of tau_{P301L} hypo-to-hyperphosphorylation coincided with conformational alterations and insolubility. This phenotypic marker may be useful to distinguish pre-clinical disease in future experimental studies. Importantly, this genotype-specific difference was first realized in neurosphere cultures and later confirmed in adult mice, which provides supporting evidence for the use of SC-based culture systems to study disease.

Overall, results from our *in vitro* and *in vivo* studies provide evidence against the long-standing hypothesis that suggests species differences between mouse and human tau prevent the development of an AD mouse. The presence of endogenous mouse tau likely resembles that of human tau in patient brains. The inability to develop an AD mouse model may arise from other species differences that could be explored using neurospheres. Based on the robust results generated by these neurospheres, and with the development of methodology to culture human olfactory mucosa-derived neurospheres, we suggest that neurospheres derived from family members carrying FAD genes will provide useful information regarding disease pathogenesis.

REFERENCES CITED

1. Alzheimer A, Stelzmann RA, Schnitzlein HN, Murtagh FR (1995) An English translation of Alzheimer's 1907 paper, "Uber eine eigenartige Erkankung der Hirnrinde". Clin Anat 8: 429-431.

2. Thies W, Bleiler L (2011) 2011 Alzheimer's disease facts and figures. Alzheimers Dement 7: 208-244.

3. Brookmeyer R, Corrada MM, Curriero FC, Kawas C (2002) Survival following a diagnosis of Alzheimer disease. Arch Neurol 59: 1764-1767.

4. Larson EB, Shadlen MF, Wang L, McCormick WC, Bowen JD, et al. (2004) Survival after initial diagnosis of Alzheimer disease. Ann Intern Med 140: 501-509.

5. Ganguli M, Dodge HH, Shen C, Pandav RS, DeKosky ST (2005) Alzheimer disease and mortality: a 15-year epidemiological study. Arch Neurol 62: 779-784.

6. Helzner EP, Scarmeas N, Cosentino S, Tang MX, Schupf N, et al. (2008) Survival in Alzheimer disease: a multiethnic, population-based study of incident cases. Neurology 71: 1489-1495.

7. Hansson O, Zetterberg H, Buchhave P, Londos E, Blennow K, et al. (2006) Association between CSF biomarkers and incipient Alzheimer's disease in patients with mild cognitive impairment: a follow-up study. Lancet Neurol 5: 228-234.

8. Braak H, Braak E (1991) Neuropathological stageing of Alzheimer-related changes. Acta Neuropathol 82: 239-259.

9. Goate A, Chartier-Harlin MC, Mullan M, Brown J, Crawford F, et al. (1991) Segregation of a missense mutation in the amyloid precursor protein gene with familial Alzheimer's disease. Nature 349: 704-706.

10. Chartier-Harlin MC, Crawford F, Houlden H, Warren A, Hughes D, et al. (1991) Early-onset Alzheimer's disease caused by mutations at codon 717 of the beta-amyloid precursor protein gene. Nature 353: 844-846.

11. Murrell J, Farlow M, Ghetti B, Benson MD (1991) A mutation in the amyloid precursor protein associated with hereditary Alzheimer's disease. Science 254: 97-99.

12. Hendriks L, van Duijn CM, Cras P, Cruts M, Van Hul W, et al. (1992) Presenile dementia and cerebral haemorrhage linked to a mutation at codon 692 of the beta-amyloid precursor protein gene. Nat Genet 1: 218-221.

13. Mullan M, Crawford F, Axelman K, Houlden H, Lilius L, et al. (1992) A pathogenic mutation for probable Alzheimer's disease in the APP gene at the N-terminus of beta-amyloid. Nat Genet 1: 345-347.

14. Sherrington R, Rogaev EI, Liang Y, Rogaeva EA, Levesque G, et al. (1995) Cloning of a gene bearing missense mutations in early-onset familial Alzheimer's disease. Nature 375: 754-760.

15. Levy-Lahad E, Wasco W, Poorkaj P, Romano DM, Oshima J, et al. (1995) Candidate gene for the chromosome 1 familial Alzheimer's disease locus. Science 269: 973-977.

16. Rogaev EI, Sherrington R, Rogaeva EA, Levesque G, Ikeda M, et al. (1995) Familial Alzheimer's disease in kindreds with missense mutations in a gene on chromosome 1 related to the Alzheimer's disease type 3 gene. Nature 376: 775-778.

17. Masters CL, Multhaup G, Simms G, Pottgiesser J, Martins RN, et al. (1985) Neuronal origin of a cerebral amyloid: neurofibrillary tangles of Alzheimer's disease contain the same protein as the amyloid of plaque cores and blood vessels. EMBO J 4: 2757-2763.

18. Hardy J, Selkoe DJ (2002) The amyloid hypothesis of Alzheimer's disease: progress and problems on the road to therapeutics. Science 297: 353-356.

19. Games D, Adams D, Alessandrini R, Barbour R, Berthelette P, et al. (1995) Alzheimer-type neuropathology in transgenic mice overexpressing V717F beta-amyloid precursor protein. Nature 373: 523-527.

20. Hsiao K, Chapman P, Nilsen S, Eckman C, Harigaya Y, et al. (1996) Correlative memory deficits, Abeta elevation, and amyloid plaques in transgenic mice. Science 274: 99-102.

21. Irizarry MC, McNamara M, Fedorchak K, Hsiao K, Hyman BT (1997) APPSw transgenic mice develop age-related A beta deposits and neuropil abnormalities, but no neuronal loss in CA1. J Neuropathol Exp Neurol 56: 965-973.

22. Elder GA, Gama Sosa MA, De Gasperi R, Dickstein DL, Hof PR (2010) Presenilin transgenic mice as models of Alzheimer's disease. Brain Struct Funct 214: 127-143.

23. Lewis J, McGowan E, Rockwood J, Melrose H, Nacharaju P, et al. (2000) Neurofibrillary tangles, amyotrophy and progressive motor disturbance in mice expressing mutant (P301L) tau protein. Nat Genet 25: 402-405.

24. Oddo S, Caccamo A, Shepherd JD, Murphy MP, Golde TE, et al. (2003) Triple-transgenic model of Alzheimer's disease with plaques and tangles: intracellular Abeta and synaptic dysfunction. Neuron 39: 409-421.

25. Weingarten MD, Lockwood AH, Hwo SY, Kirschner MW (1975) A protein factor essential for microtubule assembly. Proc Natl Acad Sci U S A 72: 1858-1862.

26. Horio T, Hotani H (1986) Visualization of the dynamic instability of individual microtubules by dark-field microscopy. Nature 321: 605-607.

27. Goedert M, Crowther RA, Garner CC (1991) Molecular characterization of microtubule-associated proteins tau and MAP2. Trends Neurosci 14: 193-199.

28. Hirokawa N (1994) Microtubule organization and dynamics dependent on microtubule-associated proteins. Curr Opin Cell Biol 6: 74-81.

29. Goedert M, Spillantini MG, Jakes R, Rutherford D, Crowther RA (1989) Multiple isoforms of human microtubule-associated protein tau: sequences and localization in neurofibrillary tangles of Alzheimer's disease. Neuron 3: 519-526.

30. Goedert M, Spillantini MG, Potier MC, Ulrich J, Crowther RA (1989) Cloning and sequencing of the cDNA encoding an isoform of microtubule-associated protein tau containing four tandem repeats: differential expression of tau protein mRNAs in human brain. EMBO J 8: 393-399.

31. Himmler A, Drechsel D, Kirschner MW, Martin DW, Jr. (1989) Tau consists of a set of proteins with repeated C-terminal microtubule-binding domains and variable N-terminal domains. Mol Cell Biol 9: 1381-1388.

32. Kosik KS, Orecchio LD, Bakalis S, Neve RL (1989) Developmentally regulated expression of specific tau sequences. Neuron 2: 1389-1397.

33. Lee G, Cowan N, Kirschner M (1988) The primary structure and heterogeneity of tau protein from mouse brain. Science 239: 285-288.

34. Kanai Y, Chen J, Hirokawa N (1992) Microtubule bundling by tau proteins in vivo: analysis of functional domains. EMBO J 11: 3953-3961.

35. Chen J, Kanai Y, Cowan NJ, Hirokawa N (1992) Projection domains of MAP2 and tau determine spacings between microtubules in dendrites and axons. Nature 360: 674-677.

36. Brandt R, Leger J, Lee G (1995) Interaction of tau with the neural plasma membrane mediated by tau's amino-terminal projection domain. J Cell Biol 131: 1327-1340.

37. Goedert M, Jakes R (1990) Expression of separate isoforms of human tau protein: correlation with the tau pattern in brain and effects on tubulin polymerization. EMBO J 9: 4225-4230.

38. Goode BL, Feinstein SC (1994) Identification of a novel microtubule binding and assembly domain in the developmentally regulated inter-repeat region of tau. J Cell Biol 124: 769-782.

39. Panda D, Goode BL, Feinstein SC, Wilson L (1995) Kinetic stabilization of microtubule dynamics at steady state by tau and microtubule-binding domains of tau. Biochemistry 34: 11117-11127.

40. Gustke N, Trinczek B, Biernat J, Mandelkow EM, Mandelkow E (1994) Domains of tau protein and interactions with microtubules. Biochemistry 33: 9511-9522.

41. Cleveland DW, Hwo SY, Kirschner MW (1977) Purification of tau, a microtubule-associated protein that induces assembly of microtubules from purified tubulin. J Mol Biol 116: 207-225.

42. Cleveland DW, Hwo SY, Kirschner MW (1977) Physical and chemical properties of purified tau factor and the role of tau in microtubule assembly. J Mol Biol 116: 227-247.

43. Lindwall G, Cole RD (1984) Phosphorylation affects the ability of tau protein to promote microtubule assembly. J Biol Chem 259: 5301-5305.

44. Biernat J, Gustke N, Drewes G, Mandelkow EM, Mandelkow E (1993) Phosphorylation of Ser262 strongly reduces binding of tau to microtubules: distinction between PHF-like immunoreactivity and microtubule binding. Neuron 11: 153-163.

45. Bramblett GT, Goedert M, Jakes R, Merrick SE, Trojanowski JQ, et al. (1993) Abnormal tau phosphorylation at Ser396 in Alzheimer's disease recapitulates development and contributes to reduced microtubule binding. Neuron 10: 1089-1099.

46. Brion JP, Smith C, Couck AM, Gallo JM, Anderton BH (1993) Developmental changes in tau phosphorylation: fetal tau is transiently phosphorylated in a manner similar to paired helical filament-tau characteristic of Alzheimer's disease. J Neurochem 61: 2071-2080.

47. Kenessey A, Yen SH (1993) The extent of phosphorylation of fetal tau is comparable to that of PHF-tau from Alzheimer paired helical filaments. Brain Res 629: 40-46.

48. Himmler A (1989) Structure of the bovine tau gene: alternatively spliced transcripts generate a protein family. Mol Cell Biol 9: 1389-1396.

49. Alonso A, Zaidi T, Novak M, Grundke-Iqbal I, Iqbal K (2001) Hyperphosphorylation induces self-assembly of tau into tangles of paired helical filaments/straight filaments. Proc Natl Acad Sci U S A 98: 6923-6928.

50. Bancher C, Brunner C, Lassmann H, Budka H, Jellinger K, et al. (1989) Accumulation of abnormally phosphorylated tau precedes the formation of neurofibrillary tangles in Alzheimer's disease. Brain Res 477: 90-99.

51. Weaver CL, Espinoza M, Kress Y, Davies P (2000) Conformational change as one of the earliest alterations of tau in Alzheimer's disease. Neurobiol Aging 21: 719-727.

52. Ihara Y (1988) Massive somatodendritic sprouting of cortical neurons in Alzheimer's disease. Brain Res 459: 138-144.

53. Wischik CM (1989) Cell biology of the Alzheimer tangle. Curr Opin Cell Biol 1: 115-122.

54. Braak E, Braak H, Mandelkow EM (1994) A sequence of cytoskeleton changes related to the formation of neurofibrillary tangles and neuropil threads. Acta Neuropathol 87: 554-567.

55. Kosik KS, Crandall JE, Mufson EJ, Neve RL (1989) Tau in situ hybridization in normal and Alzheimer brain: localization in the somatodendritic compartment. Ann Neurol 26: 352-361.

56. Braak H, Braak E (1995) Staging of Alzheimer's disease-related neurofibrillary changes. Neurobiol Aging 16: 271-278; discussion 278-284.

57. Buee L, Bussiere T, Buee-Scherrer V, Delacourte A, Hof PR (2000) Tau protein isoforms, phosphorylation and role in neurodegenerative disorders. Brain Res Brain Res Rev 33: 95-130.

58. Schweers O, Schonbrunn-Hanebeck E, Marx A, Mandelkow E (1994) Structural studies of tau protein and Alzheimer paired helical filaments show no evidence for beta-structure. J Biol Chem 269: 24290-24297.

59. Kidd M (1963) Paired helical filaments in electron microscopy of Alzheimer's disease. Nature 197: 192-193.

60. Kidd M (1964) Alzheimer's Disease--an Electron Microscopical Study. Brain 87: 307-320.

61. Wolozin BL, Pruchnicki A, Dickson DW, Davies P (1986) A neuronal antigen in the brains of Alzheimer patients. Science 232: 648-650.

62. Goedert M, Wischik CM, Crowther RA, Walker JE, Klug A (1988) Cloning and sequencing of the cDNA encoding a core protein of the paired helical filament of Alzheimer disease: identification as the microtubule-associated protein tau. Proc Natl Acad Sci U S A 85: 4051-4055.

63. Lee VM, Balin BJ, Otvos L, Jr., Trojanowski JQ (1991) A68: a major subunit of paired helical filaments and derivatized forms of normal Tau. Science 251: 675-678.

64. Ksiezak-Reding H, Binder LI, Yen SH (1990) Alzheimer disease proteins (A68) share epitopes with tau but show distinct biochemical properties. J Neurosci Res 25: 420-430.

65. Delacourte A, Flament S, Dibe EM, Hublau P, Sablonniere B, et al. (1990) Pathological proteins Tau 64 and 69 are specifically expressed in the somatodendritic domain of the degenerating cortical neurons during Alzheimer's disease. Demonstration with a panel of antibodies against Tau proteins. Acta Neuropathol 80: 111-117.

66. Hasegawa M, Morishima-Kawashima M, Takio K, Suzuki M, Titani K, et al. (1992) Protein sequence and mass spectrometric analyses of tau in the Alzheimer's disease brain. J Biol Chem 267: 17047-17054.

67. Flament S, Delacourte A, Mann DM (1990) Phosphorylation of Tau proteins: a major event during the process of neurofibrillary degeneration. A comparative study between Alzheimer's disease and Down's syndrome. Brain Res 516: 15-19.

68. Crowe A, Ksiezak-Reding H, Liu WK, Dickson DW, Yen SH (1991) The N terminal region of human tau is present in Alzheimer's disease protein A68 and is incorporated into paired helical filaments. Am J Pathol 139: 1463-1470.

69. Goedert M, Spillantini MG, Cairns NJ, Crowther RA (1992) Tau proteins of Alzheimer paired helical filaments: abnormal phosphorylation of all six brain isoforms. Neuron 8: 159-168.

70. Goedert M, Jakes R, Crowther RA, Six J, Lubke U, et al. (1993) The abnormal phosphorylation of tau protein at Ser-202 in Alzheimer disease recapitulates phosphorylation during development. Proc Natl Acad Sci U S A 90: 5066-5070.

71. Grundke-Iqbal I, Iqbal K, Tung YC, Quinlan M, Wisniewski HM, et al. (1986) Abnormal phosphorylation of the microtubule-associated protein tau (tau) in Alzheimer cytoskeletal pathology. Proc Natl Acad Sci U S A 83: 4913-4917.

72. Ksiezak-Reding H, Liu WK, Yen SH (1992) Phosphate analysis and dephosphorylation of modified tau associated with paired helical filaments. Brain Res 597: 209-219.

73. Lichtenberg-Kraag B, Mandelkow EM, Biernat J, Steiner B, Schroter C, et al. (1992) Phosphorylation-dependent epitopes of neurofilament antibodies on tau protein and relationship with Alzheimer tau. Proc Natl Acad Sci U S A 89: 5384-5388.

74. Wood JG, Mirra SS, Pollock NJ, Binder LI (1986) Neurofibrillary tangles of Alzheimer disease share antigenic determinants with the axonal microtubule-associated protein tau (tau). Proc Natl Acad Sci U S A 83: 4040-4043.

75. Grundke-Iqbal I, Iqbal K, Quinlan M, Tung YC, Zaidi MS, et al. (1986) Microtubule-associated protein tau. A component of Alzheimer paired helical filaments. J Biol Chem 261: 6084-6089.

76. Wischik CM, Crowther RA, Stewart M, Roth M (1985) Subunit structure of paired helical filaments in Alzheimer's disease. J Cell Biol 100: 1905-1912.

77. Crowther RA, Wischik CM (1985) Image reconstruction of the Alzheimer paired helical filament. EMBO J 4: 3661-3665.

78. Wischik CM, Novak M, Thogersen HC, Edwards PC, Runswick MJ, et al. (1988) Isolation of a fragment of tau derived from the core of the paired helical filament of Alzheimer disease. Proc Natl Acad Sci U S A 85: 4506-4510.

79. Heutink P, Stevens M, Rizzu P, Bakker E, Kros JM, et al. (1997) Hereditary frontotemporal dementia is linked to chromosome 17q21-q22: a genetic and clinicopathological study of three Dutch families. Ann Neurol 41: 150-159.

80. Hutton M, Lendon CL, Rizzu P, Baker M, Froelich S, et al. (1998) Association of missense and 5'-splice-site mutations in tau with the inherited dementia FTDP-17. Nature 393: 702-705.

81. Mayford M, Bach ME, Huang YY, Wang L, Hawkins RD, et al. (1996) Control of memory formation through regulated expression of a CaMKII transgene. Science 274: 1678-1683.

82. Erondu NE, Kennedy MB (1985) Regional distribution of type II Ca2+/calmodulin-dependent protein kinase in rat brain. J Neurosci 5: 3270-3277.

83. Bayer KU, Lohler J, Schulman H, Harbers K (1999) Developmental expression of the CaM kinase II isoforms: ubiquitous gamma- and delta-CaM kinase II are the early isoforms and most abundant in the developing nervous system. Brain Res Mol Brain Res 70: 147-154.

84. Ramsden M, Kotilinek L, Forster C, Paulson J, McGowan E, et al. (2005) Age-dependent neurofibrillary tangle formation, neuron loss, and memory impairment in a mouse model of human tauopathy (P301L). J Neurosci 25: 10637-10647.

85. Santacruz K, Lewis J, Spires T, Paulson J, Kotilinek L, et al. (2005) Tau suppression in a neurodegenerative mouse model improves memory function. Science 309: 476-481.

86. Gossen M, Bujard H (1992) Tight control of gene expression in mammalian cells by tetracycline-responsive promoters. Proc Natl Acad Sci U S A 89: 5547-5551.

87. Mercken M, Vandermeeren M, Lubke U, Six J, Boons J, et al. (1992) Monoclonal antibodies with selective specificity for Alzheimer Tau are directed against phosphatase-sensitive epitopes. Acta Neuropathol 84: 265-272.

88. Dickey C, Kraft C, Jinwal U, Koren J, Johnson A, et al. (2009) Aging analysis reveals slowed tau turnover and enhanced stress response in a mouse model of tauopathy. Am J Pathol 174: 228-238.

89. Brich J, Shie FS, Howell BW, Li R, Tus K, et al. (2003) Genetic modulation of tau phosphorylation in the mouse. J Neurosci 23: 187-192.

90. Hiesberger T, Trommsdorff M, Howell BW, Goffinet A, Mumby MC, et al. (1999) Direct binding of Reelin to VLDL receptor and ApoE receptor 2 induces tyrosine phosphorylation of disabled-1 and modulates tau phosphorylation. Neuron 24: 481-489.

91. Kocherhans S, Madhusudan A, Doehner J, Breu KS, Nitsch RM, et al. (2010) Reduced Reelin expression accelerates amyloid-beta plaque formation and tau pathology in transgenic Alzheimer's disease mice. J Neurosci 30: 9228-9240.

92. Ohkubo N, Lee YD, Morishima A, Terashima T, Kikkawa S, et al. (2003) Apolipoprotein E and Reelin ligands modulate tau phosphorylation through an apolipoprotein E receptor/disabled-1/glycogen synthase kinase-3beta cascade. FASEB J 17: 295-297.

93. Terwel D, Lasrado R, Snauwaert J, Vandeweert E, Van Haesendonck C, et al. (2005) Changed conformation of mutant Tau-P301L underlies the moribund tauopathy, absent in progressive, nonlethal axonopathy of Tau-4R/2N transgenic mice. J Biol Chem 280: 3963-3973.

94. Boekhoorn K, Terwel D, Biemans B, Borghgraef P, Wiegert O, et al. (2006) Improved long-term potentiation and memory in young tau-P301L transgenic mice before onset of hyperphosphorylation and tauopathy. J Neurosci 26: 3514-3523.

95. Hasegawa M, Smith MJ, Goedert M (1998) Tau proteins with FTDP-17 mutations have a reduced ability to promote microtubule assembly. FEBS Lett 437: 207-210.

96. Hong M, Zhukareva V, Vogelsberg-Ragaglia V, Wszolek Z, Reed L, et al. (1998) Mutation-specific functional impairments in distinct tau isoforms of hereditary FTDP-17. Science 282: 1914-1917.

97. Morsch R, Simon W, Coleman PD (1999) Neurons may live for decades with neurofibrillary tangles. J Neuropathol Exp Neurol 58: 188-197.

98. Spires TL, Orne JD, SantaCruz K, Pitstick R, Carlson GA, et al. (2006) Region-specific dissociation of neuronal loss and neurofibrillary pathology in a mouse model of tauopathy. Am J Pathol 168: 1598-1607.

99. de Calignon A, Fox LM, Pitstick R, Carlson GA, Bacskai BJ, et al. (2010) Caspase activation precedes and leads to tangles. Nature 464: 1201-1204.

100. Rocher AB, Crimins JL, Amatrudo JM, Kinson MS, Todd-Brown MA, et al. (2009) Structural and functional changes in tau mutant mice neurons are not linked to the presence of NFTs. Exp Neurol.

101. Rissman RA, Poon WW, Blurton-Jones M, Oddo S, Torp R, et al. (2004) Caspase-cleavage of tau is an early event in Alzheimer disease tangle pathology. J Clin Invest 114: 121-130.

102. Gamblin TC, Chen F, Zambrano A, Abraha A, Lagalwar S, et al. (2003) Caspase cleavage of tau: linking amyloid and neurofibrillary tangles in Alzheimer's disease. Proc Natl Acad Sci U S A 100: 10032-10037.

103. Zhang Q, Zhang X, Sun A (2009) Truncated tau at D421 is associated with neurodegeneration and tangle formation in the brain of Alzheimer transgenic models. Acta Neuropathol 117: 687-697.

104. Delobel P, Lavenir I, Fraser G, Ingram E, Holzer M, et al. (2008) Analysis of tau phosphorylation and truncation in a mouse model of human tauopathy. Am J Pathol 172: 123-131.

105. Gilley J, Seereeram A, Ando K, Mosely S, Andrews S, et al. (2011) Age-dependent axonal transport and locomotor changes and tau hypophosphorylation in a "P301L" tau knockin mouse. Neurobiol Aging.

106. Eidenmuller J, Fath T, Hellwig A, Reed J, Sontag E, et al. (2000) Structural and functional implications of tau hyperphosphorylation: information from phosphorylation-mimicking mutated tau proteins. Biochemistry 39: 13166-13175.

107. Hundelt M, Fath T, Selle K, Oesterwind K, Jordan J, et al. (2011) Altered phosphorylation but no neurodegeneration in a mouse model of tau hyperphosphorylation. Neurobiol Aging 32: 991-1006.

108. Zhang B, Higuchi M, Yoshiyama Y, Ishihara T, Forman MS, et al. (2004) Retarded axonal transport of R406W mutant tau in transgenic mice with a neurodegenerative tauopathy. J Neurosci 24: 4657-4667.

109. Tatebayashi Y, Miyasaka T, Chui DH, Akagi T, Mishima K, et al. (2002) Tau filament formation and associative memory deficit in aged mice expressing mutant (R406W) human tau. Proc Natl Acad Sci U S A 99: 13896-13901.

110. von Bergen M, Friedhoff P, Biernat J, Heberle J, Mandelkow EM, et al. (2000) Assembly of tau protein into Alzheimer paired helical filaments depends on a local sequence motif ((306)VQIVYK(311)) forming beta structure. Proc Natl Acad Sci U S A 97: 5129-5134.

111. von Bergen M, Barghorn S, Li L, Marx A, Biernat J, et al. (2001) Mutations of tau protein in frontotemporal dementia promote aggregation of paired helical filaments by enhancing local beta-structure. J Biol Chem 276: 48165-48174.

112. Eckermann K, Mocanu MM, Khlistunova I, Biernat J, Nissen A, et al. (2007) The beta-propensity of Tau determines aggregation and synaptic loss in inducible mouse models of tauopathy. J Biol Chem 282: 31755-31765.

113. Barghorn S, Mandelkow E (2002) Toward a unified scheme for the aggregation of tau into Alzheimer paired helical filaments. Biochemistry 41: 14885-14896.

114. Hoover BR, Reed MN, Su J, Penrod RD, Kotilinek LA, et al. (2010) Tau mislocalization to dendritic spines mediates synaptic dysfunction independently of neurodegeneration. Neuron 68: 1067-1081.

115. Gotz J, Probst A, Spillantini MG, Schafer T, Jakes R, et al. (1995) Somatodendritic localization and hyperphosphorylation of tau protein in transgenic mice expressing the longest human brain tau isoform. EMBO J 14: 1304-1313.

116. Brion JP, Tremp G, Octave JN (1999) Transgenic expression of the shortest human tau affects its compartmentalization and its phosphorylation as in the pretangle stage of Alzheimer's disease. Am J Pathol 154: 255-270.

117. Ishihara T, Hong M, Zhang B, Nakagawa Y, Lee MK, et al. (1999) Age-dependent emergence and progression of a tauopathy in transgenic mice overexpressing the shortest human tau isoform. Neuron 24: 751-762.

118. Spittaels K, Van den Haute C, Van Dorpe J, Bruynseels K, Vandezande K, et al. (1999) Prominent axonopathy in the brain and spinal cord of transgenic mice overexpressing four-repeat human tau protein. Am J Pathol 155: 2153-2165.

119. Probst A, Gotz J, Wiederhold KH, Tolnay M, Mistl C, et al. (2000) Axonopathy and amyotrophy in mice transgenic for human four-repeat tau protein. Acta Neuropathol 99: 469-481.

120. Duff K, Knight H, Refolo LM, Sanders S, Yu X, et al. (2000) Characterization of pathology in transgenic mice over-expressing human genomic and cDNA tau transgenes. Neurobiol Dis 7: 87-98.

121. Adams SJ, Crook RJ, Deture M, Randle SJ, Innes AE, et al. (2009) Overexpression of wild-type murine tau results in progressive tauopathy and neurodegeneration. Am J Pathol 175: 1598-1609.

122. D'Souza I, Schellenberg GD (2005) Regulation of tau isoform expression and dementia. Biochim Biophys Acta 1739: 104-115.

123. Stanford PM, Shepherd CE, Halliday GM, Brooks WS, Schofield PW, et al. (2003) Mutations in the tau gene that cause an increase in three repeat tau and frontotemporal dementia. Brain 126: 814-826.

124. Liu F, Gong CX (2008) Tau exon 10 alternative splicing and tauopathies. Mol Neurodegener 3: 8.

125. Sergeant N, Delacourte A, Buee L (2005) Tau protein as a differential biomarker of tauopathies. Biochim Biophys Acta 1739: 179-197.

126. Ishihara T, Zhang B, Higuchi M, Yoshiyama Y, Trojanowski JQ, et al. (2001) Age-dependent induction of congophilic neurofibrillary tau inclusions in tau transgenic mice. Am J Pathol 158: 555-562.

127. Ikegami S, Harada A, Hirokawa N (2000) Muscle weakness, hyperactivity, and impairment in fear conditioning in tau-deficient mice. Neurosci Lett 279: 129-132.

128. Harada A, Oguchi K, Okabe S, Kuno J, Terada S, et al. (1994) Altered microtubule organization in small-calibre axons of mice lacking tau protein. Nature 369: 488-491.

129. Tucker KL, Meyer M, Barde YA (2001) Neurotrophins are required for nerve growth during development. Nat Neurosci 4: 29-37.

130. Dawson HN, Ferreira A, Eyster MV, Ghoshal N, Binder LI, et al. (2001) Inhibition of neuronal maturation in primary hippocampal neurons from tau deficient mice. J Cell Sci 114: 1179-1187.

131. Drubin DG, Feinstein SC, Shooter EM, Kirschner MW (1985) Nerve growth factor-induced neurite outgrowth in PC12 cells involves the coordinate induction of microtubule assembly and assembly-promoting factors. J Cell Biol 101: 1799-1807.

132. Takei Y, Teng J, Harada A, Hirokawa N (2000) Defects in axonal elongation and neuronal migration in mice with disrupted tau and map1b genes. J Cell Biol 150: 989-1000.

133. DiTella MC, Feiguin F, Carri N, Kosik KS, Caceres A (1996) MAP-1B/TAU functional redundancy during laminin-enhanced axonal growth. J Cell Sci 109 (Pt 2): 467-477.

134. Schoenfeld TA, McKerracher L, Obar R, Vallee RB (1989) MAP 1A and MAP 1B are structurally related microtubule associated proteins with distinct developmental patterns in the CNS. J Neurosci 9: 1712-1730.

135. Riederer BM, Innocenti GM (1991) Differential Distribution of Tau Proteins in Developing Cat Cerebral Cortex and Corpus Callosum. Eur J Neurosci 3: 1134-1145.

136. Pacheco CD, Elrick MJ, Lieberman AP (2009) Tau deletion exacerbates the phenotype of Niemann-Pick type C mice and implicates autophagy in pathogenesis. Hum Mol Genet 18: 956-965.

137. Pacheco CD, Elrick MJ, Lieberman AP (2009) Tau normal function influences Niemann-Pick type C disease pathogenesis in mice and modulates autophagy in NPC1-deficient cells. Autophagy 5: 548-550.

138. Andorfer C, Acker CM, Kress Y, Hof PR, Duff K, et al. (2005) Cell-cycle reentry and cell death in transgenic mice expressing nonmutant human tau isoforms. J Neurosci 25: 5446-5454.

139. Ando K, Leroy K, Heraud C, Yilmaz Z, Authelet M, et al. (2011) Accelerated human mutant tau aggregation by knocking out murine tau in a transgenic mouse model. Am J Pathol 178: 803-816.

140. Poorkaj P, Kas A, D'Souza I, Zhou Y, Pham Q, et al. (2001) A genomic sequence analysis of the mouse and human microtubule-associated protein tau. Mamm Genome 12: 700-712.

141. Chohan MO, Haque N, Alonso A, El-Akkad E, Grundke-Iqbal I, et al. (2005) Hyperphosphorylation-induced self assembly of murine tau: a comparison with human tau. J Neural Transm 112: 1035-1047.

142. Goedert M, Jakes R, Spillantini MG, Hasegawa M, Smith MJ, et al. (1996) Assembly of microtubule-associated protein tau into Alzheimer-like filaments induced by sulphated glycosaminoglycans. Nature 383: 550-553.

143. Kampers T, Pangalos M, Geerts H, Wiech H, Mandelkow E (1999) Assembly of paired helical filaments from mouse tau: implications for the neurofibrillary pathology in transgenic mouse models for Alzheimer's disease. FEBS Lett 451: 39-44.

144. Yanagisawa M, Planel E, Ishiguro K, Fujita SC (1999) Starvation induces tau hyperphosphorylation in mouse brain: implications for Alzheimer's disease. FEBS Lett 461: 329-333.

145. Planel E, Miyasaka T, Launey T, Chui DH, Tanemura K, et al. (2004) Alterations in glucose metabolism induce hypothermia leading to tau hyperphosphorylation through differential inhibition of kinase and phosphatase activities: implications for Alzheimer's disease. J Neurosci 24: 2401-2411.

146. Planel E, Richter KE, Nolan CE, Finley JE, Liu L, et al. (2007) Anesthesia leads to tau hyperphosphorylation through inhibition of phosphatase activity by hypothermia. J Neurosci 27: 3090-3097.

147. Okawa Y, Ishiguro K, Fujita SC (2003) Stress-induced hyperphosphorylation of tau in the mouse brain. FEBS Lett 535: 183-189.

148. Arendt T, Stieler J, Strijkstra AM, Hut RA, Rudiger J, et al. (2003) Reversible paired helical filament-like phosphorylation of tau is an adaptive process associated with neuronal plasticity in hibernating animals. J Neurosci 23: 6972-6981.

149. Hartig W, Stieler J, Boerema AS, Wolf J, Schmidt U, et al. (2007) Hibernation model of tau phosphorylation in hamsters: selective vulnerability of cholinergic basal forebrain neurons - implications for Alzheimer's disease. Eur J Neurosci 25: 69-80.

150. Su B, Wang X, Drew KL, Perry G, Smith MA, et al. (2008) Physiological regulation of tau phosphorylation during hibernation. J Neurochem 105: 2098-2108.

151. Clavaguera F, Bolmont T, Crowther RA, Abramowski D, Frank S, et al. (2009) Transmission and spreading of tauopathy in transgenic mouse brain. Nat Cell Biol 11: 909-913.

152. Frost B, Jacks RL, Diamond MI (2009) Propagation of tau misfolding from the outside to the inside of a cell. J Biol Chem 284: 12845-12852.

153. Buee L, Delacourte A (1999) Comparative biochemistry of tau in progressive supranuclear palsy, corticobasal degeneration, FTDP-17 and Pick's disease. Brain Pathol 9: 681-693.

154. Frost B, Ollesch J, Wille H, Diamond MI (2009) Conformational diversity of wild-type Tau fibrils specified by templated conformation change. J Biol Chem 284: 3546-3551.

155. Pan KM, Baldwin M, Nguyen J, Gasset M, Serban A, et al. (1993) Conversion of alpha-helices into beta-sheets features in the formation of the scrapie prion proteins. Proc Natl Acad Sci U S A 90: 10962-10966.

156. Konstantinov IE (2000) In search of Alexander A. Maximow: the man behind the unitarian theory of hematopoiesis. Perspect Biol Med 43: 269-276.

157. Till JE, Mc CE (1963) Early repair processes in marrow cells irradiated and proliferating in vivo. Radiat Res 18: 96-105.

158. Till JE, Mc CE (1961) A direct measurement of the radiation sensitivity of normal mouse bone marrow cells. Radiat Res 14: 213-222.

159. Becker AJ, Mc CE, Till JE (1963) Cytological demonstration of the clonal nature of spleen colonies derived from transplanted mouse marrow cells. Nature 197: 452-454.

160. Evans MJ, Kaufman MH (1981) Establishment in culture of pluripotential cells from mouse embryos. Nature 292: 154-156.

161. Martin GR (1981) Isolation of a pluripotent cell line from early mouse embryos cultured in medium conditioned by teratocarcinoma stem cells. Proc Natl Acad Sci U S A 78: 7634-7638.

162. Ting AE, Mays RW, Frey MR, Hof WV, Medicetty S, et al. (2008) Therapeutic pathways of adult stem cell repair. Crit Rev Oncol Hematol 65: 81-93.

163. Hess DC, Borlongan CV (2008) Stem cells and neurological diseases. Cell Prolif 41 Suppl 1: 94-114.

164. Thomson JA, Itskovitz-Eldor J, Shapiro SS, Waknitz MA, Swiergiel JJ, et al. (1998) Embryonic stem cell lines derived from human blastocysts. Science 282: 1145-1147.

165. Martinat C, Shendelman S, Jonason A, Leete T, Beal MF, et al. (2004) Sensitivity to oxidative stress in DJ-1-deficient dopamine neurons: an ES- derived cell model of primary Parkinsonism. PLoS Biol 2: e327.

166. Di Giorgio FP, Carrasco MA, Siao MC, Maniatis T, Eggan K (2007) Non-cell autonomous effect of glia on motor neurons in an embryonic stem cell-based ALS model. Nat Neurosci 10: 608-614.

167. Goldberg MS, Fleming SM, Palacino JJ, Cepeda C, Lam HA, et al. (2003) Parkin-deficient mice exhibit nigrostriatal deficits but not loss of dopaminergic neurons. J Biol Chem 278: 43628-43635.

168. Itier JM, Ibanez P, Mena MA, Abbas N, Cohen-Salmon C, et al. (2003) Parkin gene inactivation alters behaviour and dopamine neurotransmission in the mouse. Hum Mol Genet 12: 2277-2291.

169. Masliah E, Rockenstein E, Veinbergs I, Mallory M, Hashimoto M, et al. (2000) Dopaminergic loss and inclusion body formation in alpha-synuclein mice: implications for neurodegenerative disorders. Science 287: 1265-1269.

170. Giasson BI, Duda JE, Quinn SM, Zhang B, Trojanowski JQ, et al. (2002) Neuronal alpha-synucleinopathy with severe movement disorder in mice expressing A53T human alpha-synuclein. Neuron 34: 521-533.

171. Lee MK, Stirling W, Xu Y, Xu X, Qui D, et al. (2002) Human alpha-synuclein-harboring familial Parkinson's disease-linked Ala-53 --> Thr mutation causes neurodegenerative disease with alpha-synuclein aggregation in transgenic mice. Proc Natl Acad Sci U S A 99: 8968-8973.

172. Bonifati V, Rizzu P, van Baren MJ, Schaap O, Breedveld GJ, et al. (2003) Mutations in the DJ-1 gene associated with autosomal recessive early-onset parkinsonism. Science 299: 256-259.

173. Nagakubo D, Taira T, Kitaura H, Ikeda M, Tamai K, et al. (1997) DJ-1, a novel oncogene which transforms mouse NIH3T3 cells in cooperation with ras. Biochem Biophys Res Commun 231: 509-513.

174. Shendelman S, Jonason A, Martinat C, Leete T, Abeliovich A (2004) DJ-1 is a redox-dependent molecular chaperone that inhibits alpha-synuclein aggregate formation. PLoS Biol 2: e362.

175. Pasinelli P, Brown RH (2006) Molecular biology of amyotrophic lateral sclerosis: insights from genetics. Nat Rev Neurosci 7: 710-723.

176. McGrath J, Solter D (1983) Nuclear transplantation in the mouse embryo by microsurgery and cell fusion. Science 220: 1300-1302.

177. Campbell KH, McWhir J, Ritchie WA, Wilmut I (1996) Sheep cloned by nuclear transfer from a cultured cell line. Nature 380: 64-66.

178. Wilmut I, Schnieke AE, McWhir J, Kind AJ, Campbell KH (1997) Viable offspring derived from fetal and adult mammalian cells. Nature 385: 810-813.

179. Cowan CA, Atienza J, Melton DA, Eggan K (2005) Nuclear reprogramming of somatic cells after fusion with human embryonic stem cells. Science 309: 1369-1373.

180. Tada M, Takahama Y, Abe K, Nakatsuji N, Tada T (2001) Nuclear reprogramming of somatic cells by in vitro hybridization with ES cells. Curr Biol 11: 1553-1558.

181. Takahashi K, Yamanaka S (2006) Induction of pluripotent stem cells from mouse embryonic and adult fibroblast cultures by defined factors. Cell 126: 663-676.

182. Takahashi K, Tanabe K, Ohnuki M, Narita M, Ichisaka T, et al. (2007) Induction of pluripotent stem cells from adult human fibroblasts by defined factors. Cell 131: 861-872.

183. Damjanov I (2005) The road from teratocarcinoma to human embryonic stem cells. Stem Cell Rev 1: 273-276.

184. Wernig M, Meissner A, Foreman R, Brambrink T, Ku M, et al. (2007) In vitro reprogramming of fibroblasts into a pluripotent ES-cell-like state. Nature 448: 318-324.

185. Meissner A, Wernig M, Jaenisch R (2007) Direct reprogramming of genetically unmodified fibroblasts into pluripotent stem cells. Nat Biotechnol 25: 1177-1181.

186. Okita K, Ichisaka T, Yamanaka S (2007) Generation of germline-competent induced pluripotent stem cells. Nature 448: 313-317.

187. Park IH, Arora N, Huo H, Maherali N, Ahfeldt T, et al. (2008) Disease-specific induced pluripotent stem cells. Cell 134: 877-886.

188. Soldner F, Hockemeyer D, Beard C, Gao Q, Bell GW, et al. (2009) Parkinson's disease patient-derived induced pluripotent stem cells free of viral reprogramming factors. Cell 136: 964-977.

189. Dimos JT, Rodolfa KT, Niakan KK, Weisenthal LM, Mitsumoto H, et al. (2008) Induced pluripotent stem cells generated from patients with ALS can be differentiated into motor neurons. Science 321: 1218-1221.

190. Kostova FV, Williams VC, Heemskerk J, Iannaccone S, Didonato C, et al. (2007) Spinal muscular atrophy: classification, diagnosis, management, pathogenesis, and future research directions. J Child Neurol 22: 926-945.

191. Lefebvre S, Burglen L, Reboullet S, Clermont O, Burlet P, et al. (1995) Identification and characterization of a spinal muscular atrophy-determining gene. Cell 80: 155-165.

192. Coovert DD, Le TT, McAndrew PE, Strasswimmer J, Crawford TO, et al. (1997) The survival motor neuron protein in spinal muscular atrophy. Hum Mol Genet 6: 1205-1214.

193. Crawford TO, Pardo CA (1996) The neurobiology of childhood spinal muscular atrophy. Neurobiol Dis 3: 97-110.

194. Ebert AD, Yu J, Rose FF, Jr., Mattis VB, Lorson CL, et al. (2009) Induced pluripotent stem cells from a spinal muscular atrophy patient. Nature 457: 277-280.

195. Pearson J, Pytel B (1978) Quantitative studies of ciliary and sphenopalatine ganglia in familial dysautonomia. J Neurol Sci 39: 123-130.

196. Pearson J, Pytel BA (1978) Quantitative studies of sympathetic ganglia and spinal cord intermedio-lateral gray columns in familial dysautonomia. J Neurol Sci 39: 47-59.

197. Pearson J, Pytel BA, Grover-Johnson N, Axelrod F, Dancis J (1978) Quantitative studies of dorsal root ganglia and neuropathologic observations on spinal cords in familial dysautonomia. J Neurol Sci 35: 77-92.

198. Slaugenhaupt SA, Blumenfeld A, Gill SP, Leyne M, Mull J, et al. (2001) Tissue-specific expression of a splicing mutation in the IKBKAP gene causes familial dysautonomia. Am J Hum Genet 68: 598-605.

199. Lee G, Papapetrou EP, Kim H, Chambers SM, Tomishima MJ, et al. (2009) Modelling pathogenesis and treatment of familial dysautonomia using patient-specific iPSCs. Nature 461: 402-406.

200. Bontekoe CJ, de Graaff E, Nieuwenhuizen IM, Willemsen R, Oostra BA (1997) FMR1 premutation allele (CGG)81 is stable in mice. Eur J Hum Genet 5: 293-298.

201. Bontekoe CJ, Bakker CE, Nieuwenhuizen IM, van der Linde H, Lans H, et al. (2001) Instability of a (CGG)98 repeat in the Fmr1 promoter. Hum Mol Genet 10: 1693-1699.

202. Peier AM, Nelson DL (2002) Instability of a premutation-sized CGG repeat in FMR1 YAC transgenic mice. Genomics 80: 423-432.

203. Lavedan C, Grabczyk E, Usdin K, Nussbaum RL (1998) Long uninterrupted CGG repeats within the first exon of the human FMR1 gene are not intrinsically unstable in transgenic mice. Genomics 50: 229-240.

204. Lavedan CN, Garrett L, Nussbaum RL (1997) Trinucleotide repeats (CGG)22TGG(CGG)43TGG(CGG)21 from the fragile X gene remain stable in transgenic mice. Hum Genet 100: 407-414.

205. Brouwer JR, Mientjes EJ, Bakker CE, Nieuwenhuizen IM, Severijnen LA, et al. (2007) Elevated Fmr1 mRNA levels and reduced protein expression in a mouse model with an unmethylated Fragile X full mutation. Exp Cell Res 313: 244-253.

206. Eiges R, Urbach A, Malcov M, Frumkin T, Schwartz T, et al. (2007) Developmental study of fragile X syndrome using human embryonic stem cells derived from preimplantation genetically diagnosed embryos. Cell Stem Cell 1: 568-577.

207. Markoulaki S, Hanna J, Beard C, Carey BW, Cheng AW, et al. (2009) Transgenic mice with defined combinations of drug-inducible reprogramming factors. Nat Biotechnol 27: 169-171.

208. Kaji K, Norrby K, Paca A, Mileikovsky M, Mohseni P, et al. (2009) Virus-free induction of pluripotency and subsequent excision of reprogramming factors. Nature.

209. Murrell W, Feron F, Wetzig A, Cameron N, Splatt K, et al. (2005) Multipotent stem cells from adult olfactory mucosa. Dev Dyn 233: 496-515.

210. Feron F, Perry C, McGrath JJ, Mackay-Sim A (1998) New techniques for biopsy and culture of human olfactory epithelial neurons. Arch Otolaryngol Head Neck Surg 124: 861-866.

211. Leung CT, Coulombe PA, Reed RR (2007) Contribution of olfactory neural stem cells to tissue maintenance and regeneration. Nat Neurosci 10: 720-726.

212. Mackay-Sim A, Kittel PW (1991) On the Life Span of Olfactory Receptor Neurons. Eur J Neurosci 3: 209-215.

213. Reynolds BA, Tetzlaff W, Weiss S (1992) A multipotent EGF-responsive striatal embryonic progenitor cell produces neurons and astrocytes. J Neurosci 12: 4565-4574.

214. Reynolds BA, Weiss S (1992) Generation of neurons and astrocytes from isolated cells of the adult mammalian central nervous system. Science 255: 1707-1710.

215. Reynolds BA, Weiss S (1996) Clonal and population analyses demonstrate that an EGF-responsive mammalian embryonic CNS precursor is a stem cell. Dev Biol 175: 1-13.

216. Suslov ON, Kukekov VG, Ignatova TN, Steindler DA (2002) Neural stem cell heterogeneity demonstrated by molecular phenotyping of clonal neurospheres. Proc Natl Acad Sci U S A 99: 14506-14511.

217. Lobo MV, Alonso FJ, Redondo C, Lopez-Toledano MA, Caso E, et al. (2003) Cellular characterization of epidermal growth factor-expanded free-floating neurospheres. J Histochem Cytochem 51: 89-103.

218. Jacques TS, Relvas JB, Nishimura S, Pytela R, Edwards GM, et al. (1998) Neural precursor cell chain migration and division are regulated through different beta1 integrins. Development 125: 3167-3177.

219. Campos LS, Leone DP, Relvas JB, Brakebusch C, Fassler R, et al. (2004) Beta1 integrins activate a MAPK signalling pathway in neural stem cells that contributes to their maintenance. Development 131: 3433-3444.

220. Jessberger S, Clemenson GD, Jr., Gage FH (2007) Spontaneous fusion and nonclonal growth of adult neural stem cells. Stem Cells 25: 871-874.

221. Coles-Takabe BL, Brain I, Purpura KA, Karpowicz P, Zandstra PW, et al. (2008) Don't look: growing clonal versus nonclonal neural stem cell colonies. Stem Cells 26: 2938-2944.

222. Mori H, Fujitani T, Kanemura Y, Kino-Oka M, Taya M (2007) Observational examination of aggregation and migration during early phase of neurosphere culture of mouse neural stem cells. J Biosci Bioeng 104: 231-234.

223. Singec I, Knoth R, Meyer RP, Maciaczyk J, Volk B, et al. (2006) Defining the actual sensitivity and specificity of the neurosphere assay in stem cell biology. Nat Methods 3: 801-806.

224. Ferron SR, Andreu-Agullo C, Mira H, Sanchez P, Marques-Torrejon MA, et al. (2007) A combined ex/in vivo assay to detect effects of exogenously added factors in neural stem cells. Nat Protoc 2: 849-859.

225. Chojnacki A, Weiss S (2008) Production of neurons, astrocytes and oligodendrocytes from mammalian CNS stem cells. Nat Protoc 3: 935-940.

226. Cordey M, Limacher M, Kobel S, Taylor V, Lutolf MP (2008) Enhancing the Reliability and Throughput of Neurosphere Culture on Hydrogel Microwell Arrays. Stem Cells.

227. Louis SA, Rietze RL, Deleyrolle L, Wagey RE, Thomas TE, et al. (2008) Enumeration of neural stem and progenitor cells in the neural colony-forming cell assay. Stem Cells 26: 988-996.

228. Conti L, Pollard SM, Gorba T, Reitano E, Toselli M, et al. (2005) Niche-independent symmetrical self-renewal of a mammalian tissue stem cell. PLoS Biol 3: e283.

229. Pollard SM, Yoshikawa K, Clarke ID, Danovi D, Stricker S, et al. (2009) Glioma stem cell lines expanded in adherent culture have tumor-specific phenotypes and are suitable for chemical and genetic screens. Cell Stem Cell 4: 568-580.

230. Johe KK, Hazel TG, Muller T, Dugich-Djordjevic MM, McKay RD (1996) Single factors direct the differentiation of stem cells from the fetal and adult central nervous system. Genes Dev 10: 3129-3140.

231. Ahmed S, Reynolds BA, Weiss S (1995) BDNF enhances the differentiation but not the survival of CNS stem cell-derived neuronal precursors. J Neurosci 15: 5765-5778.

232. Kim JB, Sebastiano V, Wu G, Arauzo-Bravo MJ, Sasse P, et al. (2009) Oct4-induced pluripotency in adult neural stem cells. Cell 136: 411-419.

233. Matigian N, Abrahamsen G, Sutharsan R, Cook AL, Vitale AM, et al. (2010) Disease-specific, neurosphere-derived cells as models for brain disorders. Dis Model Mech.

234. Abrams MT, Kaufmann WE, Rousseau F, Oostra BA, Wolozin B, et al. (1999) FMR1 gene expression in olfactory neuroblasts from two males with fragile X syndrome. Am J Med Genet 82: 25-30.

235. Arnold SE, Han LY, Moberg PJ, Turetsky BI, Gur RE, et al. (2001) Dysregulation of olfactory receptor neuron lineage in schizophrenia. Arch Gen Psychiatry 58: 829-835.

236. McCurdy RD, Feron F, Perry C, Chant DC, McLean D, et al. (2006) Cell cycle alterations in biopsied olfactory neuroepithelium in schizophrenia and bipolar I disorder using cell culture and gene expression analyses. Schizophr Res 82: 163-173.

237. Ronnett GV, Leopold D, Cai X, Hoffbuhr KC, Moses L, et al. (2003) Olfactory biopsies demonstrate a defect in neuronal development in Rett's syndrome. Ann Neurol 54: 206-218.

238. Andorfer CA, Davies P (2000) PKA phosphorylations on tau: developmental studies in the mouse. Dev Neurosci 22: 303-309.

239. Goedert M, Crowther RA (1989) Amyloid plaques, neurofibrillary tangles and their relevance for the study of Alzheimer's disease. Neurobiol Aging 10: 405-406; discussion 412-404.

240. Kopke E, Tung YC, Shaikh S, Alonso AC, Iqbal K, et al. (1993) Microtubule-associated protein tau. Abnormal phosphorylation of a non-paired helical filament pool in Alzheimer disease. J Biol Chem 268: 24374-24384.

241. Gotz J, Deters N, Doldissen A, Bokhari L, Ke Y, et al. (2007) A decade of tau transgenic animal models and beyond. Brain Pathol 17: 91-103.

242. Andorfer C, Kress Y, Espinoza M, de Silva R, Tucker KL, et al. (2003) Hyperphosphorylation and aggregation of tau in mice expressing normal human tau isoforms. J Neurochem 86: 582-590.

243. Brion JP, Octave JN, Couck AM (1994) Distribution of the phosphorylated microtubule-associated protein tau in developing cortical neurons. Neuroscience 63: 895-909.

244. Yu Y, Run X, Liang Z, Li Y, Liu F, et al. (2009) Developmental regulation of tau phosphorylation, tau kinases, and tau phosphatases. J Neurochem 108: 1480-1494.

245. Mocanu MM, Nissen A, Eckermann K, Khlistunova I, Biernat J, et al. (2008) The potential for beta-structure in the repeat domain of tau protein determines aggregation, synaptic decay, neuronal loss, and coassembly with endogenous Tau in inducible mouse models of tauopathy. J Neurosci 28: 737-748.

246. Gotz J, Chen F, van Dorpe J, Nitsch RM (2001) Formation of neurofibrillary tangles in P301l tau transgenic mice induced by Abeta 42 fibrils. Science 293: 1491-1495.

247. Lewis J, Dickson DW, Lin WL, Chisholm L, Corral A, et al. (2001) Enhanced neurofibrillary degeneration in transgenic mice expressing mutant tau and APP. Science 293: 1487-1491.

248. Greenberg SG, Davies P (1990) A preparation of Alzheimer paired helical filaments that displays distinct tau proteins by polyacrylamide gel electrophoresis. Proc Natl Acad Sci U S A 87: 5827-5831.

249. Fuster-Matanzo A, de Barreda EG, Dawson HN, Vitek MP, Avila J, et al. (2009) Function of tau protein in adult newborn neurons. FEBS Lett 583: 3063-3068.

250. Komori T, Arai N, Oda M, Nakayama H, Mori H, et al. (1998) Astrocytic plaques and tufts of abnormal fibers do not coexist in corticobasal degeneration and progressive supranuclear palsy. Acta Neuropathol 96: 401-408.

251. Sun Y, Chen X, Xiao D (2007) Tetracycline-inducible expression systems: new strategies and practices in the transgenic mouse modeling. Acta Biochim Biophys Sin (Shanghai) 39: 235-246.

252. Terwel D, Muyllaert D, Dewachter I, Borghgraef P, Croes S, et al. (2008) Amyloid activates GSK-3beta to aggravate neuronal tauopathy in bigenic mice. Am J Pathol 172: 786-798.

253. Carlson GA, Kingsbury DT, Goodman PA, Coleman S, Marshall ST, et al. (1986) Linkage of prion protein and scrapie incubation time genes. Cell 46: 503-511.

254. Westaway D, Goodman PA, Mirenda CA, McKinley MP, Carlson GA, et al. (1987) Distinct prion proteins in short and long scrapie incubation period mice. Cell 51: 651-662.

255. Legname G, Nguyen HO, Peretz D, Cohen FE, DeArmond SJ, et al. (2006) Continuum of prion protein structures enciphers a multitude of prion isolate-specified phenotypes. Proc Natl Acad Sci U S A 103: 19105-19110.

256. Tanaka M, Chien P, Naber N, Cooke R, Weissman JS (2004) Conformational variations in an infectious protein determine prion strain differences. Nature 428: 323-328.

257. Hamano T, Gendron TF, Ko LW, Yen SH (2009) Concentration-dependent effects of proteasomal inhibition on tau processing in a cellular model of tauopathy. Int J Clin Exp Pathol 2: 561-573.

258. Goedert M, Jakes R (2005) Mutations causing neurodegenerative tauopathies. Biochim Biophys Acta 1739: 240-250.

259. Lein ES, Hawrylycz MJ, Ao N, Ayres M, Bensinger A, et al. (2007) Genome-wide atlas of gene expression in the adult mouse brain. Nature 445: 168-176.

260. Braak H, Del Tredici K (2011) The pathological process underlying Alzheimer's disease in individuals under thirty. Acta Neuropathol 121: 171-181.

261. Urbach A, Schuldiner M, Benvenisty N (2004) Modeling for Lesch-Nyhan disease by gene targeting in human embryonic stem cells. Stem Cells 22: 635-641.

262. Urbach A, Benvenisty N (2009) Studying early lethality of 45,XO (Turner's syndrome) embryos using human embryonic stem cells. PLoS One 4: e4175.

263. Brennand KJ, Simone A, Jou J, Gelboin-Burkhart C, Tran N, et al. (2011) Modelling schizophrenia using human induced pluripotent stem cells. Nature 473: 221-225.

264. Giri RK, Young R, Pitstick R, DeArmond SJ, Prusiner SB, et al. (2006) Prion infection of mouse neurospheres. Proc Natl Acad Sci U S A 103: 3875-3880.

265. Mroz K, Carrel L, Hunt PA (1999) Germ cell development in the XXY mouse: evidence that X chromosome reactivation is independent of sexual differentiation. Dev Biol 207: 229-238.

266. Barten DM, Cadelina GW, Hoque N, DeCarr LB, Guss VL, et al. Tau transgenic mice as models for cerebrospinal fluid tau biomarkers. J Alzheimers Dis 24 Suppl 2: 127-141.

267. Takuma H, Arawaka S, Mori H (2003) Isoforms changes of tau protein during development in various species. Brain Res Dev Brain Res 142: 121-127.

268. McMillan P, Korvatska E, Poorkaj P, Evstafjeva Z, Robinson L, et al. (2008) Tau isoform regulation is region- and cell-specific in mouse brain. J Comp Neurol 511: 788-803.

269. Loomis PA, Howard TH, Castleberry RP, Binder LI (1990) Identification of nuclear tau isoforms in human neuroblastoma cells. Proc Natl Acad Sci U S A 87: 8422-8426.

270. Thurston VC, Pena P, Pestell R, Binder LI (1997) Nucleolar localization of the microtubule-associated protein tau in neuroblastomas using sense and anti-sense transfection strategies. Cell Motil Cytoskeleton 38: 100-110.

271. Sjoberg MK, Shestakova E, Mansuroglu Z, Maccioni RB, Bonnefoy E (2006) Tau protein binds to pericentromeric DNA: a putative role for nuclear tau in nucleolar organization. J Cell Sci 119: 2025-2034.

272. Ahmed S (2009) The culture of neural stem cells. J Cell Biochem 106: 1-6.

273. Guan K, Chang H, Rolletschek A, Wobus AM (2001) Embryonic stem cell-derived neurogenesis. Retinoic acid induction and lineage selection of neuronal cells. Cell Tissue Res 305: 171-176.

274. Smith AG (2001) Embryo-derived stem cells: of mice and men. Annu Rev Cell Dev Biol 17: 435-462.

275. Csete M (2005) Oxygen in the cultivation of stem cells. Ann N Y Acad Sci 1049: 1-8.

276. Caceres A, Binder LI, Payne MR, Bender P, Rebhun L, et al. (1984) Differential subcellular localization of tubulin and the microtubule-associated protein MAP2 in brain tissue as revealed by immunocytochemistry with monoclonal hybridoma antibodies. J Neurosci 4: 394-410.

277. Kosik KS, Finch EA (1987) MAP2 and tau segregate into dendritic and axonal domains after the elaboration of morphologically distinct neurites: an immunocytochemical study of cultured rat cerebrum. J Neurosci 7: 3142-3153.

278. Kleiman R, Banker G, Steward O (1994) Development of subcellular mRNA compartmentation in hippocampal neurons in culture. J Neurosci 14: 1130-1140.

279. Kempf M, Clement A, Faissner A, Lee G, Brandt R (1996) Tau binds to the distal axon early in development of polarity in a microtubule- and microfilament-dependent manner. J Neurosci 16: 5583-5592.

280. Harris KM, Jensen FE, Tsao B (1992) Three-dimensional structure of dendritic spines and synapses in rat hippocampus (CA1) at postnatal day 15 and adult ages: implications for the maturation of synaptic physiology and long-term potentiation. J Neurosci 12: 2685-2705.

281. Dailey ME, Buchanan J, Bergles DE, Smith SJ (1994) Mossy fiber growth and synaptogenesis in rat hippocampal slices in vitro. J Neurosci 14: 1060-1078.

282. Papa M, Bundman MC, Greenberger V, Segal M (1995) Morphological analysis of dendritic spine development in primary cultures of hippocampal neurons. J Neurosci 15: 1-11.

283. Ziv NE, Smith SJ (1996) Evidence for a role of dendritic filopodia in synaptogenesis and spine formation. Neuron 17: 91-102.

284. Fiala JC, Feinberg M, Popov V, Harris KM (1998) Synaptogenesis via dendritic filopodia in developing hippocampal area CA1. J Neurosci 18: 8900-8911.

285. Bayreuther K, Rodemann HP, Hommel R, Dittmann K, Albiez M, et al. (1988) Human skin fibroblasts in vitro differentiate along a terminal cell lineage. Proc Natl Acad Sci U S A 85: 5112-5116.

286. Ciccolini F (2001) Identification of two distinct types of multipotent neural precursors that appear sequentially during CNS development. Mol Cell Neurosci 17: 895-907.

287. Perez M, Lim F, Arrasate M, Avila J (2000) The FTDP-17-linked mutation R406W abolishes the interaction of phosphorylated tau with microtubules. J Neurochem 74: 2583-2589.

288. Connell JW, Gibb GM, Betts JC, Blackstock WP, Gallo J, et al. (2001) Effects of FTDP-17 mutations on the in vitro phosphorylation of tau by glycogen synthase kinase 3beta identified by mass spectrometry demonstrate certain mutations exert long-range conformational changes. FEBS Lett 493: 40-44.

289. DeTure M, Ko LW, Easson C, Yen SH (2002) Tau assembly in inducible transfectants expressing wild-type or FTDP-17 tau. Am J Pathol 161: 1711-1722.

290. Sakaue F, Saito T, Sato Y, Asada A, Ishiguro K, et al. (2005) Phosphorylation of FTDP-17 mutant tau by cyclin-dependent kinase 5 complexed with p35, p25, or p39. J Biol Chem 280: 31522-31529.

291. Wada Y, Ishiguro K, Itoh TJ, Uchida T, Hotani H, et al. (1998) Microtubule-stimulated phosphorylation of tau at Ser202 and Thr205 by cdk5 decreases its microtubule nucleation activity. J Biochem 124: 738-746.

292. Bugiani O, Murrell JR, Giaccone G, Hasegawa M, Ghigo G, et al. (1999) Frontotemporal dementia and corticobasal degeneration in a family with a P301S mutation in tau. J Neuropathol Exp Neurol 58: 667-677.

293. Dayanandan R, Van Slegtenhorst M, Mack TG, Ko L, Yen SH, et al. (1999) Mutations in tau reduce its microtubule binding properties in intact cells and affect its phosphorylation. FEBS Lett 446: 228-232.

294. Lu M, Kosik KS (2001) Competition for microtubule-binding with dual expression of tau missense and splice isoforms. Mol Biol Cell 12: 171-184.

295. Matsuo ES, Shin RW, Billingsley ML, Van deVoorde A, O'Connor M, et al. (1994) Biopsy-derived adult human brain tau is phosphorylated at many of the same sites as Alzheimer's disease paired helical filament tau. Neuron 13: 989-1002.

296. Lovestone S, Reynolds CH (1997) The phosphorylation of tau: a critical stage in neurodevelopment and neurodegenerative processes. Neuroscience 78: 309-324.

297. Ding H, Matthews TA, Johnson GV (2006) Site-specific phosphorylation and caspase cleavage differentially impact tau-microtubule interactions and tau aggregation. J Biol Chem 281: 19107-19114.

298. Vandebroek T, Terwel D, Vanhelmont T, Gysemans M, Van Haesendonck C, et al. (2006) Microtubule binding and clustering of human Tau-4R and Tau-P301L proteins isolated from yeast deficient in orthologues of glycogen synthase kinase-3beta or cdk5. J Biol Chem 281: 25388-25397.

299. Braak H, Braak E (1997) Frequency of stages of Alzheimer-related lesions in different age categories. Neurobiol Aging 18: 351-357.

300. Delobel P, Flament S, Hamdane M, Jakes R, Rousseau A, et al. (2002) Functional characterization of FTDP-17 tau gene mutations through their effects on Xenopus oocyte maturation. J Biol Chem 277: 9199-9205.

301. Illenberger S, Zheng-Fischhofer Q, Preuss U, Stamer K, Baumann K, et al. (1998) The endogenous and cell cycle-dependent phosphorylation of tau protein in living cells: implications for Alzheimer's disease. Mol Biol Cell 9: 1495-1512.

302. Preuss U, Mandelkow EM (1998) Mitotic phosphorylation of tau protein in neuronal cell lines resembles phosphorylation in Alzheimer's disease. Eur J Cell Biol 76: 176-184.

303. D'Arcangelo G, Miao GG, Chen SC, Soares HD, Morgan JI, et al. (1995) A protein related to extracellular matrix proteins deleted in the mouse mutant reeler. Nature 374: 719-723.

304. Singh TJ, Grundke-Iqbal I, Wu WQ, Chauhan V, Novak M, et al. (1997) Protein kinase C and calcium/calmodulin-dependent protein kinase II phosphorylate three-repeat and four-repeat tau isoforms at different rates. Mol Cell Biochem 168: 141-148.

305. Haas MA, Chuckowree JA, Chung RS, Vickers JC, Dickson TC (2007) Identification and characterization of a population of motile neurons in long-term cortical culture. Cell Motil Cytoskeleton 64: 274-287.

306. Klein C, Fishell G (2004) Neural stem cells: progenitors or panacea? Dev Neurosci 26: 82-92.

307. Klein C, Butt SJ, Machold RP, Johnson JE, Fishell G (2005) Cerebellum- and forebrain-derived stem cells possess intrinsic regional character. Development 132: 4497-4508.

308. Garrick D, Fiering S, Martin DI, Whitelaw E (1998) Repeat-induced gene silencing in mammals. Nat Genet 18: 56-59.

309. Henikoff S (1998) Conspiracy of silence among repeated transgenes. Bioessays 20: 532-535.

310. Feng G, Mellor RH, Bernstein M, Keller-Peck C, Nguyen QT, et al. (2000) Imaging neuronal subsets in transgenic mice expressing multiple spectral variants of GFP. Neuron 28: 41-51.

311. Yasuda M, Mayford MR (2006) CaMKII activation in the entorhinal cortex disrupts previously encoded spatial memory. Neuron 50: 309-318.

APPENDICES

APPENDIX A

HISTOLOGY: NEUN AND PHF1/NFT CELL COUNTS

NEUN CELL COUNT ESTIMATION WITH PHOTOSHOP CS5

NeuN Cell Counts

Bright field 5x NeuN images (Figure 4.1) were acquired with a Zeiss Axio Imager.M1 microscope using AxioVision release 4.5 sp1 PixeLINK Capture Standard Edition (IHC). Four to six mice of each genotype were imaged and analyzed. Images were analyzed in PhotoShop CS5 (Figure 4.2). The hippocampal formation was selected using the "magic wand tool". This function takes into account a range of color variations based on the tolerance setting. The tolerance was set to select only chromogen stained cells. The extracted hippocampal region was copied into a transparent background to allow for more precise data selection (Figure 4.2B). The area stained was calculated with the Area Measurement tool and data was exported into an excel document. To determine the average size of a NeuN positive cell, individual NeuN stained cells were selected and extracted into transparent backgrounds (Figure 4.2C and 4.2D). The average area of 21 cells was used as the average NeuN cell size. To determine total hippocampal cell number, the total hippocampal area value was divided by calculated average NeuN size. Multiple sections of individual mice were average.

Specific CA1 counts were determined by arranging all extracted hippocampi in the same orientation. To do so, a template document was generated containing vertical and horizontal guides to form four quadrants. All extracted hippocampi were rotated until the edge of the DG abutted the vertical guide and was bisected by the horizontal guide; the bottom of CA3 rested on the horizontal guide (Figure 4.2E). All cells within the top left quadrant (Quadrant 1) were counted as CA1. Every hippocampi was opened in the

same template and aligned identically (Figure 4.2F). All cells in the CA1 quadrant were extracted and measured as for whole hippocampi.

PHF1 and NFT Cell Counts.

Entire hemibrains were sectioned at 5μm. Six 5μm sections from each mouse were stained with PHF1 or Bielschowsky silver staining (Figure 4.1). We chose sections spaced approximately 60μm apart to encompass approximately 300μm brain region. Initial sections from each brain were stained with H&E to assess brain region. Based on H&E findings we selected sections of comparable brain depth/location for immunostaining. We counted 3-6 5μm sections for each mouse/antibody.

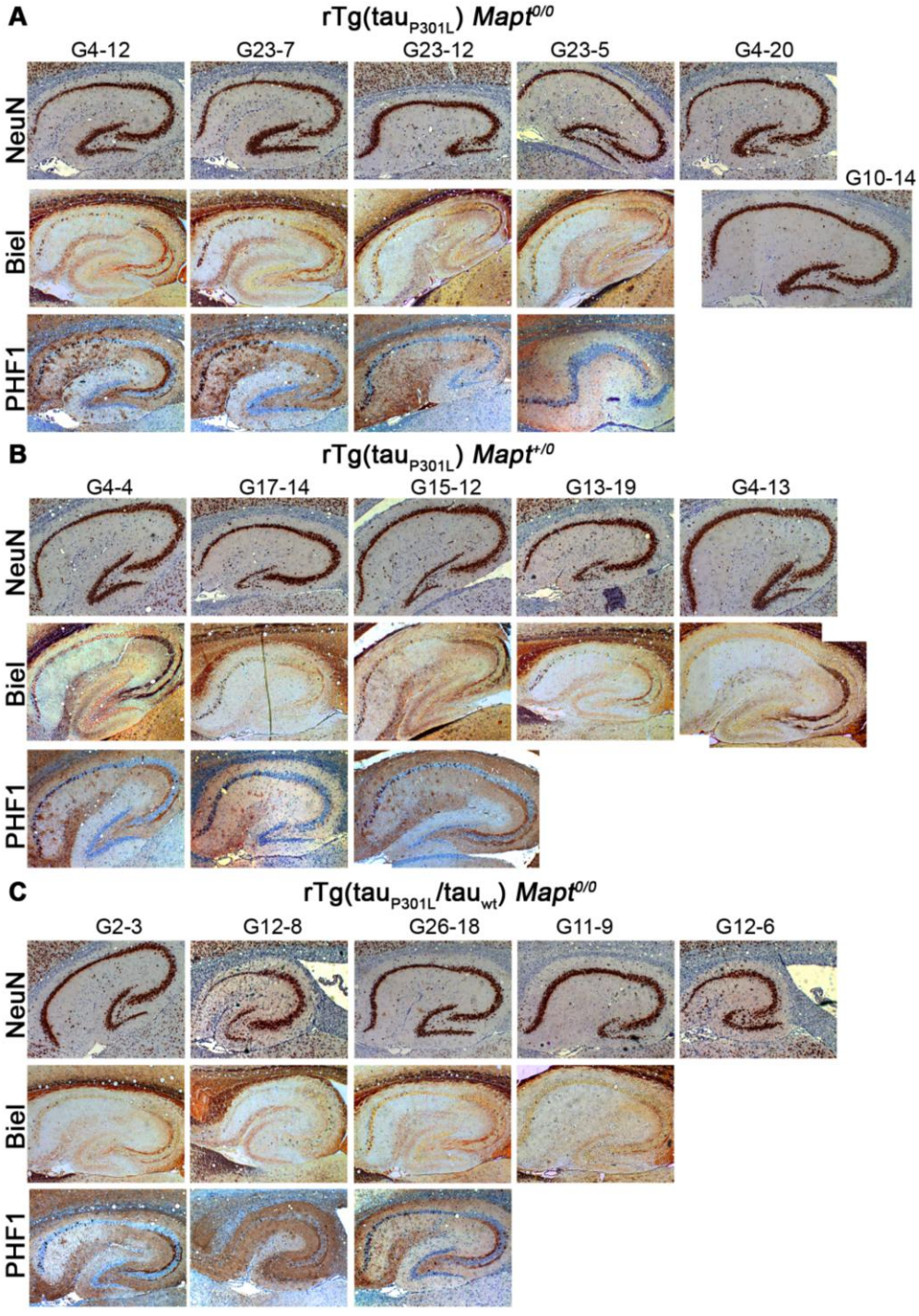

Figure Appendix A1: Representative NeuN, PHF1, and NFT Images Used For Analyses**.** Representative sections from each mouse stained with NeuN, Bielschowsky silver stain, or PHF1 are shown. (A) rTg(tau$_{P301L}$)*Mapt*$^{0/0}$, (B) rTg(tau$_{P301L}$)*Mapt*$^{+/0}$, and (C) rTg(tau$_{P301L}$/tau$_{wt}$)*Mapt*$^{0/0}$; (5x power).

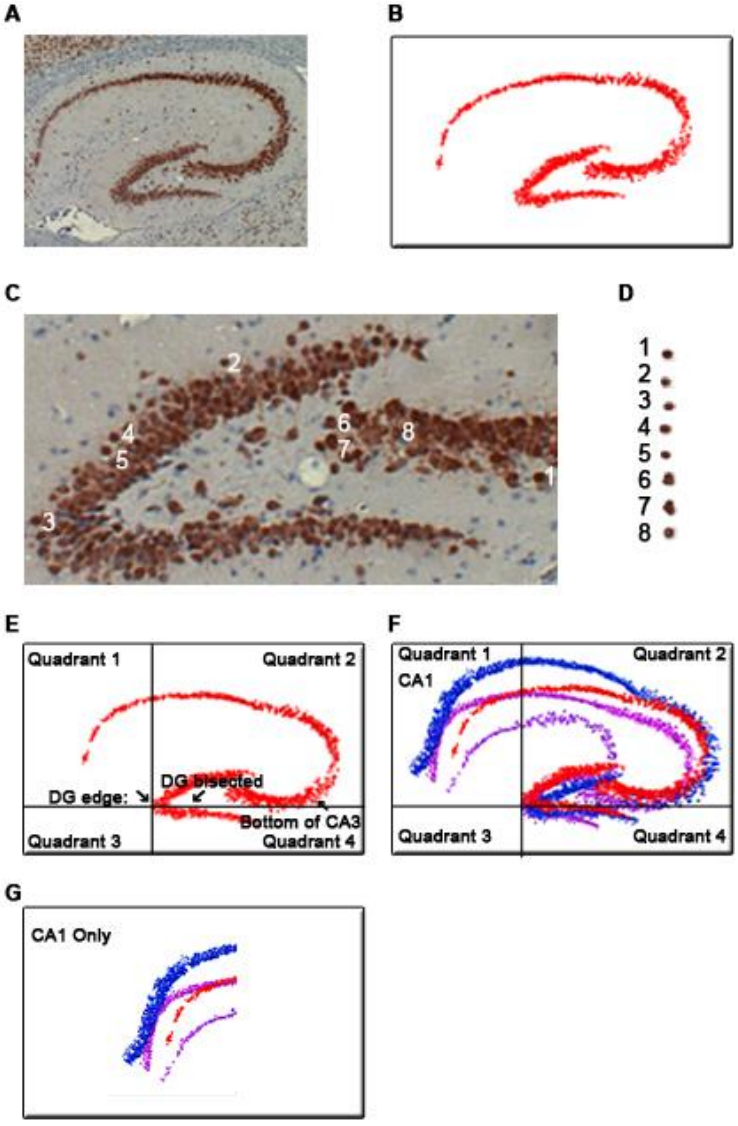

Figure Appendix A2: NeuN Cell Counting With PhotoShop CS5.
(A) Representative 5x NeuN image opened in PS CS5. (B) The Magic Wand was used to select the hippocampal formation. The selected pixels were extracted to a transparent background so the area could be measured. (C) Individual NeuN stained cells were selected and extracted to transparent backgrounds for area measurement. (D) Individual NeuN cells extracted from C. (E) In order to specifically count CA1 NeuN positive cells a template document was divided into quadrants. Hippocampi were rotated until their DG was bisected by the horizontal axis with the CA3 resting on the horizontal axis, and DG abutted the vertical axis. (F) All hippocampi were arranged in the same manner. Shown is the alignment of 4 different mouse hippocampi. (G) All cells within quadrant 1 were extracted to a separate transparent document and for area measurement. Each hippocampi was measured individually, 4 are shown together for purposed of illustration only.

APPENDIX B

AUTOMATED IMMUNOFLUORESCENCE IMAGING

MULTI DIMENSIONAL ACQUISITION USING METAMORPH

Before Imaging

1. Adjust microscope diaphragm. Using the computer screen as a reference adjust the diaphragm circle so it is just out of view on the "live" view. This is to ensure that the field you see through the microscope eyepieces will match the field imaged by the camera.
2. Adjust the microscope focus to the computer focus. Click "live" on the computer and adjust the focus so that DAPI is in focus on the computer screen. Once DAPI is in good focus on the computer, look through the microscope eyepieces and adjust the eyepieces, not the stage, until DAPI is in focus. At this point the computer and microscope focus should be the same.
3. Using a positive control cell take sample images at each wavelength. To do so the Z-focus will be slightly different for each wavelength due to different focal planes in which the protein of interest was located in the cell. Focus each wavelength on the computer and acquire separately. Open "image information" and record the Z-axis reading for each wavelength. Compare each of these values to that of DAPI. Open "M-Change Z-UV to 488" Journal. Based on DAPI, record the + or – Z-value difference for each wavelength.
4. On the Multi-Dimensional Acquisition (MDA) "Journal" tab, click the box for each of the following: Before each image—M-change Z UV to 488; Start at stage position—M-Focus at start.

5. MDA “Main tab” check the boxes for: multiple stage positions, multiple wavelengths, save in series
6. MDA “Wavelength tab” make sure auto-focus and auto-acquire are NOT checked. Record appropriate exposure time for each wavelength based on intensity of individual wavelength on positive control cells. Note: do not set an exposure time that will result in saturated fluorescence. It is better to error on the side of shorter exposure time.
7. MDA “Main tab” select directory to save images.

Imaging

1. Image no primary control fields for each wavelength and record the minimum intensity
2. Image positive control fields for each wavelength and record maximum intensity
3. Values from (1) and (2) will be used to later scale all images if desired
4. Select fields to image based on DAPI distribution, focus DAPI and select field by pressing F11 to add each field to be acquired (Multiple stage positions).
5. Press acquire on MDA window. (A small portion of images will be out of focus so select 5% more than you need to make sure you have enough cells).

Multi Wavelength Cell Scoring:

Multi Wavelength Cell Scoring can only be conducted on images that were acquired as a journal. If they were acquired separately, manual cell counts must be conducted. Multi Wavelength Cell Scoring allows automated determination of whether a cell was

positive or negative for the antibody used. The program recognizes a cell based on DAPI staining, which are the first set of parameters that need to be set.

1. Determine nuclei based on DAPI.
    a. Size parameters
        i. Using the caliper tool measure the narrowest nuclei visible.
        ii. Use this value as the minimum width parameter.
        iii. Measure the broadest nuclei visible.
        iv. Use this value for the maximum width parameters.
    b. Fluorescence Parameters: Determine the "Intensity above background" parameter.
        i. Subtract the background gray scale (place the cursor over an area without staining and record the gray scale) from the gray scale of the dimmest nuclei (place the cursor over the dimmest nuclei and record the gray scale value. Subtract the values.
        ii. Click "Preview" to determine if all nuclei are appropriately selected.
2. Determine cytoplasmic stain parameters. The steps are similar to DAPI.
    a. Negative control images were used to set the minimum fluorescence intensity (cells that received only secondary antibody)
    b. Positive control images were used to set minimum stained area (smallest positive control cell for minimum stained area).

c. Once the parameters were set for all three wavelengths (DAPI, nestin, tau), each image was analyzed. Data was exported to excel files.

Percent Positive Cells and Histograms:

The Multi Wavelength Cell Scoring program scored each cell as positive (1) or negative (0) for each wavelength. The proportion of cells stained with nestin and Tau13 were recorded for each cell line. To generate fluorescence intensity histograms only the positive cells were used. The "average intensity" values for each cell line were exported into a new excel spreadsheet. The lowest value was subtracted from the highest value. This was the total fluorescence range. This number was divided by the number of desired bins (typically 10). This number represented the bin size. The bin size value was added to the lowest value to get the cut-off range for bin 1, the bin 1 value was added to the bin size value to get the cut-off range for bin 2, etc. through bin 10. Using StatPlus:mac LE.2009 I generated histograms. The "Continuous Variable" was the average intensity output generated by MetaMorph and the Bin Range were the values I described above. StatPlus output data consisted of histograms, raw counts, and percentage of cells in each bin. The percentage of cells in each bin was exported into a separate spreadsheet. This was repeated for each cell line. If more than three independent cell lines of the same genotype were included in the analysis I averaged the proportion of cells in each bin and calculated the standard deviation and plotted the averages against bin number. If less than three lines of each genotype were analyzed, they were plotted individually.

APPENDIX C

CRYOPRESERVATION AND THAWING OF NEUROSPHERES

CRYOPRESERVATION OF CULTURED NEUROSPHERE FORMING CELLS

Adopted From StemCells Inc.

Materials and Equipment

1. Bovine Serum Albumin—Sigma
2. DMSO—Sigma
3. Nalgene cryovials
4. 50mL Polystyrene conical tubes
5. Complete NeuroCult Media
6. Nalgene Freezing Containers
7. Cryo-Medium **Part A 50mL**
    a. 20mL 20% BSA
    b. 30mL NeuroCult Basal Media (Stem Cell Technologies)
8. Cryo-Medium **Part B 50mL**
    a. 7.5mL DMSO
    b. 42.5mL NeuroCult Basal Media
9. **Final Cryo-medium formulation for cell cryo=50/50, A/B**

Procedure

1. Cell cultures are frozen 2-3 days post papain passage. The culture flask will contain ~$6x10^6$ cells at this time.
2. Place the Nalgene freezing container on ice to chill while collecting cells.
3. Make cryo-medium **Part A** and **Part B** and place on ice.

4. Transfer the entire T75 flask volume into polystyrene conical tube and centrifuge at 1100RPM (200xg) for 5 min RT.
5. Resuspend the pellet in 500μL cryo-medium **part A**/number cryovials and gently triturate.
    a. Each T75 flask will yield 3 frozen vials of ~2-4x10^6 cells.
    b. For 3 cryovials resuspend pellet in 1.5mL.
6. Aliquot 500μL of resuspended cells into each cryovial.
7. Add 500μL ice-cold cryo-medium **part B** to each cell suspension. Add **part B** slowly, one drop/second and swirl.
8. Immediately place into chilled Nalgene freezing containers and transfer to the -80C freezer.
9. Transfer to liquid N_2 the following day.

Procedure: Thawing Cryo-Preserved Cells

1. Remove the vial of cryo-preserved cells from liquid N_2 storage and place on dry ice to transport to the lab. Swirl the vial in 37°C water bath (rapid thaw) until only a small piece of ice is left in vial.
2. Pipette the cell suspension into a 15mL tube containing ~10mL of complete NeuroCult medium and centrifuge for 5 min at ~200 x g.
3. Resuspend the pellet in 10mL of fresh complete NeuroCult medium and centrifuge as above.

4. Gently resuspend the pellet in ~2mL of complete NeuroCult medium and pipette and place entire volume into T75cm flask containing 13 mL of Complete NeuroCult medium.